New Coherence Effects in Systems with Near-Degenerate Levels Driven by Intense Laser Fields

A THESIS

submitted for the Award of Ph.D degree of

Mohan Lal Sukhadia University

in the

Faculty of Science

BY

Sunish Menon

Under the Supervision of

Prof. G. S. Agarwal
Director, Physical Research Laboratory

DEPARTMENT OF LASER PHYSICS AND QUANTUM OPTICS
PHYSICAL RESEARCH LABORATORY, AHMEDABAD.

MOHANLAL SUKHADIA UNIVERSITY, UDAIPUR

Year of submission: 2000

CERTIFIED that the work incorporated in the thesis

New Coherence Effects in Systems with Near- Degenerate Levels Driven by Intense Laser Fields

submitted by Shri. **Sunish Menon** was carried out by the candidate under my guidance at the Physical Research Laboratory, Ahmedabad. The work presented in this thesis is original and has not formed basis for the award of any degree or diploma by any university or institution.

Prof. G. S. Agarwal
(Supervisor)

to

Pappa

and to the memory of
Mummy

Contents

Acknowledgement

It gives me great pleasure to express my gratitude to Prof. G. S. Agarwal for his excellent guidance and valuable suggestions. I benefited a great deal from his deep insight and excitement in the subject. I will always be indebted to him for what I have learnt from him in these five years.

I take this opportunity to also thank all my teachers, right from my early school days, to infuse in me the best part of their personalities.

I thank Drs., B. G. Anandrao, J. Banerji, D. P. Dewangan, S. Dutta Gupta, and V. B. Sheorey for important discussions and suggestions at various stages. It is a pleasure to acknowledge Drs., Anu, S. Arun, P. Dutta, Harsha, Sagar, and R. P. Singh for help and interesting academic and non-academic discussions.

I thank all the staff members at PRL for their kind support. In particular, the library staff, computer center staff, Leela, Sudheen, and Babubhai for their timely help and cooperation when required.

I thank my batch-mates at PRL, Anil the Nightingale, Alam + better-half, raving Alok, AdShukla, Dipu + Amrita, garba-girl Jitti, Koushik the gentleman, Pankaj the Assam, disturbed Rajesh, nirvana-attained Rajneesh, Sanki the Badshah, Sudhir + depression, Som, and the one-and-only Vinay, for their unforgettable and entertaining company in the last five years. I reminisce here good times I shared with many of my friends, just to name a few, Anshu, R. Arun, Chandan, c.Muthu, Dulichand, Jayendra, Kunu, Lokesh, Prashant, Rishi, Ravi, Saikrishna, Sarika, Shajesh, Sudeshna, Tarak, and Tarun. I owe a special thanks to each one of them, and in particular to Chandan for carefully proof-reading this manuscript.

Finally, I acknowledge my dear ones for making me what I am. I thank Pappa, Sudha and Bijuatten for their constant support and encouragement to me in pursuing a research career. I owe a lot to my niece Nitu for the pleasant moments I have been sharing with her.

Abstract

In chapter 1, the basic theory of radiation-matter interaction is introduced. Some properties of density matrix equations and derivation of interaction Hamiltonian are discussed. In Sec. 1.2 an overview of important atomic coherence effects like coherent population trapping, electromagnetically induced transparency etc. is presented. In Sec. 1.3 master equation formalism for the treatment of spontaneous emission is introduced. Conditions for observing coherence effects via spontaneous emission in near-degenerate V and Λ systems are also discussed.

In chapter 2, the probe absorption spectra of a strongly driven Λ system with arbitrary spacing between the two lower levels is analyzed. The key findings of this chapter are: (a) Prediction of gain regions arising from the cross talk among optical transitions. (b) Demonstration of the possibility of superluminal propagation due to cross talk. An analysis based on dressed states is presented to explain our numerical results.

In chapter 3, new coherence effects due to interfering decay channels in the V systems are reported. The presence of new gain features in the absorption spectra are predicted, and this gain is shown to arise due to a vacuum induced quasi-trapped-state. It is also shown that the quasi-trapped-state gives rise to a spectral region where the refractive index is large but the absorption is minimum.

In chapter 4, it is shown that the dynamical equations for the interaction between a heat bath and a near-degenerate V system can give rise to new coherence terms. We address the question as to whether such equations are consistent with the principles of thermodynamic equilibrium. Our key findings are that the coherences affect the dynamics but the steady states conditions are still characterized by Boltzmann factors. It is also shown that such coherences in the dynamical equations can be probed via the spectrum of fluorescence.

We next investigate the characteristics of near-degenerate Λ systems, where

additional coherence terms can arise due to interaction with a common mode of vacuum field. In chapter 5, a simple test is proposed to demonstrate and detect the presence of vacuum induced coherence (VIC) in the Λ systems. It is shown that the probe field absorption is modulated due to the presence of such a coherence which is unobservable in the fluorescence. In chapter 6, the effects of VIC on the formation of trapped state is reported. The key findings in this chapter are: (a) VIC can preserve both electromagnetically induced transparency and coherent population trapping. (b) VIC increases the time scale for the formation of trapped state. (c) Phase dependent line shapes arise due to the VIC.

Chapter 1

Introduction

The beginning of the twentieth century saw a major revolution in science, and in physics, in particular. The development of quantum mechanics was a major boon in understanding the behavior of particles at microscopic level. Later, the discovery of lasers in 1960 [1] accelerated the pace of development and opened up the previously unexplored regimes of light-matter interaction. By the end of the twentieth century, lasers had found application in almost all facets of life like bio-science, space science, defence, computing, communication etc. For experimentalists, lasers are setting a new benchmark in high precision measurements. As newer techniques are being developed, lasers are becoming the key instrument in controlling and developing tailor made optical properties of matter. The Bose-Einstein condensation, quantum teleportation, coherent control of a chemical reaction, ultra-slow group velocity of light (8 m/s), also group velocity greater than the velocity of light in vacuum etc. are now possible via controlled laser-matter interaction. The list of such new developments continues to grow and the dawn of the twenty-first century is heading for a second revolution.

1.1 Radiation-Matter Interaction

The early work of Planck and Einstein had shown that radiation should not be treated just as waves, but also as a flow of packets (quanta) of energies [2]. These quanta of radiation were later named as *photons* [3]. A significant contribution towards understanding radiation-matter interaction was made by Einstein [4] in 1917. Though his theory was based on phenomenological considerations, he was able to predict correctly the basic quantities like absorption and emission

probabilities which are still in use. Later on, rigorous quantum mechanical calculations were able to prove these results. Consider two discrete energy levels of atom, namely the excited state $|1\rangle$ and the ground state $|2\rangle$. Einstein classified interaction of radiation with matter into three important processes:

1. *Stimulated absorption*: The atom absorbs a photon and jumps up from ground state $|2\rangle$ to excited state $|1\rangle$ due to an input radiation flux with a proportionality coefficient B_{21}.

2. *Stimulated emission*: The atom jumps down from excited state $|1\rangle$ to ground state $|2\rangle$ via photon emission stimulated due to an input radiation flux with a proportionality coefficient B_{12}. The emitted photon will have the same frequency and phase characteristics as that of the stimulating photon.

3. *Spontaneous emission*: Random emission of photon from excited state $|1\rangle$ with a probability A_{12} due to background fluctuations.

The important point is that none of these A, B coefficients, by definition, depend on the applied field. They are the properties of the medium. For thermal equilibrium, Einstein's theory predicted that

$$B_{12} = \frac{g_2}{g_1} B_{21}, \tag{1.1a}$$

$$A_{12} = \frac{\hbar\omega^3}{c^3\pi^2} B_{21}, \tag{1.1b}$$

where g_1, g_2 are the degeneracies of the excited and ground levels and $\hbar\omega$ is the energy of the photon. Thus all Einstein's coefficients are interrelated. Consider a collection of N atoms with N_1 atoms in excited state and N_2 atoms in ground state. The first result above shows that for $g_1 = g_2 = 1$, if $N_2 > N_1$ then absorption will dominate and if $N_1 > N_2$ then stimulated emission will dominate. The basic idea of lasing action involves having a medium with population inversion ($N_1 > N_2$) and thus the radiation emitted is stimulated rather than spontaneous emission. Since all photons in stimulated radiation have similar phase and frequency characteristics, such a radiation is highly coherent (thus directional) and number of photons per mode can be very high. Typically, a mercury lamp will have 10^{-2} photons/mode while a continuous wave laser can have 10^{10} photons/mode. It should be noted that stimulated absorption/emission are equiprobable at thermal equilibrium [see (1.1a)] which gives the requirement of population inversion

for lasing action. It has now been realized that such a requirement may not be always essential as we will see later.

A complete quantum mechanical calculation for the two levels $|1\rangle$ and $|2\rangle$ with energy separation $\hbar\omega_{12}$ will show that (in C.G.S units)

$$B_{21} = \frac{4\pi^2|\vec{d}_{21}|^2}{3\hbar^2}, \tag{1.2a}$$

$$A_{12} = \frac{4\omega_{12}^3|\vec{d}_{12}|^2}{3\hbar c^3}. \tag{1.2b}$$

Here the parameter $\vec{d}_{12} = \langle 1|e\vec{r}|2\rangle$ is the dipole matrix element. The above results show that the spontaneous emission rate increases rapidly with increasing energy spacing $\hbar\omega_{12}$. Thus it is difficult to have population inversion at higher frequencies like VUV, X-rays and beyond. But in the last ten years or so it has been demonstrated that it is possible to control spontaneous emission. The Fermi golden rule in quantum mechanics will show that the transition rate from a discrete atomic level to a continuum of electromagnetic modes is given by [5]

$$\gamma = \frac{2\pi}{\hbar}|V|^2\rho(\omega). \tag{1.3}$$

Here $|V|^2$ is the coupling strength of the electromagnetic field with atomic levels and $\rho(\omega)$ is the density of modes available to the emitted photon. Thus by changing the density of modes or the coupling strength the spontaneous emission rate can be modified or controlled.

1.1.1 Classical Electromagnetic Field Theory

For any medium the electromagnetic (em) field propagation is governed by the four fundamental Maxwell equations (in C.G.S. units) given by [6],

$$\vec{\nabla}\cdot\vec{D} = 4\pi\varrho, \quad \vec{\nabla}\cdot\vec{B} = 0, \tag{1.4a}$$

$$\vec{\nabla}\times\vec{E} = -\frac{1}{c}\frac{\partial\vec{B}}{\partial t}, \tag{1.4b}$$

$$\vec{\nabla}\times\vec{H} = \frac{4\pi\vec{J}}{c} + \frac{1}{c}\frac{\partial\vec{D}}{\partial t}, \tag{1.4c}$$

where $\vec{E}$, $\vec{B}$ are the averaged electric, magnetic induction field vectors at some space-time point and c is the velocity of these fields in vacuum. The freely moving charges in the medium contribute via the charge density ϱ and current density $\vec{J}$.

The components of averaged displacement vector ($\vec{D}$) and magnetic field ($\vec{H}$) are given by

$$D_i = E_i + 4\pi P_i - 4\pi \sum_j \frac{\partial Q_{ij}}{\partial r_j} + \ldots, \quad H_i = B_i - 4\pi M_i + \ldots \tag{1.5}$$

Here $\vec{P}$, $\vec{M}$, Q_{ij}, ... are respectively the averaged electric dipole, magnetic dipole, electric quadrupole and the higher order moments per unit volume. The bound charges and currents in the medium contribute via these moments. For the results to be reported in this thesis, we consider interaction of em field with a gas of non-interacting neutral atoms. Thus the medium is charge-free ($\varrho = 0$), non-conducting ($\vec{J} = 0$). For such a gas electric polarization ($\vec{P}$) is the most dominant contribution at optical frequencies and the other moments can be neglected in comparison. Using the curl equations (1.4b) and (1.4c) and time derivatives it can be shown that

$$\vec{\nabla} \times \vec{\nabla} \times \vec{E} + \frac{1}{c^2}\frac{\partial^2}{\partial t^2}(\vec{E} + 4\pi\vec{P}) = 0. \tag{1.6}$$

For a medium with only bound charges, $\vec{\nabla} \cdot \vec{D} = 0$ and thus $\vec{\nabla} \cdot \vec{E} = 0$, because $\vec{D} = \mathfrak{e}\vec{E}$ where $\mathfrak{e}$ is the electric permittivity tensor. Equation (1.6) can be simplified as below:

$$\nabla^2\vec{E} - \frac{1}{c^2}\frac{\partial^2\vec{E}}{\partial t^2} = \frac{4\pi}{c^2}\frac{\partial^2\vec{P}}{\partial t^2}. \tag{1.7}$$

Though the above inhomogeneous wave equation is difficult to solve, in practice the working equations are simpler to handle. For example, consider a laser field at central frequency ω, traveling along the z-axis, incident on a medium. The variation of the field along transverse directions is typically small on the optical wavelength scale. The input field can be written as

$$\vec{E}_{\rm in}(z,t) = \hat{\epsilon}E_0(z,t)e^{i(kz-\omega t)} + \text{c.c.}, \tag{1.8}$$

where $\hat{\epsilon}$ is the direction of the field vector and E_0 is a slowly varying pulse amplitude. For a continuous wave (cw) field the time dependence of E_0 can be neglected. The linear response of the medium will result in an induced polarization given by,

$$\vec{P}(z,t) = \hat{\epsilon}P_0(z,t)e^{i(kz-\omega t)} + \text{c.c.} \tag{1.9}$$

Substituting these solutions in (1.7) and using the slowly-varying-envelop approximation which implies

$$\left|k\frac{\partial E_0}{\partial z}\right| \gg \left|\frac{\partial^2 E_0}{\partial z^2}\right|, \quad \left|\omega\frac{\partial E_0}{\partial t}\right| \gg \left|\frac{\partial^2 E_0}{\partial t^2}\right|, \quad |\omega^2 P_0| \gg \left|\omega\frac{\partial P_0}{\partial t}\right| \gg \left|\frac{\partial^2 P_0}{\partial t^2}\right|, \tag{1.10}$$

the wave equation reduces to a first order partial differential equation,

$$\frac{\partial E_0}{\partial z} + \frac{1}{c}\frac{\partial E_0}{\partial t} = 2\pi i k P_0. \tag{1.11}$$

For a steady state propagation

$$\frac{\partial E_0}{\partial z} = 2\pi i k \chi(\omega) E_0, \tag{1.12}$$

where the linear relation $P_0 = \chi(\omega)E_0$ is used and $\chi(\omega)$ is the complex susceptibility of the isotropic medium. In general, $\chi(\omega)$ is a tensor of rank 2 for an anisotropic medium. For a medium of length L the output field will be

$$\vec{E}_{\rm out}(z,t) = \hat{\epsilon} E_0 e^{(2\pi i k \chi L)} e^{i(kz-\omega t)} + \text{c.c.}, \tag{1.13}$$

and as seen from (1.13) the linear refractive index of the medium is $n(\omega) = 1 + 2\pi \mathrm{Re}\{\chi(\omega)\}$. The absorption coefficient will be $\alpha(\omega) = 4\pi k \mathrm{Im}\{\chi(\omega)\}$ where the output intensity is given by

$$I_{\rm out} = I_{\rm in} \exp\left(-\alpha L\right). \tag{1.14}$$

Note that χ may also contain information of any other strong laser field present in the medium, provided the laser field amplitude has not changed much in the medium. This is possible if the medium is an atomic beam or the field is acting on levels which are less populated. Also, by appropriate selection of atomic density and medium length, the effect of medium polarization on a strong field can be minimized. At various sections in the thesis we will discuss the effect of a strong field on the medium. The modified properties of the medium will be obtained by evaluating $\chi(\omega)$ for a probe (weak) field. This is done by using density matrix calculations for the discrete energy levels of the medium which take part in the interaction.

1.1.2 Density Matrix Formalism

A given physical system can be described by a quantum mechanical state $|\psi\rangle$ (Dirac notation) where $|\psi\rangle$ will satisfy the Schrödinger equation

$$\frac{\partial |\psi\rangle}{\partial t} = -\frac{i}{\hbar} H |\psi\rangle. \tag{1.15}$$

Here H is the Hamiltonian describing the system. The state $|\psi\rangle$ can be expressed in terms of some orthonormal basis states $|i\rangle$, i.e., $|\psi\rangle = \sum_i c_i |i\rangle$. The density

operator for the state $|\psi\rangle$ is $\rho = |\psi\rangle\langle\psi|$. When represented in a $\{|i\rangle\}$ basis, ρ is given by a matrix called the *density matrix*. The elements of this matrix are $\rho_{ij} = \langle i|\rho|j\rangle = c_j^* c_i$. Clearly, $\mathrm{Tr}(\rho) = 1$, which is a statement of conservation of probability. The expectation value of any operator A in terms of ρ is given by

$$\langle A\rangle = \langle\psi|A|\psi\rangle = \mathrm{Tr}(\rho A) = \mathrm{Tr}(A\rho). \tag{1.16}$$

Note that the expectation value is linear in ρ, but quadratic in $|\psi\rangle$. The major advantage of the density matrix formalism is in dealing with statistical mixtures.

Statistical mixture: In many situations one may have collection of such identical systems $|\psi_l\rangle$. It is possible that the state $|\psi_l\rangle$ is not known, but the probability p_l that the system is in state $|\psi_l\rangle$ is known. To give an example, the momentum of a collection of atoms which may be given by Maxwellian distribution at some temperature T. The density operator for such an ensemble is defined as

$$\rho = \sum_l p_l |\psi_l\rangle\langle\psi_l|, \tag{1.17}$$

where $\sum_l p_l = 1$. It can be shown further from Schrödinger equation (1.15) that ρ will satisfy the differential equation

$$\dot{\rho} = -\frac{i}{\hbar}[H, \rho]. \tag{1.18}$$

Equation (1.18) is often called as Liouville or Von Neumann equation of motion for the density matrix. The elements of ρ in the basis $\{|i\rangle\}$ are now given by

$$\rho_{ij} = \sum_l p_l c_{lj}^* c_{li}, \tag{1.19}$$

and ρ will still satisfy (1.16), but now $\langle A\rangle$ would mean the ensemble averaged value. If the system is in one of the states $|\psi_l\rangle$ with $p_l = 1$, then $\mathrm{Tr}(\rho^2) = 1$ and the state is called a *pure state*. From (1.19) following properties of ρ may be noted: $\mathrm{Tr}(\rho^2) \leq 1$, it is Hermitian and it is positive definite i.e. $\mathrm{Tr}\{\rho U^\dagger U\} \geq 0$, $\forall\ \ U$. The diagonal elements in (1.19) are the ensemble averaged probability to be in some state $|i\rangle$ and are referred as *populations*. The cross terms $c_{lj}^* c_{li}$ represent coherence terms between two different states $|i\rangle$ and $|j\rangle$. These terms are complex in general and if $\rho_{ij} = 0 (i \neq j)$ then it means that the average (1.19) has cancelled the coherence terms. If $\rho_{ij} \neq 0$ $(i \neq j)$ then some kind of coherent addition of interference terms exist. For this reason the off-diagonal elements are often called

coherences. The above equation (1.18) is more general than the Schrödinger equation (1.15), because one can derive both statistical as well as quantum mechanical information from (1.18). For example, one can conveniently handle spontaneous emission, collisional decay, fluctuations in laser fields etc. with density matrix formalism. In practice, the interest will be in some observable in the presence of environmental effects as for example, measuring absorption of a laser field in a medium in the presence of background electromagnetic fluctuations and collisions. The density matrix in such cases is expressed as,

$$\dot{\rho} = -\frac{i}{\hbar}[H, \rho] + \mathcal{L}(\rho), \tag{1.20}$$

where $\mathcal{L}(\rho)$ is the matrix involving decay terms. In section 1.3 master equation formalism will be discussed which can be used to derive the explicit form of $\mathcal{L}(\rho)$ [7]. In general practice, the decay terms are phenomenologically added in equation (1.18).

1.1.3 Interaction Hamiltonian

Consider an em field (plane wave) interacting with an electron bound to a nucleus (assumed to be motionless) by a central potential $V(r)$. In quantum mechanics the classical variables are replaced by their corresponding quantum mechanical operators. The Hamiltonian for the field at a distance $\vec{r}$ from the origin will be

$$H = \frac{1}{2m}[\vec{P} - \frac{q}{c}\vec{A}(\vec{r}, t)]^2 + V(r) + q\Phi(\vec{r}, t). \tag{1.21}$$

Here $\vec{A}(\vec{r}, t)$ [$\Phi(\vec{r}, t)$] is the vector [scalar], potential for the external field and $\vec{P}$ is the momentum operator for the electron. The Hamiltonian (1.21) will satisfy the Schrödinger equation (1.15). If $\psi(\vec{r}, t)$ is a solution of (1.15) so is $\psi(\vec{r}, t)\exp(i\varphi)$, where φ is some arbitrary constant phase. The probability density remains unaffected by the arbitrary choice of phase. However, if the phase is space-time dependent, the Schrödinger equation (1.15) is no longer satisfied. To satisfy phase (or gauge) invariance the following transformation of vector and scalar potentials should be inserted in (1.21).

$$\vec{A}'(\vec{r}, t) \rightarrow \vec{A}(\vec{r}, t) - \frac{\hbar c}{q}\nabla\varphi(\vec{r}, t), \tag{1.22a}$$

$$\Phi'(\vec{r}, t) \rightarrow \Phi(\vec{r}, t) + \frac{\hbar}{q}\frac{\partial\varphi}{\partial t}(\vec{r}, t). \tag{1.22b}$$

Clearly, the vector and scalar potentials are gauge-dependent and the gauge-independent quantities are the electric field and magnetic induction given by $\vec{E} = -\nabla\Phi - \frac{1}{c}\frac{\partial \vec{A}}{\partial t}$ and $\vec{B} = \vec{\nabla} \times \vec{A}$, respectively. Generally, it is convenient to work in the Coulomb gauge which implies $\Phi = 0$ and $\vec{\nabla} \cdot \vec{A} = 0$. Further, for em fields of wavelength greater than or equal to the optical wavelengths one can invoke the *dipole approximation* for (1.21). The atoms have radius of the order of Bohr radius and the positional variation of em field within this distance can be neglected. The vector potential near the atomic radius $\vec{R}$ can be written as $\vec{A}(t) \exp\{i\vec{k} \cdot (\vec{R} + \vec{r'})\}$. In the dipole approximation $\vec{A}(\vec{r}, t) \approx \vec{A}(t) \exp\{i\vec{k} \cdot \vec{R}\}$. Now consider a gauge transformation

$$\varphi(\vec{r}, t) = \frac{q}{c\hbar}\vec{A}(\vec{R}, t) \cdot \vec{r}. \tag{1.23}$$

Using (1.22) and the relation $\vec{E} = -\dot{\vec{A}}/c$ the Hamiltonian (1.21) can be written as

$$H = \frac{1}{2m}P^2 + V(r) - \vec{d} \cdot \vec{E}, \tag{1.24}$$

where $\vec{d} = q\vec{r}$ is the atomic dipole moment operator. Writing the interaction term as $-\vec{d} \cdot \vec{E}$ is called the dipole approximation. If the dipole term is zero then the higher order terms in the expansion of $\exp(i\vec{k} \cdot \vec{r'})$ becomes important. A *semiclassical treatment* of radiation-matter interaction would imply that the electric field in (1.24) is treated as a classical field and the atomic variables as operators. Such an analysis is very reliable for laser fields because of the large photons/mode. It is extensively used in nonlinear optics and laser spectroscopy. A more rigorous theory would require both field and atomic variables to be treated as operators. Such a treatment is required, for example, to study nonclassical effects like squeezed light, sub-Poissonian statistics etc. Most parts of this thesis will involve semiclassical treatment which works well for optical properties of matter in the presence of laser fields.

1.2 Atomic Coherence Effects

The phenomenal development in new experimental techniques and theoretical insight have led to a very precise control over properties of radiation and matter. Atomic coherence, which is a manifestation of coherent superposition of atomic levels, plays a central role in controlling the optical properties of matter. In the

following, some of the important atomic coherence effects are discussed. Most of these effects have found important applications in laser spectroscopy and quantum optics.

1.2.1 Two-Level Atom: Rabi Sidebands

When a strong coherent light is near-resonant with an atomic transition, then the interaction of light with the two concerned atomic states sufficiently explains the response of a medium. The other levels present in the medium can be neglected and the atom is called a *two-level atom*. The very early works on two-level atom driven by a strong field have shown that sidebands will appear in emission spectrum [8, 9], now known as Rabi splitting. Consider a two-level atom with excited state $|1\rangle$ and ground state $|2\rangle$; then by closure theorem, $|1\rangle\langle 1| + |2\rangle\langle 2| = 1$. The atomic Hamiltonian H_0 in term of its eigenstates $|1\rangle$, $|2\rangle$ will be

$$\begin{aligned} H_0 &= (|1\rangle\langle 1| + |2\rangle\langle 2|)H_0(|1\rangle\langle 1| + |2\rangle\langle 2|) \\ &= \hbar\omega_1|1\rangle\langle 1| + \hbar\omega_2|2\rangle\langle 2|, \end{aligned} \tag{1.25}$$

where $\hbar\omega_1$, $\hbar\omega_2$ are the absolute energies corresponding to the excited and ground levels. Similarly, the atomic dipole moment operator can be written as

$$\vec{d} = \vec{d}_{12}|1\rangle\langle 2| + \vec{d}_{21}|2\rangle\langle 1|, \tag{1.26}$$

where $\vec{d}_{lm} = \langle l|\vec{d}|m\rangle$ is zero for diagonal elements due to parity reasons. The off-diagonal elements of $\vec{d}$ will be non-zero only if $|1\rangle$ and $|2\rangle$ have different parities. Let this two-level system be driven by a *control* laser field

$$\vec{E}_c(\vec{r}, t) = \vec{E}_{c0}e^{i(\vec{k}\cdot\vec{r}-\omega_c t)} + \text{c.c.}, \tag{1.27}$$

of frequency ω_c. The total Hamiltonian in dipole approximation will be

$$H = \hbar\omega_{12}A_{11} - (\vec{d}_{12}A_{12} + \vec{d}_{21}A_{21}) \cdot \vec{E}_c, \tag{1.28}$$

where $A_{lm} = |l\rangle\langle m|$ and $\hbar\omega_{12} = \hbar(\omega_1 - \omega_2)$. In writing (1.28), level $|2\rangle$ is considered as the zero of energy. The Hamiltonian (1.28) will satisfy the Schrödinger equation (1.15). Making a unitary transformation $|\phi\rangle = \exp(i\omega_c A_{11}t)|\psi\rangle$ in (1.15), the effective Hamiltonian will be

$$H_{\text{eff}}/\hbar = \Delta_c A_{11} - (G_{12}A_{12} + \text{H.c.}) - (G'_{12}A_{21}e^{-2i\omega_c t} + \text{H.c.}), \tag{1.29}$$

where the coupling strengths are

$$G_{12} = \frac{\vec{d}_{12} \cdot \vec{E}_{c0}}{\hbar} e^{i\vec{k}\cdot\vec{r}}, \quad G'_{12} = \frac{\vec{d}_{12} \cdot \vec{E}^*_{c0}}{\hbar} e^{-i\vec{k}\cdot\vec{r}},$$

and $\Delta_c = \omega_{12} - \omega_c$ is the control field detuning. The rapidly oscillating terms in (1.29) are also called anti-resonant terms. A perturbative analysis (in terms of E_{c0}) will show that they contribute in orders of G'_{12}/ω_c in the probability amplitudes and thus are important only when $G'_{12} \approx \omega_c$ [5]. At optical frequencies this would imply an intensity $\approx 10^{14}\mathrm{W/cm}^2$. Thus at normal intensities one can neglect such anti-resonant terms and this is called the *rotating-wave-approximation* (RWA). If the medium length is small compared to the optical wavelength, for example for atomic beams, the position dependence of coupling strengths can be neglected. The coupling strength $2G_{12}$ is called the *Rabi frequency* - an optical analogue of frequency in magnetic resonance described by I. I. Rabi [10]. With the above approximations the equation of motion for the density matrix elements using (1.18) will be

$$\dot{\tilde{\rho}}_{11} = -\dot{\tilde{\rho}}_{22} = iG_{12}\tilde{\rho}_{21} + \text{c.c.}, \quad \dot{\tilde{\rho}}_{12} = -i\Delta_c\tilde{\rho}_{12} + iG_{12}(\tilde{\rho}_{22} - \tilde{\rho}_{11}), \tag{1.30}$$

where $\tilde{\rho}$ denotes ρ in the rotating frame. Using the initial condition that the atoms are in ground state $|2\rangle$ at $t = 0$, the above set of equations (1.30) can be readily solved. The solution will be,

$$\rho_{22} = \cos^2(\Omega_{12}t/2) + \frac{\Delta_c^2}{\Omega_{12}}\sin^2(\Omega_{12}t/2), \tag{1.31a}$$

$$\rho_{12} = \frac{G_{12}}{2\Omega_{12}}\left[2\Delta_c e^{-i\omega_c t} - (\Omega_{12} + \Delta_c)e^{-i(\omega_c+\Omega_{12})t} + (\Omega_{12} - \Delta_c)e^{-i(\omega_c-\Omega_{12})t}\right], \tag{1.31b}$$

and $\rho_{11} = 1 - \rho_{22}$ due to probability conservation. Here $\Omega_{12} = (4|G_{12}|^2 + \Delta_c^2)^{1/2}$ is called the generalized Rabi frequency. The result (1.31a) shows that for $\Delta_c = 0$ the probability oscillates with an angular frequency $2|G_{12}|$, thus the name Rabi *frequency*. As the detuning Δ_c is increased, the frequency of oscillation increases, but the amplitude decreases. The average induced dipole moment is given by

$$\langle\vec{d}\rangle = \mathrm{Tr}(\rho\vec{d}) = \vec{d}_{21}\rho_{12} + \text{c.c.}. \tag{1.32}$$

From (1.31b) it is clear that the dipole will oscillate at frequencies $\omega_c \pm \Omega_{12}$ apart from ω_c. Thus the fluorescence spectrum will have new frequency side-bands corresponding to $\omega_c \pm \Omega_{12}$. In the above analysis we have not taken spontaneous

decay, collisional decay, Doppler broadening [1] etc. into account. However, for a strong control field ($G_{12} \gg$ decays rates) the sidebands still appear at $\omega_c \pm \Omega_{12}$. The decays change the height and width of these emission bands.

Probe Absorption: Steady State Solution. The above driven two-level system can also be probed by scanning over the probe frequency ω_p and measuring the probe absorption. If the excited level decays only to the ground state then the system is referred as a *closed two-level system*, otherwise it is an *open system*. In the case of a closed system, due to the presence of decay, the Rabi oscillations will finally decay to a constant value. Thus a *steady state* solution is possible ($\dot{\rho} = 0$) with the condition $\mathrm{Tr}(\rho) = 1$. In the case of an open system, the total probability is not conserved. For a closed two-level system [e.g., the D_2 hyperfine sub-levels of Na: $|1\rangle = 3P_{3/2}(F = 3, M_F = +3)$ and $|2\rangle = 2S_{1/2}(F = 2, M_F = +2)$.] it was shown by Mollow [11] that the absorption and emission spectrum are asymmetric. He showed that the probe field gets amplified at $\omega_p = \omega_c - \Omega_{12}$ and absorbed at $\omega_p = \omega_c + \Omega_{12}$) when $\Delta_c > 0$. The reverse behaviors occur for $\Delta_c < 0$. Mollow's work led to a series of theoretical [12] and experimental [13] investigations. The gain observed is a result of *atomic coherence* term, ρ_{12}, and there is no population inversion among the levels $|1\rangle$ and $|2\rangle$. It has been demonstrated that this gain can show lasing action [14]. A physical understanding of these interesting behaviors are seen in the dressed atom picture developed by Cohen-Tannoudji and coworkers [15]. In the absorption spectra, a dispersive type feature appears around $\omega_p \approx \omega_c$, which is a kind of stimulated Rayleigh scattering. The physical origin of this feature is more involved [16] and the gain associated with this feature has been utilized for optical parametric oscillators [17].

The two-level atom interacting with a field (classical or quantized) is a generic model explaining a large number of quantum optical and nonlinear effects [18]. The resonance fluorescence from such a system was predicted to show squeezing [19] and was recently demonstrated [20]. Phase dependent features were shown to appear in the resonance fluorescence when a driven two-level atom is placed in a squeezed vacuum [21]. When a two-level atom is driven by strong bichromatic fields, the result is a more complicated Rabi splitting [22, 23]. The exact solutions for two-level atom interacting with a single mode quantized field was

[1] Doppler broadening is due to atoms moving with a velocity distribution. Details can be seen in Ref. [5], pg. 72.

provided by Jaynes and Cummings [24]. The Jaynes-Cummings model is known to exhibit non-classical effects like collapse and revival in a lossless medium [25]. Sanchez-Mondragon, Narozhuy, and Eberly [26] and Agarwal [27] have shown that a strong coupling of a single mode quantized field with a two-level atom gives rise to vacuum Rabi splitting which was verified by Thompson and coworkers [28].

1.2.2 Coherent Population Trapping

In comparison to the two-level systems, three-level systems interacting with two monochromatic fields have an enhanced atomic coherence effects. The development of monochromatic and tunable laser sources has produced a large variety of high-resolution spectroscopic investigations on three-level systems in different configurations. Among these *coherent population trapping* (CPT) has been extensively studied due to its immense applications. This phenomenon was first observed by Alzetta et al. [29] as decrease in fluorescence emission from Sodium atoms on application of two fields with certain frequency difference. Theoretical [30] and experimental [31] analysis showed that when two resonant laser fields acted on two coupled transitions, the atomic populations got trapped in certain states due to interference. Physically, the applied radiation creates an atomic coherence such that the atom's evolution is out of phase with the incoming radiation and no absorption takes place [32]. Coherence between quantum states is known to be important in quantum mechanics due to the superposition principle, but macroscopic effect of coherence like zero absorption, suppression of fluorescence etc. is unusual.

In the absence of spontaneous emission all the three laser configurations shown in Fig. 1.1 are equivalent. However, in practice, Λ system (Fig. 1.1(a)) is the most stable configuration. Here the population is trapped among the two ground states (which are metastable), and the atomic coherence among them has a large life time. A theory for Λ systems with two coherent fields of arbitrary strength was developed by Cohen-Tannoudji and Reynuad [33] using dressed state approach and by Agarwal and Jha [34] using master equation approach. Consider two laser fields of frequency ω_{c1} and ω_{c2} acting on transitions $|1\rangle \leftrightarrow |3\rangle$ and $|1\rangle \leftrightarrow |2\rangle$ of a Λ system, respectively. The Hamiltonian for this system will be:

$$H/\hbar = \omega_{13}A_{11} + \omega_{23}A_{22} - (G_{12}A_{12}\exp(-i\omega_{c2}t) + G_{13}A_{13}\exp(-i\omega_{c1}t) + \text{H.c}). \quad (1.33)$$

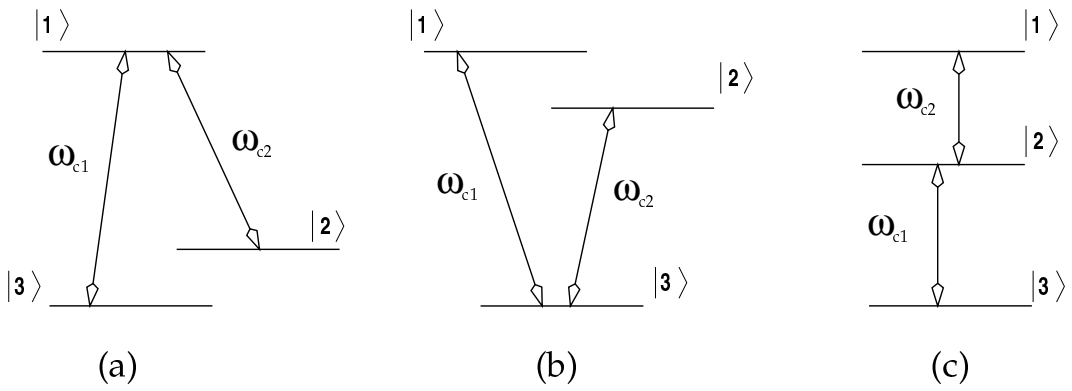

Figure 1.1: Figures show the three possible configurations in three-level system with two laser fields of frequency ω_{c1} and ω_{c2}. (a) Λ system. (b) V system (c) Ξ system. The laser field is coupling (dipole coupling) states of different parity.

Here $\hbar\omega_{lm}$ is the energy separation between the levels $|l\rangle$ and $|m\rangle$, the Rabi frequency for the transition $|l\rangle \leftrightarrow |m\rangle$ is denoted as $2G_{lm}$ and $A_{lm} = |l\rangle\langle m|$. Making a unitary transformation $|\phi\rangle = \exp\{i\omega_{c1}A_{11}t + i(\omega_{c1} - \omega_{c2})A_{22}t\}|\psi\rangle$ in the Schrödinger equation (1.15) the effective Hamiltonian is obtained as below.

$$H_{\text{eff}}/\hbar = \Delta_{1c}A_{11} + (\Delta_{1c} - \Delta_{2c})A_{22} - (G_{12}A_{12} + G_{13}A_{13} + \text{H.c.}), \tag{1.34}$$

where $\Delta_{1c} = \omega_{13} - \omega_{c1}$ and $\Delta_{2c} = \omega_{12} - \omega_{c2}$. In writing (1.34) the RWA has been made to remove the explicit time dependence. The corresponding equation for the density matrix ρ will be

$$\begin{aligned} \dot{\rho} = -\frac{i}{\hbar}[H_{\text{eff}}, \rho] \quad &- \quad \gamma_{13}(A_{11}\rho - 2A_{33}\rho_{11} + \rho A_{11}) \\ &- \quad \gamma_{12}(A_{11}\rho - 2A_{22}\rho_{11} + \rho A_{11}), \end{aligned} \tag{1.35}$$

where $2\gamma_{13}$ and $2\gamma_{12}$ are the radiative decay rates from $|1\rangle$ to $|3\rangle$ and $|2\rangle$, respectively. Here the decay terms are added by hand and a proper derivation of such terms will follow in section 1.3. The above Hamiltonian (1.34) will result in a 3×3 matrix which can be diagonalized. When $\Delta_{1c} = \Delta_{2c}$ one of the eigenvalues will be zero. The corresponding eigenstate is

$$|uc\rangle = \frac{G_{13}|2\rangle - G_{12}|3\rangle}{\Omega}, \qquad \text{where,} \qquad \Omega = \sqrt{G_{12}^2 + G_{13}^2}. \tag{1.36}$$

It implies that $H_{\text{eff}}|uc\rangle = 0$ (for $\Delta_{1c} = \Delta_{2c}$) and the electrons in the (dark) state $|uc\rangle$ are *uncoupled* from the applied field. If a basis $\{|1\rangle, |uc\rangle, |c\rangle\}$ is considered, where

$$|c\rangle = \frac{G_{12}|2\rangle + G_{13}|3\rangle}{\Omega}, \tag{1.37}$$

then using (1.35) it can be shown that for $\Delta_{1c} = \Delta_{2c} = 0$,

$$\dot{\rho}_{ucuc} = (\gamma_{13} + \gamma_{12})\rho_{11}, \tag{1.38a}$$

$$\dot{\rho}_{cc} = (\gamma_{13} + \gamma_{12})\rho_{11} + i\Omega\rho_{1c} - i\Omega\rho_{c1}. \tag{1.38b}$$

As seen from the above equations, the spontaneous emission from $|1\rangle$ populates the dark state. The external field *couples* the states $|c\rangle$ and $|1\rangle$ with an effective Rabi frequency Ω. Thus irrespective of the initial condition, under Raman resonance condition ($\Delta_{1c} = \Delta_{2c} = 0$), the steady state populations will be in the CPT state (or dark state).

However, in practice, creation of the CPT state is affected by finite laser linewidth, atomic collisions, Doppler broadening etc. When atomic motion is taken into account, the Raman resonance condition is given by

$$\Delta_{1v} - \Delta_{2v} = \Delta_{1c} - \Delta_{2c} - (\vec{k}_1 - \vec{k}_2) \cdot \vec{v},$$

where $\vec{v}$ is the velocity of the atom and $\vec{k}$'s are the propagation vectors for the two fields. Thus for a Λ system Doppler broadening can be reduced by using copropagating laser fields and $|\vec{k}_1| \approx |\vec{k}_2|$. Several authors have investigated the effect of Doppler broadening and relaxation processes on CPT [32]. Phase fluctuations of the laser fields are also known to affect the absorption and emission processes [35] and such fluctuations in the context of CPT have also been examined [36]. Further, it is difficult to find an ideal closed three-level system. The simplest atomic level configuration for CPT is $J = 1 \rightarrow J = 1$ kind of transitions with circularly polarized fields. More general level schemes have been discussed [37], and the basic requirement is odd number of total levels (≥ 3), with ground levels being one more than the excited levels. Agarwal has shown [38] that the quantized fields give rise to novel field properties under trapping conditions [38].

Various authors have investigated different aspects of CPT [39, 40, 41], and over the years important applications of CPT have been realized. Some of the early applications were in metrology [42], optical bistability [43] and laser cooling [44]. In molecules, population trapping effect has been used for adiabatic population transfer [45]. A recent work has shown generation of coherent microwave field in Cs vapor under CPT conditions [46]. Many recent phenomena like lasing without inversion, field induced transparency, pulse matching, enhanced nonlinear optical effects are closely related to CPT and a brief introduction to some of them follows.

1.2.3 Lasing Without Inversion

One of the most elaborately studied applications of atomic coherence effect is lasing without inversion (LWI). The main motivation for this study is to create coherent ("table-top") sources of short wavelengths, which will allow new regime of spectroscopic investigations and biological imaging (X-ray lasers). The underlying principle of LWI is to create asymmetry in absorption and emission processes. Though some early proposals were known to exist [47, 48], the concept got attention after the work of Kocharovskaya and Khanin [49] and Harris [50]. Ref. [49] found that ultra short pulses got amplified without inversion in a three-level Λ system due to CPT. Harris [50] discovered that decay from a discrete state to an identical continuum resulted in an interference in absorption, whereas the emission probability remained intact. This interference was of Fano-type [51] which arises due to several quantum mechanical paths for the same final continuum level. Imamoglu and Harris showed how similar interference can be generated using a control field [52]. Another interesting proposal by Scully and coworkers [53] showed that the Λ systems with coherent superposition of ground levels can give rise to LWI. Classically, the absorption from a coherent superposition of ground levels is like driving two dipoles. When they oscillate at 180^{o} out of phase, absorption will be absent. The situation is different if the atom begins life from excited state, where the phase of oscillation is governed by the applied field, which adds up the emission probability. Agarwal has shown [54] that lasers based on LWI may have interesting properties like ultra-narrow linewidths due to reduced spontaneous emission noise.

These proposals led to a series of theoretical [55, 56, 57, 58] and experimental activities [60, 61, 62, 63, 64, 65, 66]. In many of these proposals [49, 53], although there was no inversion in the bare basis, there did exist an inversion in the *dressed basis*. On the other hand, in some schemes [48, 50, 55, 56, 58] there was no inversion in any basis. Agarwal [59] showed that in such cases the gain arises due to coherence among dressed states.

The earliest experimental indication of gain without inversion (GWI) was in a four level model by Gao et al. [60]. Using coherent pulse along $3S_{1/2} \leftrightarrow 3P_{1/2}$ in Na they created atomic coherence among the ground hyperfine levels F = 1 and F = 2. They observed gain of a probe field along $3S_{1/2} \leftrightarrow 3P_{1/2}$. This work was based on the model proposed by Narducci et al. [57], but the experiment did not have any

concrete evidence that the gain was *in fact* without inversion. Nonetheless, the results did show atomic coherence effect. An unambiguous demonstration of GWI was given by Fry et al. [61] in a Λ system in Na. The gain they observed was due to population trapping and thus due to inversion in a dressed basis. Nottelmann et al. [62] demonstrated GWI in Samarium vapor. They used picosecond pulses to create population trapping among Zeeman sublevels. Transient GWI was shown by van der Veer et al. [63] in $^{112}\mathrm{Cd}$.

The first proof-in-principle of LWI was given by Zibrov et al. [64] in $^{87}\mathrm{Rb}$. This was the first experiment to use low power cw diode laser as control field, and they used D_1, D_2 lines of $^{87}\mathrm{Rb}$ in a V configuration. They applied control field along $|\mathrm{P}_{3/2}, \mathrm{F}=2\rangle \leftrightarrow |\mathrm{S}_{1/2}, \mathrm{F}=1\rangle$ transition and generated lasing action along $|\mathrm{P}_{1/2}, \mathrm{F}=2\rangle \leftrightarrow |\mathrm{S}_{1/2}, \mathrm{F}=1\rangle$. Another demonstration by Padmabandu et al. [65] used Na beams. They used a Λ-type configuration and their model was similar to the one proposed in Ref. [56]. The lasing action in both these cases can be understood in terms of coherence in the dressed basis [59].

1.2.4 Electromagnetically Induced Transparency

It is known in quantum mechanics that if several transition amplitudes exist for a process, then these transition amplitudes can interfere among themselves to give rise to either constructive or destructive interference. An example of such a process in atomic system is the well known Fano interference [51]. The principle of *electromagnetically induced transparency* (EIT) is to deliberately induce Fano type destructive interference in absorption via an external control field [52, 67]. As a result an initially opaque medium can be rendered *transparent* for a probe field.

Harris and coworkers were the first to demonstrate EIT in a Λ system in Strontium vapor [68]. As shown in Fig. 1.2(a), a control field at 570.3 nm was applied on the $|1\rangle(4\mathrm{d}5\mathrm{d}\,^1\mathrm{D}_2) \leftrightarrow |2\rangle(4\mathrm{d}5\mathrm{p}\,^1\mathrm{D}_2)$ transition. The probe transition $|1\rangle \leftrightarrow |3\rangle(5\mathrm{s}5\mathrm{p}\,^1\mathrm{P}_1)$, which was rendered transparent, had a wavelength 337.1 nm. The probe laser had an intensity 10^3 times less than the control laser, which is generally the situation for EIT studies. Thus from (1.36) the corresponding dark state will be the bare state $|3\rangle$. This is the major difference between EIT and CPT, though the physical basis for EIT is trapping. CPT is usually explained in terms of interference due to both the applied fields, while EIT is better understood in terms

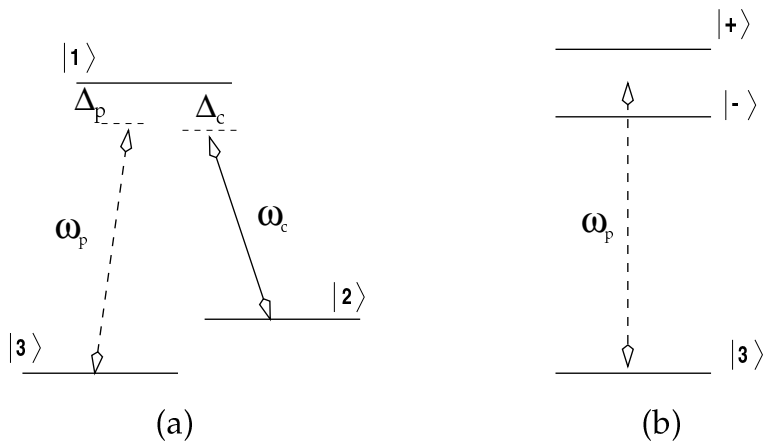

Figure 1.2: a) Schematic for EIT in the Λ systems. The control (probe) field frequency is denoted as ω_c (ω_p) and is detuned from resonance by an amount Δ_c (Δ_p). b) The dressed states created by the strong control field.

of interference among dressed states created by the control field. The control field when on resonance will produce states

$$|\pm\rangle = \frac{1}{\sqrt{2}}(|2\rangle \pm |1\rangle). \tag{1.39}$$

The probe absorption has transition amplitudes corresponding to the transitions $|\pm\rangle \leftrightarrow |3\rangle$, which interfere destructively when the Raman resonance condition is met. The $|\pm\rangle$ states give rise to new resonances in absorption and this effect is known as Autler-Townes splitting [69]. Though the transparency region lies at the center of these Autler-Townes components, it should not be confused as a result of new resonances. The Autler-Townes splitting occurs for control field Rabi frequencies much larger than the spontaneous emission rate, but EIT can, in principle, be observed even for small control fields [70]. Agarwal [71] has shown that the new resonances appear as *Lorentzian* contributions in the absorption profiles, whereas interference terms appear as *dispersive* terms.

Different groups have demonstrated EIT effects using various configurations [72, 73, 74, 75, 76], and a comparative study of these configurations (Λ, V and Ξ systems) were also carried out in different contexts [74]. EIT in laser-cooled samples has also been observed [75]. The concept of EIT has also been extended to observe transparency below the cut-off in an ideal plasma [77], and opening the bandgap in dielectric media [78].

Among the different applications of EIT, Kasapi [79] has shown that EIT can

be used for isotope discrimination. Laser pulse matching and soliton-like propagation, which have applications in optical communication, can be observed under EIT like situations [80]. EIT has also been shown to be useful as coherent switch [61], and electromagnetic field grating [81]. Agarwal and Harshawardhan [82] have generalized the idea of EIT to control two-photon processes, and based on a similar idea, Harris and Yamamoto [83] have proposed the idea of a photon switch.

Both radiative and non-radiative decay among trapping states ($|2\rangle$ and $|3\rangle$ in Fig. 1.2) can strongly affect EIT and CPT. This decay along with inhomogeneous broadening reduces the number of atoms in the trapped state. In atomic vapors, the *leak* from the trapped state can be minimized using strong control fields. (In Appendix A analytical results are derived which explains the effect of such decay terms on the EIT-spectra.) In solids, these incoherent processes are so strong that the observation of EIT in solid systems is limited to a few cases [84, 85]. Zhao et al. [84] demonstrated microwave induced changes in absorption in a Ruby sample cooled at liquid Helium temperature. The other experiments were done in Y_2SiO_5 crystal doped with Pr^{+3}.

1.2.5 Dispersion Management and Giant Nonlinear Optics

Ultra-High Refractive Index: In atomic vapors, near resonance, refractive index of the medium is very high, but at the same time absorption is also high. Using the idea of atomic coherence and quantum interference, Scully [86] has shown that it is possible to have spectral regions where absorption can be suppressed, whereas the refractive index can be kept intact. Such a medium has potential applications in optical microscopy, magnetometry, magneto-optical rotation etc. For example, in an optical microscope, its resolving power depends linearly on the refractive index of the medium. Kocharovskaya and coworkers [88] have shown that spontaneous emission can be drastically modified with a strong control field, if one of the dynamic Stark levels has energy below the ground state. This gives rise to spontaneous emission from ground state to the Stark shifted level, and as a result, they found large refractive index along with transparency. Recently, Zibrov et al. [89] gave an experimental demonstration of large refractive index with vanishing absorption in Rb vapor.

Magnetometry: Another application of refractive index modification is in mea-

suring extremely weak magnetic fields using EIT. In the transparency region in EIT spectrum, the dispersion increases linearly with probe frequency (*normal dispersion*) and the refractive index is close to unity. For a probe field (in Λ system) this linear region will correspond to a phase shift

$$\Delta\Phi \approx -\frac{3\lambda_p N L\gamma}{4\pi|G_{12}|^2}(\Delta_p - \Delta_c), \tag{1.40}$$

where N is the atomic density, L is the medium length, and γ is the population decay rate. This phase change can be measured by keeping such a medium in one arm of a Mach-Zehnder interferometer. Using this property of EIT, Scully and Fleischhauer [90] have shown that $(\Delta_p - \Delta_c)_{\min}$ of the order of $10^{-5}\mathrm{Hz}$ can be detected. Such precise measurement of frequency shifts have applications in frequency standard and magnetometry. Very small Zeeman splittings due to weak magnetic fields can be measured using this technique. They have shown that magnetic fields of the order of $10^{-12}\mathrm{G}$ can be measured, which otherwise will need large superconducting devices.

Slow Light: As already noted, normal dispersion occurs in the transparency window. The group velocity of a pulse in a dispersive media is given by

$$v_g = \frac{c}{n + \omega_p \partial n/\partial\omega_p}, \tag{1.41}$$

where the refractive index $n \approx 1 + 2\pi\mathrm{Re}\{\chi(\omega_p)\}$ for atomic vapors. In the transparency window $\chi \approx 0$, but $\mathrm{Re}(\partial\chi/\partial\omega_p)$ depends on the width of the transparency window. Thus for a sub-natural transparency window, steeper dispersion curve will be seen, and hence low group velocity. Attaining a sub-natural transparency window will require a weak control field. For weak control fields, in atomic vapors, (mainly) inelastic collisions with the walls and inhomogeneous broadening, if significant, can suppress EIT effects (for details see Appendix A). For a large control field intensity of $283\mathrm{kW/cm^2}$ in $^{208}\mathrm{Pb}$ vapor, Harris et al. [91] showed that a group velocity of c/250 can be observed in the EIT window. However, with recent development of experimental techniques, the above limitations are no more barriers. In a remarkable experiment Hau et al. [92] have shown in a Sodium condensate that group velocity of a probe field under EIT conditions can be as low as 17 m/s. They used a control field intensity as low as $1\mathrm{mW/cm^2}$. This was followed by experiments in hot gases [93] and at room temperature [94] where special techniques were used to suppress collisional effects. Budker et al. have

[94] reported a group velocity of 8 m/s in $^{85}\mathrm{Rb}$ vapor. The ground state relaxation in this experiment was as low as 1 Hz due to an anti-relaxation coating on the walls of the vapor cell. This coating suppresses the inelastic collisions with the walls of the cell.

Using the idea of slow light, Fleischhauer and Lukin [95] have shown that quantum light pulses can be decelerated and *trapped* in a medium. This will allow transfer of quantum correlations from light field to the collective atomic states [96]. The stored quantum states can be transfered back to light by reversing the storage process, and thus in principle can have applications is quantum information processing. They have also demonstrated a technique for this using cavity fields [95]. This phenomena will allow generation of atomic squeezed states, entanglement and teleportation of atomic states etc, which till date has been seen only for optical fields.

Polarization Control: Control field induced modification of refractive index has also been used for demonstrating electric field polarization rotation. Among two transitions which absorb left and right circularly polarized light, a control field can be applied to modify the refractive index of either of these two field polarizations. Thus the plane of polarization of a linearly polarized probe field can undergo rotation as shown by Wielandy and Gaeta [97]. Such an electromagnetically induced birefringence has also been observed in Thallium vapor [98], and can be used for studies of atomic parity violating effects. Combining the ideas of EIT and Faraday rotation, magneto-optical rotation can be enhanced [99].

Giant Nonlinear Optical Effects

Nonlinear optical techniques and devices are now extensively used to generate new wavelengths and to make possible new types of measurement. The nonlinear susceptibility near resonance in atomic vapors is very high, but at the same time dispersion and absorption is also very high. Tewari and Agarwal [100] had shown that by using a control field, VUV generation is a three-level system can be enhanced by orders of magnitude. They showed that the control field was modifying the *phase matching* conditions in four-wave-mixing process. Based on EIT principles, Harris et al. [101] have shown that EIT results in destructive interference in $\chi^{(1)}$, but constructive interference in $\chi^{(3)}$. The efficiency of a four-wave-mixing process critically depends on the ratio $|\chi^{(3)}|/\chi^{(1)}$, thus reduction of $\chi^{(1)}$ increases

the efficiency drastically. Both these proposals were closely related, and it was found that large efficiencies arise from the same mechanism [102].

The demonstration of constructive interference in nonlinear susceptibility was done in a series of experiments by Hakuta and coworkers [103, 104]. A resonantly enhanced second-harmonic generation accompanied with reduced absorption was achieved by coupling the 2s and 2p states of Hydrogen using a dc electric field [103]. This work has implicitly shown the possibility of EIT with a dc control field. Zhang et al. [104] demonstrated sum-frequency generation by applying a strong coupling laser on the 2s-3p transition. This coupling led to continuous growth of the 103 nm (VUV) radiation, without suffering resonant absorption and dispersion. Phase matching due to control field was observed in an off-resonance four-wave mixing scheme in $^{208}\mathrm{Pb}$ [105]. In this experiment $\Delta_c \approx 5\mathrm{GHz}$ was used and so transparency had little role in the enhancement. In the experiment by Jain et al. [106], due to CPT, the *phase coherent atoms* acted as a local oscillator that is involved in mixing with a third laser at 425 nm. This generated a new field at 293 nm with an exceptionally high conversion efficiency of about 40 %.

There is now considerable literature on nonlinear optics with atomic coherence. In addition to those discussed above, other examples include giant Kerr nonlinearity [107], efficient phase conjugation [108] and new types of nonlinear spectroscopy [109]. One recent discovery is the realization that, in media with ultra-slow group velocity [92, 93, 94], the nonlinear susceptibility is very high. In the experiment of Hau et al. [92], they found an effective nonlinear refractive index $\approx 0.18\mathrm{cm/W}^{-1}$, which is a *million* times greater than the one found in usual cold atoms. This happens because, due to slow group velocity an externally long pulse *shrinks* in the medium with a very high energy density. Such a high nonlinear cross-section can be used for nonlinear processes at extremely low light-levels (few photons per atomic cross section or equivalently at $\mathrm{nJ/cm}^2$) [110]. Recently, mirrorless parametric self-oscillation under conditions of slow group velocity has been observed [111].

1.3 Vacuum Induced Atomic Coherence

Most of the experiments discussed above had atomic coherence created by an external coherent field. However, it is also known for sometime that coherence can

also be created by *environmental* effects. For example, the vacuum (zero-point) fluctuations of electromagnetic fields, which gives rise to spontaneous emission, is also known to give rise to atomic coherence. Agarwal [112] showed that if two degenerate levels are coupled to a common ground level (V system) via same mode of vacuum field, spontaneous emission from such levels can be partially suppressed. In fact this result, in principle, shows the possibility of population trapping among excited levels. The coherence thus created among the excited levels is termed as *vacuum induced coherence* (VIC). Unlike a coherent field, vacuum field has infinite modes present, with very small correlation time, and coherence via vacuum field seems to be counter-intuitive. Conceptually, this coherence is generated because two probability amplitudes interfere due to two energy levels coupled to the same mode of electromagnetic field. The effect of such coherence terms can be conveniently handled using master equation treatment for spontaneous emission [7].

1.3.1 Master Equation Techniques

Master equation technique is useful in extracting the effect of an environment on a sub-system. Take for example the effects of random fluctuating radiation field (reservoir) on a collection of atoms. The density operator for the statistical states of such a system can be denoted as ρ_{A+R}, where A stands for atomic variables and R for reservoir variables. The Liouville equation in the Schrödinger picture can be written as below.

$$\frac{\partial \rho_{A+R}(t)}{\partial t} = -\frac{i}{\hbar}[H, \rho_{A+R}(t)] = -i\mathfrak{L}\rho_{A+R}(t), \tag{1.42}$$

where $\mathfrak{L} = (1/\hbar)[H, \ldots]$ is the commutation operator often called Liouville operator. In this total system $A + R$, in practice one is interested either on atomic variables A or the effect of atoms on reservoir R. Thus we consider a (time independent) projection operator $\mathfrak{p}$ such that $\mathfrak{p}^2 = \mathfrak{p}$, and it will project the *relevant* part $\mathfrak{p}\rho_{A+R}$ from ρ_{A+R}. The interest here is to find the effect of vacuum fluctuations on atomic variables. Thus we can select $\mathfrak{p} = \rho_R(0)\mathrm{Tr_R}$, and the *reduced* density operator will be $\rho_A(t) = \mathrm{Tr_R}\{\rho_{A+R}(t)\}$. The density operator for the system in terms of $\mathfrak{p}$ can be written as

$$\rho_{A+R}(t) = \mathfrak{p}\rho_{A+R} + (1 - \mathfrak{p})\rho_{A+R}, \tag{1.43}$$

where the second term on the right hand side is the unimportant term for the present problem. If one is interested in the statistical properties of the emitted radiation then the second term becomes *relevant*. Transforming (1.42) in interaction picture, $\mathfrak{L}(t)$ will become time dependent, and multiplying $\mathfrak{p}$ and $(1-\mathfrak{p})$ from left in (1.42), we get,

$$\mathfrak{p}\frac{\partial \rho_{A+R}}{\partial t} = -i\mathfrak{p}\mathfrak{L}(t)\mathfrak{p}\rho_{A+R}(t) - i\mathfrak{p}\mathfrak{L}(t)(1-\mathfrak{p})\rho_{A+R}(t), \tag{1.44a}$$

$$(1-\mathfrak{p})\frac{\partial \rho_{A+R}}{\partial t} = -i(1-\mathfrak{p})\mathfrak{L}(t)\mathfrak{p}\rho_{A+R}(t) - i(1-\mathfrak{p})\mathfrak{L}(t)(1-\mathfrak{p})\rho_{A+R}(t). \tag{1.44b}$$

At $t = 0$ the initial state will be $\rho_{A+R}(0) = \rho_A(0)\rho_R(0)$ where $\rho_R(0) = |\{0\}\rangle\langle\{0\}|$ is the vacuum state of field. Formally integrating (1.44b) and substituting in (1.44a) and on setting

$$\exp\left[-i(1-\mathfrak{p})\int_0^\tau \mathfrak{L}(t')dt'\right] \equiv U(\tau),$$

the result will be

$$\frac{\partial \mathfrak{p}\rho_{A+R}}{\partial t} = -i\mathfrak{p}\mathfrak{L}(t)\int_0^t U(\tau)\mathfrak{L}(t-\tau)\mathfrak{p}\rho_{A+R}(t-\tau)d\tau. \tag{1.45}$$

In writing (1.45), we have used $(1-\mathfrak{p})\rho_{A+R}(0) = 0$ and moreover since $\mathfrak{L}(t)$ is linear in a_{ks} and $a_{ks}^\dagger$, annihilation and creation operators for vacuum field, $\mathfrak{p}\mathfrak{L}(t)\mathfrak{p} = 0$. The lowest order approximation (Born approximation) is obtained by taking $U(\tau) \to 1$. This limit holds good for spontaneous emission treatment, because coupling of vacuum field with atomic transition is generally weak, unless atoms are in some high Q cavity. Thus we obtain

$$\frac{\partial \mathfrak{p}\rho_{A+R}}{\partial t} = -i\mathfrak{p}\mathfrak{L}(t)\int_0^t \mathfrak{L}(t-\tau)\mathfrak{p}\rho_{A+R}(t-\tau)d\tau. \tag{1.46}$$

Note that $\rho_A(t)$ at any time t depends on all its previous times. For a reservoir like vacuum field which has a very short correlation time, Markoff or short memory approximation holds good. This would imply replacing $\rho_A(t-\tau) \approx \rho_A(t)$ inside the integral in (1.46). Equation (1.46) is a simplified form of *Zwanzig's master equation* [7]. In the subsection below, an explicit form of the master equation for the V and Λ systems is derived. Conditions under which VIC can be observed, is also discussed.

1.3.2 Vacuum Induced Coherence in V and Λ systems

In V Systems : Consider N identical, noninteracting V type atoms in a bath of vacuum field. The excited states $|1\rangle$ and $|2\rangle$ decay to a common ground state $|3\rangle$.

The Hamiltonian for this system in dipole approximation will be

$$\begin{aligned} H &= \hbar\omega_{13}A_{11} + \hbar\omega_{23}A_{22} + \sum_{ks}\hbar\omega_{ks}a_{ks}^{\dagger}a_{ks} \\ &\quad -(\vec{d}_{13}A_{13} + \vec{d}_{23}A_{23} + \text{H.c.})\cdot\vec{E}(\vec{r}). \end{aligned} \tag{1.47}$$

Here $A_{lm} = |l\rangle\langle m|$ and the energy between states $|l\rangle$ and $|m\rangle$ is denoted as $\hbar\omega_{lm}$. The vacuum state em field operator in a quantization volume L^3 is given by

$$\vec{E}(\vec{r}) = i\sum_{ks}\left(\frac{2\pi ck}{L^3}\right)^{1/2}\hat{\epsilon}_{ks}a_{ks}e^{i\vec{k}\cdot\vec{r}} + \text{H.c.}, \tag{1.48}$$

where a_{ks} ($a_{ks}^{\dagger}$) is the field annihilation (creation) operator for the mode k with polarization index s. The field polarization is denoted as $\hat{\epsilon}_{ks}$. The Hamiltonian (1.47) in the interaction picture and RWA will be

$$H_{\text{eff}}/\hbar = -\sum_{ks}[(g_{ks}A_{13}e^{i\omega_{13}t} + f_{ks}A_{23}e^{i\omega_{23}t})a_{ks}e^{-i\omega_k t} + \text{H.c.}], \tag{1.49}$$

where we write,

$$g_{ks} = i\left(\frac{2\pi ck}{L^3}\right)^{1/2}\vec{d}_{13}\cdot\hat{\epsilon}_{ks}e^{i\vec{k}\cdot\vec{r}}, \qquad f_{ks} = i\left(\frac{2\pi ck}{L^3}\right)^{1/2}\vec{d}_{23}\cdot\hat{\epsilon}_{ks}e^{i\vec{k}\cdot\vec{r}}.$$

Substituting (1.49) in the master equation (1.46) and considering the fact that

$$\begin{aligned} \text{Tr}_{\text{R}}\{\rho_R(0)a_{ks}a_{k's'}^{\dagger}\} &= \delta_{ksk's'}, \\ \text{Tr}_{\text{R}}\{\rho_R(0)a_{ks}^{\dagger}a_{k's'}\} = \text{Tr}_{\text{R}}\{\rho_R(0)a_{ks}^{\dagger}a_{k's'}^{\dagger}\} &= \text{Tr}_{\text{R}}\{\rho_R(0)a_{ks}a_{k's'}\} = 0, \end{aligned}$$

the following master equation is obtained

$$\begin{aligned} \frac{\partial\rho}{\partial t} &= -\Gamma_{13}^{c}[A_{11}\rho - A_{33}\rho_{11}] - \Gamma_{23}^{c}[A_{22}\rho - A_{33}\rho_{22}] \\ -\Gamma_{23}^{c}d_r\cos\theta[A_{12}\rho - A_{33}\rho_{21}]e^{i\omega_{12}t} &- \frac{\Gamma_{13}^{c}\cos\theta}{d_r}[A_{21}\rho - A_{33}\rho_{12}]e^{-i\omega_{12}t} + \text{H.c}, \end{aligned} \tag{1.50}$$

where $\Gamma_{l3}^{c} = \gamma_{l3} + i\Omega_{l3}$ $(l = 1, 2)$. In deriving (1.50), Markoff approximation and long time limit were taken [7], and the relation

$$\int_0^{\infty} e^{i(\omega_{lm}-\omega_{ks})t}dt = \pi\delta(\omega_{lm} - \omega_{ks}) + i\text{P}\left(\frac{1}{\omega_{lm} - \omega_{ks}}\right),$$

was used. In (1.50) $d_r = |\vec{d}_{13}|/|\vec{d}_{23}|$, θ is the angle between the two dipole matrix elements $\vec{d}_{13}$, $\vec{d}_{23}$ and

$$\gamma_{l3} = \frac{2|\vec{d}_{l3}|^2\omega_{l3}^3}{3\hbar c^3}, \tag{1.51}$$

$$\Omega_{l3} = -\frac{2|\vec{d}_{l3}|^2}{3\pi\hbar c^3}\int_0^{\infty}\frac{\omega^3}{\omega - \omega_{l3}}d\omega \tag{1.52}$$

The master equation (1.50) is more general than the usual perturbative calculations, where the $\cos\theta$ terms are absent. In the absence of such terms, $2\gamma_{l3}$ are the Einstein A-coefficients and Ω_{l3} are the energy shift terms connected with Lamb shift calculations. The energy shift terms are generally absorbed in the unperturbed Hamiltonian via renormalization procedures [7]. Cardimona and Stroud [113] have shown that the explicit mention of even the *generalized* energy shift terms in (1.50) can be removed in an 'atom+vacuum field' dressed state basis, and in physical terms they affect the ratio of spectral intensities from the two excited levels. However, we will report new effects that arise due to interfering decay terms. Assuming that appropriate renormalization has been carried out, we avoid explicit mention of Ω_{l3} terms. For near-degenerate excited levels, $\omega_{13}/\omega_{23} \approx 1$ and the master equation (1.50) will be

$$\frac{\partial\rho}{\partial t} = -\gamma_{13}[A_{11}\rho - A_{33}\rho_{11}] - \gamma_{23}[A_{22}\rho - A_{33}\rho_{22}]$$
$$-\sqrt{\gamma_{13}\gamma_{23}}\cos\theta[A_{12}\rho - A_{33}\rho_{21}]e^{i\omega_{12}t} - \sqrt{\gamma_{13}\gamma_{23}}\cos\theta[A_{21}\rho - A_{33}\rho_{12}]e^{-i\omega_{12}t} + \text{H.c.}, \quad (1.53)$$

In terms of its various matrix elements, ρ will be

$$\dot{\rho}_{11} = -2\gamma_{13}\rho_{11} - \sqrt{\gamma_{13}\gamma_{23}}\cos\theta(\rho_{12}e^{-i\omega_{12}t} + \rho_{21}e^{i\omega_{12}t}), \quad (1.54a)$$

$$\dot{\rho}_{22} = -2\gamma_{23}\rho_{22} - \sqrt{\gamma_{13}\gamma_{23}}\cos\theta(\rho_{12}e^{-i\omega_{12}t} + \rho_{21}e^{i\omega_{12}t}), \quad (1.54b)$$

$$\dot{\rho}_{12} = -(\gamma_{13} + \gamma_{23} + i\omega_{12})\rho_{12} - \sqrt{\gamma_{13}\gamma_{23}}\cos\theta(\rho_{11} + \rho_{22})e^{i\omega_{12}t}, \quad (1.54c)$$

$$\dot{\rho}_{23} = -\gamma_{23}\rho_{23} - \sqrt{\gamma_{13}\gamma_{23}}\cos\theta\rho_{13}e^{-i\omega_{12}t}, \quad (1.54d)$$

$$\dot{\rho}_{13} = -\gamma_{13}\rho_{13} - \sqrt{\gamma_{13}\gamma_{23}}\cos\theta\rho_{23}e^{i\omega_{12}t}. \quad (1.54e)$$

Here $2\gamma_{13}$ and $2\gamma_{23}$ denote the spontaneous emission rates from $|1\rangle$ and $|2\rangle$ respectively. The $\cos\theta$ terms which couple the diagonal elements with the off-diagonal elements are the interference terms. They are important when $\omega_{12} \approx \sqrt{\gamma_{13}\gamma_{23}}$, and when the dipole matrix elements are nearly parallel. When ω_{12} is large, the rapid oscillation in the off-diagonal elements in (1.54) will average out the interference effect. Neglecting interference terms in such a situation is often called *secular approximation*.

When non-secular terms are important, coupling of off-diagonal terms will give rise to evolution of ρ_{12} even when $\rho_{12}(0) = 0$. Intuitively, this happens because spontaneous emission from one state can couple with the neighboring transition and vice-versa. This coherence is thus termed as vacuum induced coherence or VIC. As noted earlier, Agarwal [112] has shown that this coherence can give rise to

partial trapping in the degenerate V systems. For the non-degenerate V systems, Cardimona et al. [114] showed that probe absorption at certain frequencies can go to zero due to VIC. It was also shown [115] that the emission spectrum in the presence of VIC is drastically modified in V systems.

In recent times, interest in this kind of coherence has been rejuvenated because atomic coherence can be created without the use of a coherent field. It is now known that VIC can give rise to LWI [116] and quantum beats [117]. Scully, Zhu and coworkers [118] showed the possibility of population trapping among excited levels in a four-level model. They considered coupling of two non-degenerate vacuum coupled excited levels with an auxiliary metastable level via laser field. They showed that an entire spectral component from the emission spectrum disappeared as a result of this trapping, and thus possibility of quenching spontaneous emission noise was realized. Subsequently, Xia et al. [119] experimentally demonstrated quenching of spontaneous emission is Sodium dimers. Zhou and Swain showed the existence of ultra-narrow resonances [120] and GWI [121] due to VIC. Such a narrowing was also observed in four-level models, and Keitel [122] has studied the effect of incoherent pumping on sub-natural resonances. Paspalakis, Knight and coworkers have shown the possibility of phase control of spontaneous emission [123] and undistorted pulse propagation [124] via VIC. A recent work by Savchenko et al. [125] studies the effect of VIC on thermal photons and thermodynamic equilibrium. The effect of VIC on thermodynamic equilibrium will be discussed later at length in Chapter. IV.

In Λ Systems : In the Λ systems, the decay is from an excited level $|1\rangle$ to the ground levels $|2\rangle$ and $|3\rangle$. The Hamiltonian for this system can be written as below.

$$\begin{aligned} H &= \hbar\omega_{13}A_{11} + \hbar\omega_{23}A_{22} + \sum_{ks}\hbar\omega_{ks}a_{ks}^{\dagger}a_{ks} \\ &\quad -(\vec{d}_{13}A_{13} + \vec{d}_{12}A_{12} + \text{H.c.})\cdot\vec{E}(\vec{r}). \end{aligned} \tag{1.55}$$

The electric field is as given in (1.48) and all the notations are as defined previously. In the interaction picture (1.55) can be written as

$$H_{\text{eff}}/\hbar = -\sum_{ks}[(g_{ks}A_{13}e^{i\omega_{13}t} + f_{ks}A_{12}e^{i\omega_{12}t})a_{ks}e^{-i\omega_k t} + \text{H.c.}], \tag{1.56}$$

where now the coupling constants will be,

$$g_{ks} = i\left(\frac{2\pi ck}{L^3}\right)^{1/2} \vec{d}_{13}\cdot\hat{\epsilon}_{ks}e^{i\vec{k}\cdot\vec{r}}, \qquad f_{ks} = i\left(\frac{2\pi ck}{L^3}\right)^{1/2} \vec{d}_{12}\cdot\hat{\epsilon}_{ks}e^{i\vec{k}\cdot\vec{r}}.$$

Using the master equation (1.46) and the procedure discussed above, the following master equation in the interaction picture is obtained:

$$\begin{aligned}\frac{\partial\rho}{\partial t} = &-\gamma_{13}[A_{11}\rho - A_{33}\rho_{11}] - \gamma_{12}[A_{11}\rho - A_{22}\rho_{11}] \\ &+2\cos\theta\sqrt{\gamma_{13}\gamma_{12}}A_{32}\rho_{11}e^{-i\omega_{23}t} + \text{H.c.}\end{aligned} \tag{1.57}$$

Here $2\gamma_{13}$ and $2\gamma_{12}$ are the spontaneous emission rates from the state $|1\rangle$ to the states $|3\rangle$ and $|2\rangle$, respectively. The vacuum coupling affects the coherence between the two ground levels as shown below.

$$\dot{\rho}_{23} = 2\cos\theta\sqrt{\gamma_{13}\gamma_{12}}\rho_{11}e^{i\omega_{23}t}. \tag{1.58}$$

Very few studies on effects of VIC in the Λ systems have been reported [126, 127]. Chapter V and VI of this thesis will discuss in detail the effects of VIC in a Λ system.

1.4 Outline of the Thesis

Different chapters in the thesis develop the framework and models for vacuum field and laser field induced coherences in systems with near-degenerate levels. We predict many new effects arising from different types of coherences. We also discuss connection to some of the current experiments. The motivation and important results reported in various chapters are briefly outlined below.

Chapter II : When a strong field couples *both* the arms of a Λ system, Raman and Rayleigh kind of features appear in the absorption and emission spectra. However, when the control field Rabi frequency is of the order of separation between the two ground levels, the usual perturbation theory breaks down [128]. In this domain, interference between Raman and Rayleigh processes takes place. Further, in usual studies dealing with LWI and EIT both the pump and the probe act on different transitions of a Λ system.

In this chapter we analyze the probe response of strongly driven Λ systems with arbitrary spacing between the two ground levels. We consider a very general

situation where the pump and the probe fields couple with both the arms of a Λ system (cross talk) [129]. In the presence of cross talk, new coherence effects like LWI, polarization dependent response, modified dispersive properties are seen. We use density matrix approach [34], and interpret results in terms of dressed states [128]. We report strong anomalous dispersion between two closely spaced gain peaks. Such a region of dispersion can be used for observing *superluminal* (velocity greater than c) propagation, which was recently demonstrated by Wang et al. [130] for an optical pulse.

Chapter III : Autler-Townes splitting occurs in a V system when a strong control field drives one transition and it is probed along the other transition. It is a well known effect in laser spectroscopy, and has been observed in both solids and gases. However, the effect of VIC on the Autler-Townes splitting has remained unexplored.

In this chapter we study the effect of VIC on the well-known Autler-Townes doublet in the V systems. We demonstrate that VIC in a V system *can produce gain at frequencies where otherwise absorption would occur* [131]. We consider the usual situation where the control (strong field) and the probe beams couple to the different transitions of a V system. We show that in the presence of strong driving, VIC effects can be important even when the separation between the excited levels is greater than their natural linewidth. This removes one of the *hurdles* of observing the VIC effect with extremely closely spaced levels. We also show the parameter regime where one of the absorption peaks can be suppressed or where both the Autler-Townes resonances can produce gain. We introduce the concept of quasi-trapped-states (QTS) to explain the above results.

Chapter IV : In the presence of thermodynamic equilibrium, one would not expect any coherences in the system as the density matrix has the form $\exp[-\beta H]$ which is clearly diagonal in a basis in which the Hamiltonian H is diagonal. A fully quantized treatment, as shown in section 1.3, leads to coherence terms in equations of populations if the levels are near-degenerate. Clearly, one needs to demonstrate that such dynamical equations lead to a steady state consistent with the thermodynamic equilibrium.

In this chapter, we address a fundamental question of compatibility of thermodynamic principles with VIC [132]. We consider a V system with VIC among

the two excited levels. We show that though the system may evolve in a different way in the presence of such coherences, the steady state populations are given in accordance with the Boltzmann distribution. Further, we discuss cases where steady state solution can be at variance with thermodynamic equilibrium. We also give an example of pumping with a broadband field where different steady states are possible. We show that the observational effect of coherences arise in the emission spectrum.

Chapter V : Unlike a V system, where VIC affects the emission spectrum, in a Λ system the effect is more subtle. Thus the question of detection of VIC in a Λ system arises. Further, the origin of VIC and its consequence on entropy in a Λ system has also remained unexplored.

We address these questions in this chapter. We show that VIC results in oscillation of coherence among the two ground levels in a Λ system. A weak probe field can pick-up such an oscillation. We propose a four-level model to monitor VIC [133]. Spontaneous emission from an excited level generates coherence among the ground levels, and a probe absorption to a new excited level is measured. Numerical results show that the probe absorption will be modulated due to VIC. We also present analytical results in support of the numerical results.

Chapter VI : As discussed earlier the coherent population trapping (CPT) in Λ systems has led to immense development in the field of light-matter interaction. This phenomenon has been the basis for some recent experiments on laser cooling, enhancement of nonlinear signals, lasing without inversion etc. However, if the two lower levels of the Λ system are nearly degenerate then we must generalize the theory by inclusion of the effects of VIC.

In this chapter we report the effects of VIC on CPT and EIT in a Λ system. We consider two fields under a situation analogous to the usual studies on CPT [134]. Our results show a scheme to keep coherent population trapping intact even in the presence of VIC. However, VIC results in changes in the time scales associated with the formation of the CPT state, and brings in quantitative changes in the line profiles. We explain these results in terms of the *uncoupled* and *coupled* states. We also report the dependence of the line shapes on the relative phase between the two applied fields.

Chapter 2

Gain From Cross Talk Among Optical Transitions

In usual studies on LWI and EIT, one considers the interaction of a strong coherent drive and a weak probe field with different transitions of a system, i.e., control and probe (cw) fields act on different transitions. There are however situations where one has to relax the above assumption, particularly when the control field is intense. Consider for example the hyperfine levels of $^{39}\mathrm{K}$, the excited level $4\mathrm{P}_{1/2}(\mathrm{F}=1)$ and the two ground levels $4\mathrm{S}_{1/2}(\mathrm{F}=2)$ and $4\mathrm{S}_{1/2}(\mathrm{F}=1)$, where the ground level splitting is of the order of 462 MHz. In solid states systems like $\mathrm{Pr}^{+3}:\mathrm{Y}_2\mathrm{SiO}_5$, ground level separation as low as 17 MHz is known to exist [84]. In such cases, a strong control field can couple with more than one transition and gives rise to several interesting phenomena. We report the possibility of LWI. We also find that such a system can lead to superluminal propagation in certain frequency regions.

In what follows, we consider the Λ systems driven by a strong control field which couples both the transitions. Cohen-Tannoudji and Reynaud [128] have calculated the fluorescence spectrum for such a system. They studied various perturbative limits and showed that for a strong control field new Raman and Rayleigh features appear in the emission spectrum. However, these perturbative treatments fail when the control field Rabi frequency is of the order of separation between the two ground levels. In this regime, the Raman and Rayleigh components interfere, and we show that atomic coherence effects become inevitable. With recent experimental and theoretical studies on atomic coherence effects in the Λ systems, a proper theoretical and numerical study in this regime has be-

come imperative. The emphasis of this chapter is on new coherence effects generated in this regime, when probed through a weak field. We refer to the cross coupling of control and probe fields on different transitions as *cross talk*.

2.1 Model System

Consider a Λ system with one excited state, $|1\rangle$ and two ground levels, $|2\rangle$ and $|3\rangle$ (see Fig. 2.1) with arbitrary spacing $\hbar\omega_{23}$ between them. Such a configuration of levels with two fields is well studied by assuming that a given field is driving *only one transition*. This can be achieved either by selecting levels with large spacing $\hbar\omega_{23}$ or by suitable arrangement of field polarization. However, in this particular case we allow the same field to act on both the transitions, i.e. to say, the control

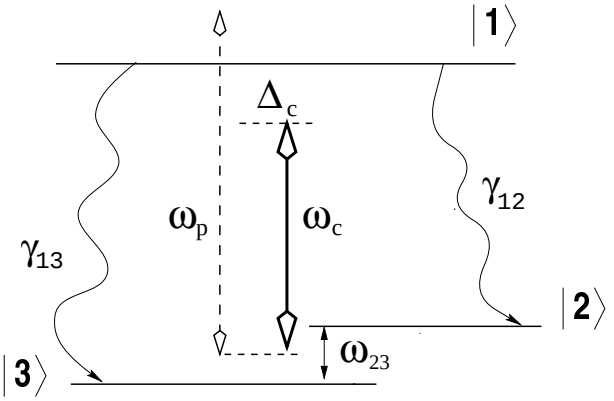

Figure 2.1: Schematic diagram of a three-level Λ system with arbitrary spacing $\hbar\omega_{23}$ between the two ground levels. The control (coupling strengths G_{13} and G_{12}) and probe fields (coupling strengths g_{13} and g_{12}) act on both the transitions.

field, $\vec{E}_c = \vec{E}_{c0}e^{-i\omega_c t} + \text{c.c.}$, which is driving $|1\rangle \leftrightarrow |2\rangle$ transition (Rabi frequency, $2G_{12} = 2\vec{E}_{c0}\cdot\vec{d}_{12}/\hbar$), can also couples with $|1\rangle \leftrightarrow |3\rangle$ transition (Rabi frequency, $2G_{13} = 2\vec{E}_{c0}\cdot\vec{d}_{13}/\hbar$). Similarly, the weak probe field, $\vec{E}_p = \vec{E}_{p0}e^{-i\omega_p t} + \text{c.c.}$, applied on $|1\rangle \leftrightarrow |3\rangle$ transition (Rabi frequency, $2g_{13} = 2\vec{E}_{p0}\cdot\vec{d}_{13}/\hbar$) can also drive $|1\rangle \leftrightarrow |2\rangle$ transition (Rabi frequency, $2g_{12} = 2\vec{E}_{p0}\cdot\vec{d}_{12}/\hbar$). Here $\vec{d}_{lm}$ is the electric transition dipole moment between the states $|l\rangle$ and $|m\rangle$. The Hamiltonian, H for this system in the dipole approximation is

$$\begin{aligned} H &= \hbar\omega_{13}A_{11} + \hbar\omega_{23}A_{22} \\ &\quad -(\vec{d}_{12}A_{12} + \vec{d}_{13}A_{13} + \text{H.c.})\cdot(\vec{E}_{c0}e^{-i\omega_c t} + \vec{E}_{p0}e^{-i\omega_p t} + \text{c.c.}), \end{aligned} \tag{2.1}$$

where $\hbar\omega_{lm}$ is the energy difference between the states $|l\rangle$ and $|m\rangle$. Here the fields are treated classically, and $A_{lm} = |l\rangle\langle m|$ are the atomic operators. The state $|\psi\rangle$ of this system is the solution of the Schrödinger equation (1.15). Under a unitary transformation, $|\phi\rangle = e^{i\omega_c A_{11} t}|\psi\rangle$, the Schrödinger equation for $|\phi\rangle$ will have the effective Hamiltonian, $H_{\rm eff} = -\hbar\omega_c A_{11} + e^{i\omega_c A_{11} t} H e^{-i\omega_c A_{11} t}$, which can be further written as

$$\begin{aligned} H_{\rm eff}/\hbar &= (\Delta_c + \omega_{23}/2)A_{11} + \omega_{23}A_{22} \\ &\quad -(G_{12} + g_{12}e^{-i\delta t})A_{12} - (G_{13} + g_{13}e^{-i\delta t})A_{13} + \text{H.c.}, \end{aligned} \tag{2.2}$$

where $\Delta_c = (\omega_{13}+\omega_{12})/2 - \omega_c$ is the control field detuning with respect to the center of the two ground levels and $\delta = \omega_p - \omega_c$. In writing (2.2), we have made RWA to neglect rapidly oscillating terms. The density matrix equations for (2.2) will be

$$\dot\rho_{11} = -2(\gamma_{13}+\gamma_{12})\rho_{11} + i(G_{13} + g_{13}e^{-i\delta t})\rho_{31} + i(G_{12} + g_{12}e^{-i\delta t})\rho_{21} - i(G_{12}^* + g_{12}^* e^{i\delta t})\rho_{12} - i(G_{13}^* + g_{13}^* e^{i\delta t})\rho_{13}, \tag{2.3a}$$

$$\dot\rho_{22} = 2\gamma_{12}\rho_{11} + i(G_{12}^* + g_{12}^* e^{i\delta t})\rho_{12} - i(G_{12} + g_{12}e^{-i\delta t})\rho_{21}, \tag{2.3b}$$

$$\dot\rho_{12} = -\{\gamma_{13}+\gamma_{12} + i(\Delta_c - \omega_{23}/2)\}\rho_{12} + i(G_{13} + g_{13}e^{-i\delta t})\rho_{32} - i(G_{12} + g_{12}e^{-i\delta t})(\rho_{11} - \rho_{22}), \tag{2.3c}$$

$$\dot\rho_{13} = -\{\gamma_{13}+\gamma_{12} + i(\Delta_c + \omega_{23}/2)\}\rho_{13} + i(G_{12} + g_{12}e^{-i\delta t})\rho_{23} - i(G_{13} + g_{13}e^{-i\delta t})(2\rho_{11} + \rho_{22} - 1), \tag{2.3d}$$

$$\dot\rho_{23} = -i\omega_{23}\rho_{23} + i(G_{12}^* + g_{12}^* e^{i\delta t})\rho_{13} - i(G_{13} + g_{13}e^{-i\delta t})\rho_{21}, \tag{2.3e}$$

where γ's are the spontaneous emission rates. Note that the density matrix elements in the original frame are given by $\rho_{12}e^{-i\omega_c t}$, $\rho_{13}e^{-i\omega_c t}$, ρ_{23}, ρ_{11}, ρ_{22} and ρ_{33}.

The above model in the absence of probe field can be connected with the well known Raman and Rayleigh lines in the fluorescence spectrum when $G_{1j} < \gamma_{1j} \ll \omega_{23}$, $(j = 2, 3)$. Cohen-Tannoudji and Reynaud [128] have studied the perturbative limits when $\omega_{23} \gg G_{1j} \gg \gamma_{1j}$ and $G_{1j} \gg \gamma_{1j} \gg \omega_{23}$. They noted the mixing of Raman and Rayleigh lines in the latter case. Our interest lies in the case when $\omega_{23} \approx G_{1j} \gg \gamma_{1j}$. Such a situation can be realized in the D_1 lines of ^{39}K or ^{85}Rb using a Ti:sapphire laser of intensity around 200-250 W/cm^2. Other possibilities will include Zeeman levels in the presence of magnetic field and linearly polarized electromagnetic fields. Expanding the solutions of equations (2.3) in terms of the

harmonics of δ,

$$\rho_{lm} = \sum_{\mathrm{n}} \rho_{lm}^{(\mathrm{n})} e^{-i\mathrm{n}\delta t}, \tag{2.4}$$

the set of equations for $\rho_{lm}^{(\mathrm{n})}$ can be solved for the steady state. Since the probe field is assumed to be weak enough ($G_{1j} \gg \gamma_{1j} \gg g_{1j}$), a perturbative solution up to $\mathrm{n} = 0, \pm 1$ will suffice. However, note that G_{1j} and ω_{23} are treated up to all orders. The probe field absorption $\mathcal{A}$ per unit volume due to the average induced polarization $\vec{P}$ is known to be [6]

$$\mathcal{A} = \overline{\vec{E}_p \cdot \frac{\partial \vec{P}}{\partial t}}, \tag{2.5}$$

where bar denotes the time average. The average polarization for N atoms per unit volume is

$$\vec{P} = N\{\vec{d}_{21}\rho_{12}e^{-i\omega_c t} + \vec{d}_{31}\rho_{13}e^{-i\omega_c t} + \text{c.c.}\}. \tag{2.6}$$

Here ρ_{lm}'s are the steady state solutions of equation (2.3). The probe absorption using (2.4), (2.5) and (2.6) is

$$\begin{aligned} \mathcal{A} &= N\hbar\{i\omega_p[g_{13}\rho_{31}^{(-1)} + g_{12}\rho_{21}^{(-1)} - g_{13}^*\rho_{13}^{(+1)} - g_{12}^*\rho_{12}^{(+1)}] \\ &\quad + i\omega_c[(g_{13}\rho_{31}^{(0)} + g_{12}\rho_{21}^{(0)})\overline{e^{-i\delta t}} - (g_{13}^*\rho_{13}^{(0)} - g_{12}^*\rho_{12}^{(0)})\overline{e^{i\delta t}}]\}. \end{aligned} \tag{2.7}$$

Thus the energy absorption per unit volume is

$$\mathcal{A} = iN\hbar\omega_p[g_{13}\rho_{13}^{*(+1)} + g_{12}\rho_{12}^{*(+1)} - g_{13}^*\rho_{13}^{(+1)} - g_{12}^*\rho_{12}^{(+1)}], \tag{2.8}$$

where we use the fact that $\rho_{lm} = \rho_{ml}^*$. The probe absorption coefficient α per unit length (the ratio of $\mathcal{A}$ and the input probe intensity $c|E_{p0}|^2/2\pi$) is

$$\alpha = \frac{\alpha_0}{g_{13}^2}[g_{13}\gamma_{13}\mathrm{Im}(\rho_{13}^{(+1)}) + g_{12}\gamma_{13}\mathrm{Im}(\rho_{12}^{(+1)})], \tag{2.9}$$

where we treat the probe Rabi frequencies as real, $\alpha_0 = 4\pi N\omega_p|d_{13}|^2/c\gamma_{13}\hbar$ and c is the velocity of light in vacuum. Note that the absorption now involves both $\mathrm{Im}(\rho_{12}^{(+1)})$ and $\mathrm{Im}(\rho_{13}^{(+1)})$ because the probe is acting on both the transitions.

We take the polarization of both control and probe fields along $(\hat{\epsilon}_2 + \hat{\epsilon}_3)/\sqrt{2}$ [except in Fig. 2.4(b)] where $\hat{\epsilon}_2$ and $\hat{\epsilon}_3$ are the unit vectors along $\vec{d}_{12}$ and $\vec{d}_{13}$ ($\vec{d}_{12} \perp \vec{d}_{13}$), respectively. For simplicity, we take $\gamma_{12} = \gamma_{13} = \gamma$. In Fig. 2.2(a), the probe absorption coefficient is plotted in units of α_0 as a function of δ for $\omega_{23} = G_{12} = G_{13}$. The

negative absorption in the profile corresponds to stimulated emission. *The solid curve in Fig. 2.2(a) shows the remarkable result that the cross talk between different optical transitions gives rise to gain provided the energy separation between the two ground levels is of the order of one half the control field Rabi frequency.* When cross talk is not taken into account, as shown in the figure, the usual Autler-Townes components [69] are seen.

The complex linear susceptibility χ ($\vec{P} = \chi \vec{E}_{p0}$) is given by

$$\chi = \frac{N|\vec{d}_{13}|^2}{\gamma_{13}\hbar g_{13}^2}[g_{13}\gamma_{13}\rho_{13}^{(+1)} + g_{12}\gamma_{13}\rho_{12}^{(+1)}]. \tag{2.10}$$

The dispersion properties of the medium corresponding to the real part of χ are plotted in Fig. 2.2(b), both in the presence and absence of cross talk. Clearly, the cross talk significantly changes the dispersion characteristics also. The imaginary part of χ corresponds to absorption as can be seen from (2.9).

Three gain peaks along with an absorption peak and a central dispersive profile are the clear features of the solid curve in Fig. 2.2 (a). The dispersive gain around $\omega_p \approx \omega_c$ is a kind of stimulated Rayleigh gain, also seen in a driven two-level system. The origin of such dispersive features are known [16], and lasing based on similar dispersive gain mechanism has been observed [17]. The features at the two extreme shows gain or absorption depending on the Δ_c. They appear as dispersive profiles when $\Delta_c = 0$, as shown in Fig. 2.3. The spectra is symmetric about $\delta = 0$ for this detuning. On the other hand the two intermediate gain regions depend significantly on the control field Rabi frequency. These gains are maximum for $\omega_{23} \approx G_{12} = G_{13}$, and disappears for both $\omega_{23} \gg G_{12}, G_{13}$ and $\omega_{23} \ll G_{12}, G_{13}$. The gain is observed for both $\delta > 0$ and $\delta < 0$ for a given Δ_c, and this supplements to the recently observed gain by Brown et al. in ^{39}K vapor [135] as a result of atomic coherence. It should be noted that these gains are not because of any inversion in the bare states. The steady state population in the three bare states and the ground state coherence in the absence of probe field are

$$\rho_{11}^{(0)} = \frac{2G^2\omega_{23}^2}{8G^4 + 8\omega_{23}^2 + 2G^2\omega_{23}^2 + \omega_{23}^4}, \tag{2.11a}$$

$$\rho_{22}^{(0)} = \frac{4G^4 + 4\omega_{23}^2 + G^2\omega_{23}^2}{8G^4 + 8\omega_{23}^2 + 2G^2\omega_{23}^2 + \omega_{23}^4}, \tag{2.11b}$$

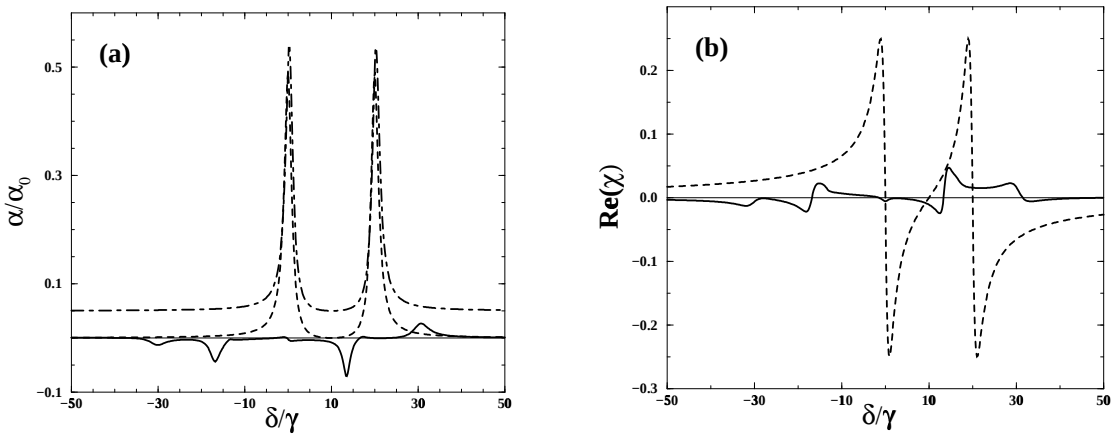

Figure 2.2: (a) Probe absorption coefficient, α in dimensionless units as a function of δ/γ. The parameters are $G_{12} = G_{13} = \omega_{23} = 10\gamma$, $g_{13} = g_{12} = 0.1\gamma$, and $\Delta_c = 5\gamma$. For comparison we also plot (dashed curve) the usual Autler-Townes components when $G_{13} = g_{12} = 0$. For large separation between $|2\rangle$ and $|3\rangle$, $\omega_{23} = 500\gamma$, the gain disappears (dot-dashed) and the standard Autler-Townes splitting emerges. The X-axis for the dot-dashed curve is taken as $\delta - \omega_{23}$ and Y-axis as $\alpha/\alpha_0 + 0.05$ for comparison and clarity. (b) Real χ in units of $N|\vec{d}_{13}|^2/\gamma\hbar$. The parameter for the solid and the dashed curves are same as the solid and the dashed curves in (a).

$$\rho_{33}^{(0)} = \frac{4G^4 + \omega_{23}^4 + 4\omega_{23}^2 - G^2\omega_{23}^2}{8G^4 + 8\omega_{23}^2 + 2G^2\omega_{23}^2 + \omega_{23}^4}, \tag{2.11c}$$

$$\rho_{23}^{(0)} = \frac{G^2(\omega_{23}^2 - 4G^2 + 4i\omega_{23})}{8G^4 + 8\omega_{23}^2 + 2G^2\omega_{23}^2 + \omega_{23}^4}, \tag{2.11d}$$

where we take $G = G_{12} = G_{13}$, $\Delta_c = \omega_{23}/2$, and $\gamma = 1$ as in Fig. 2.2. Comparing the numerators, it can be shown from the above three expressions that (i) $\rho_{33}^{(0)} > \rho_{11}^{(0)}$ for all values ω_{23} and (ii) $\rho_{22}^{(0)} > \rho_{11}^{(0)}$ for $\omega_{23} < 2G$. The coherence $|\mathrm{Re}(\rho_{23}^{(0)})|$ is significant only for the range of $\omega_{23} < 2G$, and is negligible for $\omega_{23} \gg 2G$. We show in the next section that this coherence is giving rise to gain.

2.2 New Interference Effects

We next analyze the spectra in the Fig. 2.2 and will isolate the new features as due to interference effects arising from cross talk among optical transitions. For this, we separate the different effects of the probe field on the two transitions $|1\rangle \leftrightarrow |2\rangle$ and $|1\rangle \leftrightarrow |3\rangle$ by writing, $\rho_{lm}^{(+1)} = g_{13}\sigma_{lm} + g_{12}\sigma'_{lm}$ and $\rho_{lm}^{(-1)} = g_{13}\sigma^*_{ml} + g_{12}\sigma'^*_{ml}$. Here we use the fact that $\rho_{lm} = \rho^*_{ml}$ to write the latter part and treat the probe

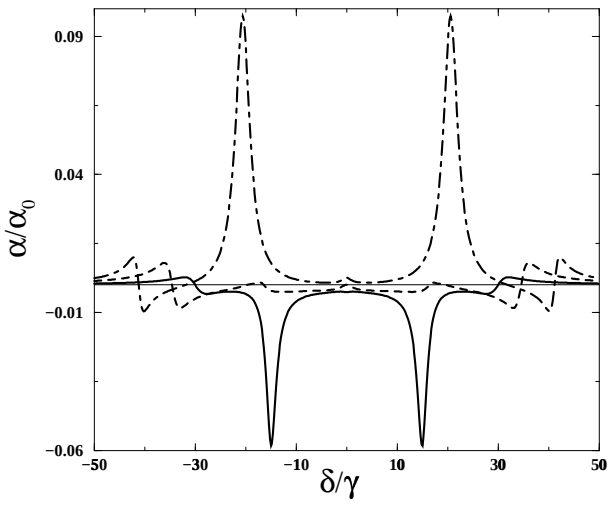

Figure 2.3: Probe absorption spectra for various values of ω_{23} when $\Delta_c = 0$. The solid curve is for $\omega_{23} = G$, the dashed curve for $\omega_{23} = 2G$ and the dot-dashed curve for $\omega_{23} = 3G$. The parameters are $G = G_{12} = G_{13} = 10\gamma$, $g_{13} = g_{12} = 0.1\gamma$. The two intermediate gains appear as dispersive profiles when $\omega_{23} = 2G$ and for $\omega_{23} > 2G$; these regions show absorption features.

Rabi frequency as real. The probe absorption coefficient α in this case will be

$$\alpha = \frac{\alpha_0 \gamma}{g_{13}^2}[g_{13}^2 \mathrm{Im}(\sigma_{13}) + g_{12}^2 \mathrm{Im}(\sigma'_{12}) + g_{13} g_{12} \mathrm{Im}(\sigma_{12}) + g_{12} g_{13} \mathrm{Im}(\sigma'_{13})]. \qquad (2.12)$$

In (2.12) the first two terms correspond to *absorption* along $|1\rangle \leftrightarrow |3\rangle$ and $|1\rangle \leftrightarrow |2\rangle$ transitions. The last two terms correspond to an *interference* among the probe field along the two transitions - a result of cross talk among the two transitions. As observed, this interference term plays a prominent role for small ω_{23} and disappears for large ω_{23}. For our numerical results we separate out the contribution of the direct *absorption* term and the *interference* term in equation (2.12). In Fig. 2.4(a) we plot the net absorption coefficient along with the contribution of absorption and interference terms. Note that the gain peaks around δ/γ = -16.8 and 13.5 are *enhanced* by the interference. On the other hand, the strong absorptions around δ/γ = -13.3 and 16.6 are almost *nullified* by the interference, though the refractive index [see Fig. 2.2(b), especially in the region $17 \leq \delta/\gamma \leq 25$] is still large. The interference thus leads to dispersion enhancement in the region of very low absorption as has been realized earlier by Scully and coworkers [86, 88, 89] for a different model. The interference term is also sensitive to the relative orientation of the probe and control field polarizations. In Fig. 2.4(b) we

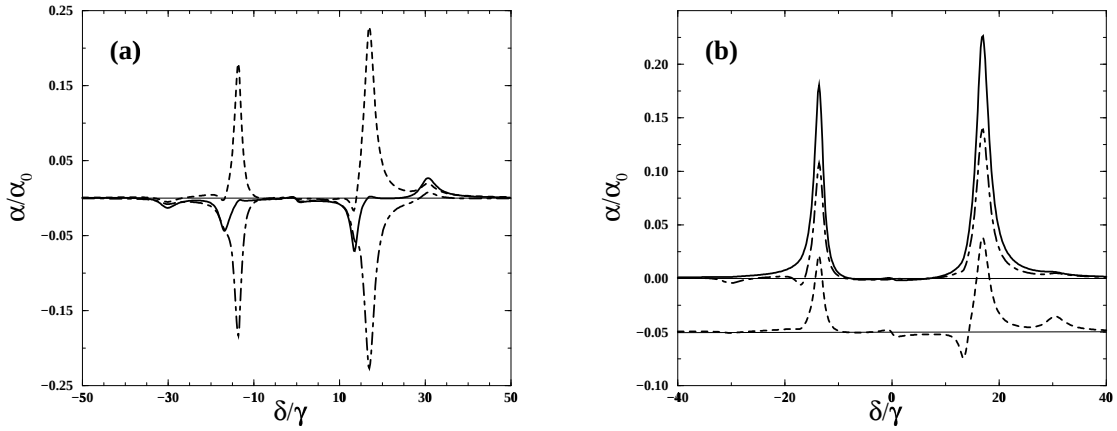

Figure 2.4: (a) Probe absorption spectra for $\omega_{23} = G_{12} = G_{13} = 10\gamma$. The interference term (dot-dashed curve) and the absorption term (dashed curve) as in equation (2.12) are separated to see their individual contribution on the net result (solid curve). The other parameters are $\Delta_c = 5\gamma$, $g_{12} = g_{13} = 0.1\gamma$. (b) Probe absorption for different orientation of probe field $\vec{E}_p$ with respect to the control field $\vec{E}_c$. The solid curve is for $g_{12} = -g_{13}$, the dashed curve for $g_{12} = 0$ (shifted by -0.05 units along the Y-axis for clarity) and the dot-dashed curve for $g_{13} = 0$. For all the cases $\vec{E}_c$ is along an axis at 45^o to both $\vec{d}_{12}$ and $\vec{d}_{13}$. The remaining parameters are as in frame (a).

show the probe absorption for various probe polarizations. For control and probe fields perpendicular to each other ($f = -g$), the interference term will flip to give rise to strong absorption. We also show in Fig. 2.4(b) the result when probe acts only on transition $|1\rangle \leftrightarrow |3\rangle$ ($f = 0$) or $|1\rangle \leftrightarrow |2\rangle$ ($g = 0$).

The origin of interference can be understood by explicitly writing down the equations of density matrix elements appearing in (2.12):

$$\begin{aligned}
\dot{\sigma}'_{12} &= -\{\gamma_{13} + \gamma_{12} + i(\Delta_c - \omega_{23}/2 - \delta)\}\sigma'_{12} + iG_{13}\sigma'_{32} \\
&\quad -iG_{12}(\sigma'_{11} - \sigma'_{22}) - i(\rho^{(0)}_{11} - \rho^{(0)}_{22}), \qquad (2.13a) \\
\dot{\sigma}_{12} &= -\{\gamma_1 + \gamma_2 + i(\Delta_c - \omega_{23}/2 - \delta)\}\sigma_{12} + iG_{13}\sigma_{32} \\
&\quad -iG_{12}(\sigma_{11} - \sigma_{22}) + i\rho^{(0)}_{32}, \qquad (2.13b) \\
\dot{\sigma}_{13} &= -\{\gamma_{13} + \gamma_{12} + i(\Delta_c + \omega_{23}/2 - \delta\}\sigma_{13} + iG_{12}\sigma_{23} \\
&\quad -iG_{13}(\sigma_{11} - \sigma_{33}) - i(\rho^{(0)}_{11} - \rho^{(0)}_{33}), \qquad (2.13c) \\
\dot{\sigma}'_{13} &= -\{\gamma_{13} + \gamma_{12} + i(\Delta_c + \omega_{23}/2 - \delta)\}\sigma'_{13} + iG_{12}\sigma'_{23} \\
&\quad -iG_{13}(\sigma'_{11} - \sigma'_{33}) + i\rho^{(0)}_{23}. \qquad (2.13d)
\end{aligned}$$

The elements in the interference term (σ_{12}, σ'_{13}) are governed by the zeroth order coherence between the states $|2\rangle$ and $|3\rangle$, created by the control field. On the other hand, the elements in the absorption term depends on the zeroth order inversion terms.

In order to explore the contribution of the interference term further, we look at large and intermediate values of ω_{23} with respect to the control field Rabi frequency. For ω_c tuned to $|1\rangle \leftrightarrow |2\rangle$ transition and large ω_{23}, the coherence due to control field is not expected due to the feeble cross talk effect. Figure 2.5(a) shows the Autler-Townes components at $\delta = \omega_{23} \pm G_{12}$. At $\delta = \omega_{23}$ the figure shows the transparency point due to CPT [32]. The dot-dashed curve in the figure represents the cross talk contribution which is negligible as expected. For intermediate values of ω_{23}, the control field driving both the transitions is to be considered, and one expects two set of Autler-Townes components as shown in Fig. 2.5(b). The transparency points will appear at $\delta = \pm\omega_{23}$ due to the two three-level configu-

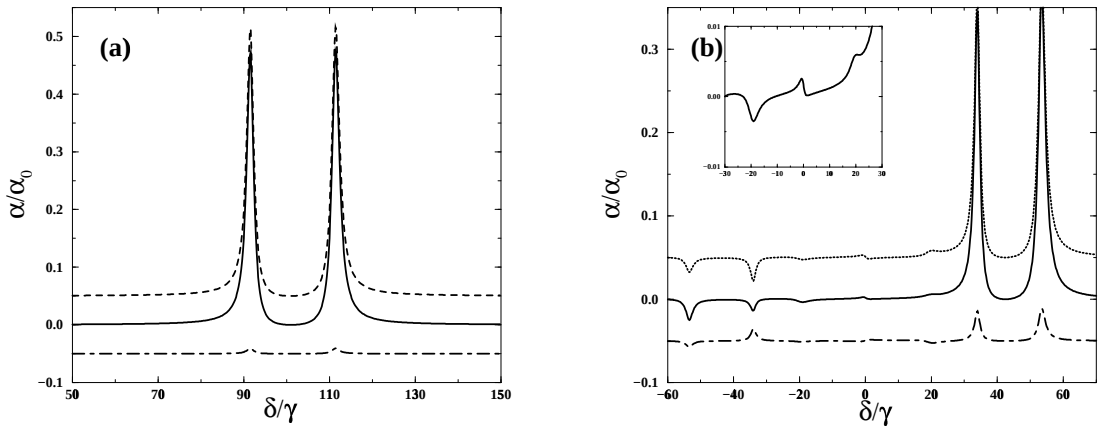

Figure 2.5: Probe absorption spectra for large and intermediate values of ω_{23}. The interference term (dot-dashed curve) is displaced by -0.05 units and the usual absorption term (dashed curve) by +0.05 units along the Y-axis for clarity. The net result is the solid curve. In frame (a) $\omega_{23} = 100\gamma$ and in (b) $\omega_{23} = 40\gamma$. The other parameters are as in Fig. 2.4(a). In frame (b) two set of Autler-Townes doublets are observed around $\delta = \pm\omega_{23}$ and Mollow type features (see inset) around $\delta = \pm 2G_{12}, 0$.

rations (G_{13}, g_{12}) and (G_{12}, g_{13}) possible in Fig. 1.1. Also seen in Fig. 2.5(b) are the Mollow [11] kind of features around $\delta = \pm 2G_{12}(= 2G_{13}), 0$. This is the result of two coupled two-level systems (G_{12}, g_{12}) and (G_{13}, g_{13}) present in Fig. 1.1. Since

both these set of two levels are like open systems, the resulting feature is very diminished. In the fluorescence spectrum these features were identified as modified Rayleigh scattering due to strong control field [128]. For $|\Delta_c| \gg G_{12}, G_{13}$, instead of Autler-Townes splitting, the usual Stokes and anti-Stokes Raman features appear at $\delta = \pm\omega_{23}$. In Fig. 2.5(b) the gain in the Autler-Townes doublet at $\delta = -\omega_{23}$ is the modified stimulated Raman gain due to resonant control field. Recently, Bowie et al. [136] measured stimulated Raman gain in $^{85}\mathrm{Rb}$ for different values of control field intensity in the presence of cross talk effect. They considered the ground

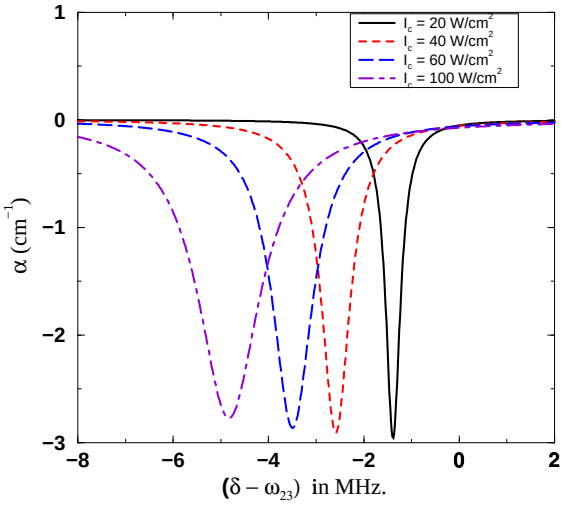

Figure 2.6: Stimulated Raman gain as observed in Ref. [136] for different values of control field intensity $\mathrm{I_c}$ as shown in the frame. The control field detuning is kept $22.6\mathrm{rad.GHz}$ above the $|1\rangle \leftrightarrow |2\rangle$ resonance.

levels $5\mathrm{S}_{1/2}(\mathrm{F}=2)$, $5\mathrm{S}_{1/2}(\mathrm{F}=3)$ and the excited level $5\mathrm{P}_{1/2}(\mathrm{F}=2)$. For these levels $\omega_{23} = 18.216$ rad.GHz, $\gamma_{12} \approx 7.43$ rad.MHz, $\gamma_{13} \approx 1.85$ rad.MHz and $\alpha_0 \approx 1455$ cm^{-1}, where $N = 5 \times 10^{11}\mathrm{atoms/cm}^3$ in their experiment. Using the model discussed above, we observe similar Raman gain as shown in Fig. 2.6. In these calculations we have not taken into account, the hyperfine magnetic sublevels, Doppler broadening etc. Nonetheless, the Raman gain shown in Fig. 2.6, qualitatively agrees well with their experimental results.

For ω_{23} close to G_{12}, G_{13} the Raman and Mollow type features discussed above are important and they superpose over each other. The coherence between states $|2\rangle$ and $|3\rangle$ also increases due to cross talk. Thus the interference term plays a dominant role as noted in Fig. 2.4(a), giving rise to enhanced stimulated emission.

If ω_{23} is reduced further, strong absorption and interference features are seen around $\delta \approx \sqrt{G_{12}^2 + G_{13}^2}$. At $\omega_{23} = 0$ the interference term completely cancels the absorption as a result of CPT [32].

2.3 Semiclassical Dressed States

In this section we examine the impact of the coherence created by cross talk in a dressed basis. In particular, to understand the presence of pronounced gain features around $\omega_{23} = G_{12} = G_{13}$. We first ignore all the incoherent terms in (2.3). We can thus work with the state $|\phi\rangle$ of the system given by

$$|\phi\rangle = C_1(t)|1\rangle + C_2(t)|2\rangle + C_3(t)|3\rangle. \tag{2.14}$$

Here $C_m(t)$ are the probability amplitudes of the states $|m\rangle$, $m = 1, 2, 3$. For simplicity, we take $G = G_{12} = G_{13}$ and $\omega_c = \omega_{12}$. However, we will present numerical results for the symmetric case ($\Delta_c = 0$) as well. Substituting (2.14) in the Schrödinger equation along with the Hamiltonian (2.2) with only the control field terms, we arrive at the matrix equation

$$i\dot{C} = H_{\text{eff}} C \tag{2.15}$$

where C and H_{eff} are 3×1 and 3×3 matrices:

$$C = \begin{bmatrix} C_1(t) \\ C_2(t) \\ C_3(t) \end{bmatrix}, H_{\text{eff}} = \begin{bmatrix} \omega_{23} & -G & -G \\ -G & \omega_{23} & 0 \\ -G & 0 & 0 \end{bmatrix}. \tag{2.16}$$

The dressed state analysis involves the evaluation of stationary states for the 'atom + control field' system. The matrix Hamiltonian in (2.16) can be diagonalised by taking $\det|H_{\text{eff}} - I\lambda| = 0$. This will result in a cubic equation of the form $\lambda^3 + A\lambda^2 + B\lambda + C = 0$, where $A = -2\omega_{23}, B = \omega_{23}^2 - 2G^2$ and $C = \omega_{23}G^2$. The two extreme roots of the above cubic equation are

$$\lambda_{\pm} = -A/3 \pm \frac{2}{3}\sqrt{(A^2 - 3B)}\cos[\frac{1}{3}\cos^{-1}(\mp L)], \tag{2.17}$$

where $L = (27C + 2A^3 - 9AB)/2(A^2 - 3B)^{3/2}$ and the third root is $\lambda_0 = -A - \lambda_+ - \lambda_-$. In Figs. 2.7(a,b) we plot the eigenvalues as a function of ω_{23} for $\Delta_c = \omega_{23}/2, 0$. For small ω_{23}, $\lambda_0 \to 0$. At $\omega_{23} = 0$ the eigenvalues $\lambda_{\pm}$ are symmetrically situated about

λ_0 for case (a), but for case (b) this symmetry is maintained for the entire range of ω_{23}. For large ω_{23} either λ_+ or λ_- goes to zero and hence the corresponding eigenstate becomes the ground state $|3\rangle$. The two remaining excited eigenstates give rise to the Autler-Townes doublet. Physically the above eigenvalue analysis means a unitary transformation of the Hamiltonian $H_{\rm eff} \rightarrow SH_{\rm eff}S^{\dagger}$ where S is the unitary matrix given by

$$S = \begin{bmatrix} -G\lambda_+\mathcal{N}_+ & (\lambda_+(\lambda_+ - \omega_{23}) - G^2)\mathcal{N}_+ & G^2\mathcal{N}_+ \\ -G\lambda_0\mathcal{N}_0 & (\lambda_0(\lambda_0 - \omega_{23}) - G^2)\mathcal{N}_0 & G^2\mathcal{N}_0 \\ -G\lambda_-\mathcal{N}_- & (\lambda_-(\lambda_- - \omega_{23}) - G^2)\mathcal{N}_- & G^2\mathcal{N}_- \end{bmatrix}, \tag{2.18}$$

where $\mathcal{N}_b$'s ($b = 0, \pm$) are the normalization factors given by $\mathcal{N}_b = [\lambda_b^2 G^2 + (\lambda_b(\lambda_b - \omega_{23}) - G^2)^2 + G^4]^{-1/2}$. Population in the three dressed states will be the diagonal

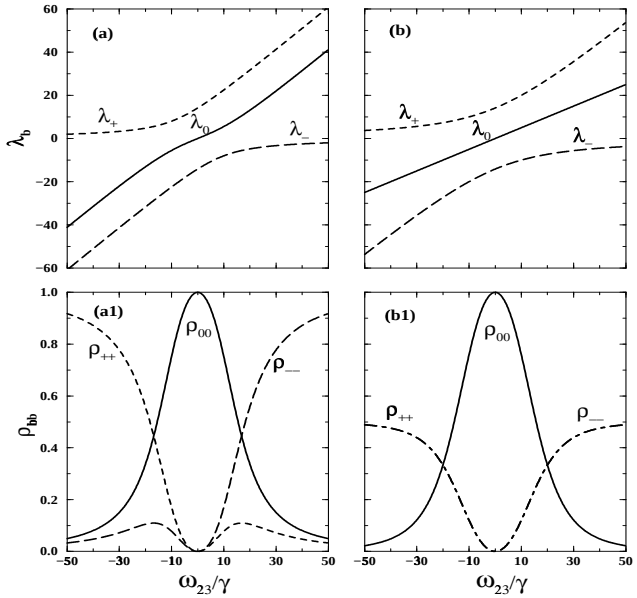

Figure 2.7: Eigenvalues λ_b and the corresponding dressed state populations ρ_{bb} as a function of spacing ω_{23}. Here $G = 10\gamma$ and $\Delta_c = \omega_{23}/2$ for (a,a1) while $\Delta_c = 0$ for (b,b1). Note that most of the population is in state $|0\rangle$ for $\omega_{23} < 2G$, giving rise to stimulated emissions as shown later in Fig. 2.8(b).

elements $\rho_{bb} = \langle b|\rho|b\rangle$ where $|b\rangle$'s are the three orthonormal dressed eigenstates. Explicitly, these dressed states are given by

$$|b\rangle = \mathcal{N}_b\{G^2|3\rangle - G\lambda_b|1\rangle + (\lambda_b(\lambda_b - \omega_{23}) - G^2)|2\rangle\}. \tag{2.19}$$

We evaluate the steady state population in the three dressed states in the presence of dissipation terms by using (2.3) (without the probe field terms) and (2.19). In

Fig. 2.7(a1,b1) we plot the steady state population in the three dressed states as a function of ω_{23}. For $\omega_{23} = 0$ only the state $|0\rangle$ is occupied due to population trapping; but for $\omega_{23} \neq 0$ there is still *population inversion* for $\omega_{23} < 2G$, thus giving rise to the possibility of stimulated emission from state $|0\rangle$. We also plot the population for the symmetric case when $\Delta_c = 0$ and note that for this case, population in both the dressed states $|+\rangle$ and $|-\rangle$ are the same for all values of ω_{23}. It can be shown from (2.19) that the weight factor for the state $|1\rangle$ is small in the state $|0\rangle$ compared to states $|\pm\rangle$ for the range of $\omega_{23} \leq G$.

The various peaks in the absorption spectrum correspond to the transitions among the dressed states, and this can be seen from the quantized dressed state description where the control field is quantized. The classical nature of the laser modes is still preserved by taking mean number of photons $\langle n\rangle$ very large, and $\langle n\rangle \gg \Delta n \gg 1$, where Δn is the fluctuation about the mean value $\langle n\rangle$. The Hamiltonian H_0 of the system without the interaction term is given by

$$H_0 = \hbar(\omega_{13}A_{11} + \omega_{23}A_{22}) + \hbar\omega_c(a^\dagger a + 1/2), \tag{2.20}$$

where a and $a^\dagger$ are the annihilation and creation operators, respectively for the laser mode at frequency ω_c. The uncoupled eigenstates for the above Hamiltonian with positive ω_{23} are shown in Fig. 2.8(a). The two manifolds M(n-1) and M(n) are shown and their centers have energy separation of $\hbar\omega_c$. The interaction with the field results in the mixing of various uncoupled eigenstates in a given manifold and the eigenvalues for each manifold can be evaluated as done above. The control field mixing the uncoupled eigenstates of two different manifolds can be neglected by invoking RWA [15]. In a strict sense, all the atomic variables, the coupling strengths G's and the eigenvalues will be different for different manifolds, but since we have assumed a laser mode with a large mean number of photons and a relatively narrow distribution, the difference between n and $n \pm 1$ can be neglected. The dressed states in a given manifold, say M(n-1), can be generalized from (2.19) by replacing states $|1\rangle$, $|2\rangle$ and $|3\rangle$ by the eigenstates of (2.20), i.e. $|1, n-1\rangle$, $|2, n\rangle$, and $|3, n\rangle$, respectively. The sequence of dressed states for two adjacent manifolds are shown in Fig. 2.8(b). Populations in the states $|b, n-1\rangle$ and $|b, n\rangle$ can be considered equal in the semi-classical limit and a transition among these states correspond to the the control frequency ω_c.

Case - I: Emission from $|0, n\rangle$ states

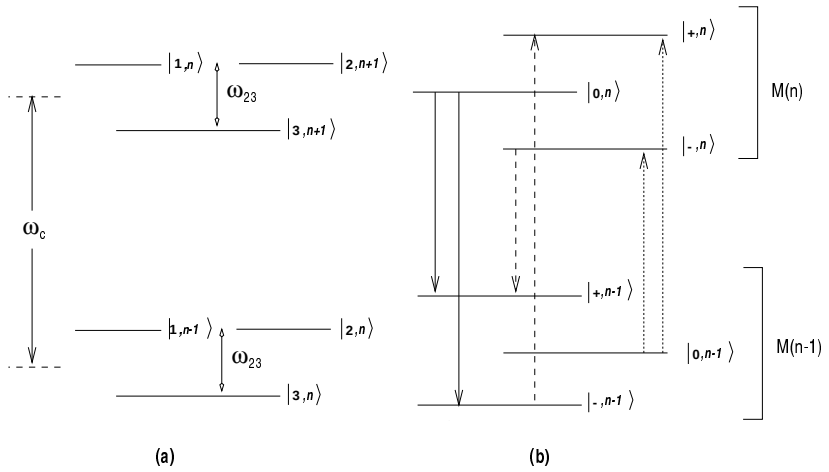

Figure 2.8: Quantized dress state picture: (a) The uncoupled eigenstates of two adjacent manifolds, M(n) and M(n-1) separated by $\omega_c(\hbar = 1)$. (b) The corresponding dressed states when coupling is included. The arrows indicate various absorption and emission processes among the dressed states. As noted in Fig. 2.4(a), the interference minimizes the absorption from states $|0, n-1\rangle$ but enhances the stimulated emission from states $|0, n\rangle$.

As shown in Fig. 2.7 the population in state $|0\rangle$ is greater than that in $|\pm\rangle$ for $|\omega_{23}| < 2G$. This gives rise to the possibility of stimulated emission from states $|0, n\rangle$ to states $|\pm, n-1\rangle$ at probe frequencies $\omega_p = \omega_c + \lambda_0 - \lambda_\pm$. For $\omega_{23} = G = 10\gamma$ and $\Delta_c = 5\gamma$, λ_+ = 22.46, λ_0 = 5.549, and λ_- = -8.02. Thus there is a possibility of gain around δ/γ = -16.9 and 13.5, and this is in tune with the numerical result in Fig. 2.4(a). The small discrepancy in the numerical and analytical values arise because of the inclusion of dissipative terms in the the numerical results.

Apart from inversion it is the coupling of the dressed atom with the probe field that governs the enhancement of gain, and as we see for $|\omega_{23}| \ll G$, though there is population inversion, the coupling strength reduces because the system is close to the CPT state. The coupling strength of the probe field will depend on the induced transition dipoles among the dressed states given by,

$$\vec{d}_{ab} = -\mathcal{N}_a\mathcal{N}_b\lambda_a G\{G^2\vec{d}_{13} + [\lambda_b(\lambda_b - \omega_{23}) - G^2]\vec{d}_{12}\}e^{i(\omega_c+\lambda_a-\lambda_b)t}. \tag{2.21}$$

Here the indices a and b are $0, \pm$. The above expression explains the existence of seven frequencies at which the dipole moment of the dressed atom will oscillate. This explains the seven different features at $\delta = \lambda_a - \lambda_b$ in Fig. 2.4 (around $\delta \approx 0, \pm 13.5, \pm 16.9, \pm 30.4$). From the above expression it is evident that the gain

components $\omega_c + \lambda_0 - \lambda_\pm$ will have a coupling strength proportional to λ_0. As seen in Fig. 2.7(a,b) $\lambda_0 \to 0$ for $|\omega_{23}| \ll G$, and hence the coupling strength reduces in this region. The coupling is absent at $\omega_{23} = 0$. For $|\omega_{23}| > G$, the population inversion reduces, and as an interplay between these two the optimum gain is observed only around $|\omega_{23}| \approx G$. To further clarify the existence of specific characteristic around $|\omega_{23}| \approx G$, we plot one of the gain components $\delta = \lambda_0 - \lambda_-$ as a

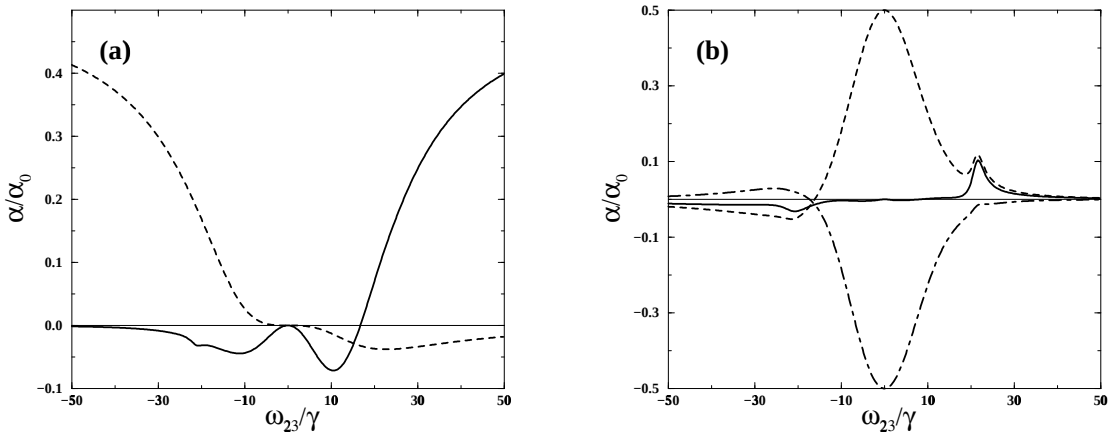

Figure 2.9: (a) Absorption coefficient for different values of probe frequencies as a function of ω_{23}. The solid curve is for $\delta = \lambda_0 - \lambda_-$, dotted curve for $\delta = \lambda_- - \lambda_+$. Other parameters include $G = 10\gamma$, $g_{13} = g_{12} = 0.1\gamma$ and $\omega_c = \omega_{12}$. (b) Absorption coefficient for one of the transparency components at $\delta = \lambda_+ - \lambda_0$ as a function of ω_{23}. The interference term (dot-dashed curve) almost nullifies the absorption (dashed curve) for a range of $|\omega_{23}|$ approximately up to G. There is a net transparency of around 99% in this range. The other parameters are as in frame (a).

function of ω_{23} in Fig. 2.9(a), and compare it with the component at $\delta = \lambda_- - \lambda_+$, the transition among extreme dressed states. Note that the gain features are prominent at $|\omega_{23}| \approx G$ for $\delta = \lambda_0 - \lambda_-$, and no such special features are seen for probe frequency at $\delta = \lambda_- - \lambda_+$. This validates the point that stimulated emission from $|0, n\rangle$ is optimum only around $|\omega_{23}| \approx G$.

Case - II: Absorption from $|0, n-1\rangle$ states

In Fig. 2.4(a), it was noted that the possibility of strong absorption at δ = -13.3 and 16.6, is minimized by the interference term. This corresponds to the probe frequencies at $\omega_p = \omega_c + \lambda_\pm - \lambda_0$ [the dotted arrows in Fig. 2.8(b)] and we show here the reasons for this kind of *transparency*. In Fig. 2.9(b) we plot one of the

components, $\delta = \lambda_+ - \lambda_0$ as a function of ω_{23}. As seen, the strong absorption is nullified by the interference term. The net absorption is zero at $\omega_{23} = 0$ due to the formation of CPT state, and continues to remain *minimum* for a range of $|\omega_{23}| < 2G$ due to state $|0\rangle$ being close to a CPT like state. Physically this can be understood in terms of destructive interference leading to small dipole matrix elements for these transitions. This can be seen from the expression (2.21) where we see that the frequency component at $\omega_c + \lambda_\pm - \lambda_0$ will have an induced dipole moment given by

$$-\mathcal{N}_0\mathcal{N}_\pm\lambda_\pm G\{G^2\vec{d}_{13} + [\lambda_0(\lambda_0 - \omega_{23}) - G^2]\vec{d}_{12}\}, \tag{2.22}$$

where we have verified that $\lambda_0(\lambda_0 - \omega_{23}) - G^2 < 0$ for all values of ω_{23}. This gives rise to opposite contributions from the dipoles oscillating along $|1\rangle \leftrightarrow |2\rangle$ and $|1\rangle \leftrightarrow |3\rangle$ transitions and the amplitudes along these transitions hardly differ for $|\omega_{23}| \leq G$. For frequency components at $\omega_c + \lambda_0 - \lambda\pm$ and $\omega_c + \lambda_\pm - \lambda_\mp$, the dipoles add up in phase because we find that $\lambda_\pm(\lambda_\pm - \omega_{23}) - G^2 > 0$ for all values of ω_{23}. Thus the net coupling for these components are important for any $\omega_{23} > 0$. On the other hand, retaining the control field polarization and taking the probe polarization along $(\hat{\epsilon}_2 - \hat{\epsilon}_3)/\sqrt{2}$ ($g_{12} = -g_{13}$) the coupling at $\delta = \lambda_\pm - \lambda_0$ will be the strongest compared to the other components.

Case - III: The transition among $|\pm\rangle$ states

In Fig. 2.4(a) the gain peak at δ = -30.4 and the absorption peak at δ = 30.4 arise because of transition among the dressed states $|\pm\rangle$ shown in Fig. 2.8(b) with dashed lines. They correspond to the probe frequencies $\omega_p = \omega_c + \lambda_\pm - \lambda_\mp$. The gain at $\omega_p = \omega_c + \lambda_- - \lambda_+$ is because of the small population inversion as seen in Fig. 2.7(a1) at $\omega_{23} = 10/\gamma$. Also note from Figs. 2.7(a1,b1) that the population in $|\pm\rangle$ states, unlike in state $|0\rangle$, is very sensitive to the Δ_c. The gain will appear at $\delta = \lambda_- - \lambda_+$ for $\Delta_c > 0$, and at $\omega_{12} = \lambda_+ - \lambda_-$ for $\Delta_c < 0$. This is because unlike state $|0\rangle$ which has a major contribution from coherence due to cross talk, both $|\pm\rangle$ states have contributions from optical coherences $\rho_{12}^{(0)}$ and $\rho_{13}^{(0)}$.

When $\Delta_c = 0$ the plot for eigenvalues in Fig. 2.7(b) shows that $\lambda_+ - \lambda_0 = \lambda_0 - \lambda_-$, because of the eigenvalues $\lambda_\pm$ placed symmetrically about λ_0 for all values of ω_{23}. This explains the presence of very symmetric profiles about $\delta = 0$ in Fig. 2.3. Also, as shown in Fig. 2.7(b1) the population in the states $|\pm\rangle$, for this case, are same for all values of ω_{23}. This gives rise to the dispersive kind of profiles as noted in

Fig. 2.3 at $\delta = \lambda_{\pm} - \lambda_{\mp}$ due to transition among dressed states of equal population. These dispersive profiles can be explained by taking into account the non-secular terms in the dressed state analysis [16]. The gain observed here is not because of any inversion, either in dressed states or in bare states, but due to coherence among dressed states [59]. Further, when $\omega_{23} = 2G$ in Fig. 2.7(b1) the population in all the three dressed states are equal. This explains the presence of dispersive profiles even at $\delta = \pm(\lambda_0 - \lambda_+)$ for this particular case.

2.4 Superluminal Propagation

In this section we report the unusual effect of cross talk on the propagation of a pulse of light. An important parameter characterizing propagation of a pulse is its group velocity which as noted in (1.41) is given by

$$v_g = \frac{c}{n + \omega_p \partial n/\partial \omega_p}. \tag{2.23}$$

In a spectral region of steep anomalous dispersion ($\partial n/\partial \omega_p < 0$) it is clear that *abnormal* group velocity like $v_g > c, \infty, -\text{ve}$ is possible [137, 138]. It is also known that such velocities need not be unphysical, and within the frame work of special relativity and principles of causality, such a phenomenon can be explained. For example a negative group velocity would mean that a new pulse center is formed at the output of the medium before the *previous* pulse center (as defined in vacuum) has entered the medium [130, 138]. Bolda and Chiao [139] have shown that in any dispersive dielectric, there will exist a spectral region where group velocity will be abnormal, the simplest example begin the region where attenuation is maximum [137, 138]. Anomalous dispersion near an amplifying region is also known to give rise to abnormal group velocity [140]. But most of these proposals and demonstrations were based on spectral regions where pulse distortion is inevitable. Recently, Chiao and coworkers [141] noted that in the region between two gain doublet, there exist a point of zero dispersion and large anomalous dispersion. Thus they predicted transport of narrow band, analytic pulses with abnormal group velocity without much distortion. Following this proposal, Wang et al. [130] created two Raman gain doublet with a well resolved separation of few MHz in Cs vapor. In the region between these gain peaks they observed a group index $n_g = -330$ ($v_g = c/n_g$) for a Gaussian pulse of bandwidth of $\approx 100\text{KHz}$.

This is the highest negative group velocity observed till date in the optical region. But it should be noted that the limitation on bandwidth and pulse shape does not allow any *information* to travel faster than the velocity of light in vacuum [142].

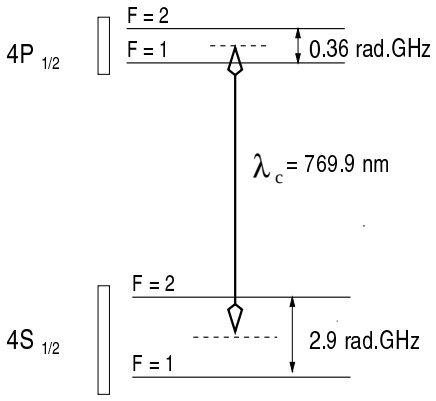

Figure 2.10: Energy level diagram of ^{39}K, D_1 transition. The separation between the hyperfine levels are as noted in the figure. The control field is tuned between the two excited and ground levels.

In Fig. 2.2(a) it was already noted that due to cross talk two close gain peaks can arise when $\omega_{23} \approx G$. For $\Delta_c = 0$ (Fig. 2.3) these gains appear symmetrically about $\delta = 0$. The separation between these two gain peaks depends crucially on ω_{23} and G, and for appropriate parameters it is possible to observe superluminal effects due to cross talk. In the following we predict the possibility of superluminal propagation for a system like ^{39}K. We consider the experimental situation reported in previous experiments [135] where ^{39}K was maintained as vapor at temperature $\mathrm{T} = 150^{\circ}\mathrm{C}$. The Doppler broadening at this temperature is $\approx 5.76\mathrm{GHz}$ and we include the Doppler effect in this calculation. The inclusion of Doppler broadening will imply a velocity dependent detuning $\Delta_v \equiv \Delta_c - v_z k_c$ where $\hat{z}$ is the direction of propagation of the control field. We consider the control and probe field as co-propagating to reduce the Doppler broadening effect. Thus δ remains unchanged since $k_p \approx k_c$. Doppler averaging of atomic variables is done for a Maxwellian velocity distribution as shown below.

$$\rho_{lm}(\delta, \Delta_c) = \frac{2\sqrt{\ln 2/\pi}}{\omega_D} \int_{-\infty}^{\infty} \rho_{lm}(\delta, \Delta_v) \exp\left[-4\ln 2(\Delta_v - \Delta_c)^2/\omega_D^2\right] d\Delta_v, \qquad (2.24)$$

where $\omega_D \approx \sqrt{8\ln 2 \omega_c^2 KT/c^2 M}$ is the Doppler width, K is the Boltzmann constant and M is the mass of each atom. A control field Rabi frequency $G = 2.2\mathrm{GHz}$ is considered which can be achieved with an intensity around $\mathrm{I_c} = 200\mathrm{W/cm^2}$. The

energy levels and their separations are shown in Fig. 2.10. Since the control field is strong, we also include the correction from the excited level $4P_{1/2}(F = 2)$. In Fig. 2.11 the probe absorption coefficient and refractive index change are plotted as a function of δ. For these calculations we have considered $\gamma = 20\text{MHz}$ and collisional dephasing rate $\approx 10\text{MHz}$. The decay of the ground and excited state coherences are taken as 0.1 MHz and 1 MHz, respectively. As can be noted from Fig. 2.11,

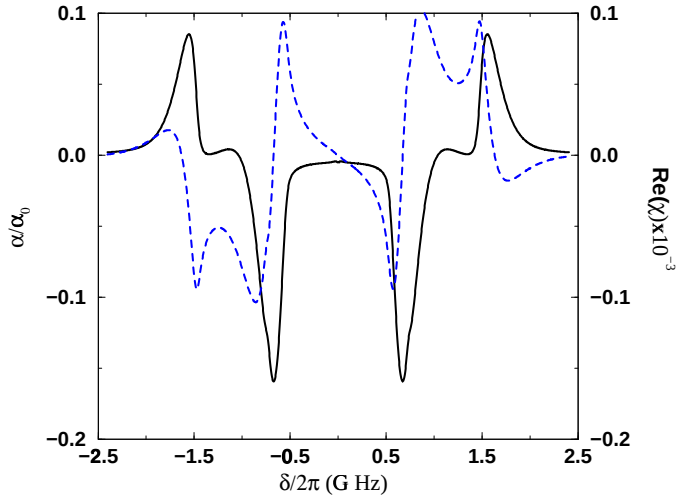

Figure 2.11: Absorption (solid, left scale) and dispersion (dashed, right scale) curve for the levels shown in Fig. 2.10 as a function of δ. The parameters are given in the text.

in the region around $\delta \approx 0$, the dispersion is close to zero and the slope is -ve. The separation between the two gain peaks is of the order of GHz range, and thus a pulse of this bandwidth can travel with superluminal velocity in this spectral region. We have measured an average group index $n_g = -60$ for a number density of $N = 10^{13}\text{atoms/cm}^3$ in this region. A detail investigation will need inclusion of all the $2F + 1$ magnetic sublevels, laser linewidth and propagation effects. However, one can work with selective magnetic sublevels and static magnetic fields [92, 94, 130]. In any case, these effects will not change the qualitative results discussed above. Further, there exist a vast parameter regime for various atomic vapors like Rb, Cs, Na, and superluminal behavior via cross talk in these systems need further investigation.

2.5 Summary

In summary, we have shown new features in the probe absorption spectra that arise in the Λ systems due to cross talk. In Sec. 2.1 we have shown the possibility of gain without inversion and new dispersive features that arise due to cross talk. In Sec. 2.2 we explain these new features in terms of new coherence effects that arise due to cross talk. We show the possibility of both gain and weak transparency as a result of interfering terms. We also connect our results with the previously well studied regimes where cross talk effects were negligible, and show that new coherence effects arise when the Rayleigh and Raman kind of phenomena interfere. The physical explanation to the gain and transparency is given in Sec. 2.3 in terms of the dressed basis. We give a general analytical expression for the position of various features in the spectra. We show that gain arise due to inversion in the dressed basis, and transparency as a result of weak coupling among dressed states. Finally, in Sec. 2.4 we discuss the possibility of superluminal propagation due to cross talk. For the parameters of ^{39}K vapor, we evaluate the group index with the inclusion of Doppler broadening and collisional effects.

Chapter 3

Gain Components in Autler-Townes Doublet

It is well known that the absorption spectrum of a probe tuned to one of the transition of a V system will show new resonances when a strong coherent field is driving the other transition. The strong drive splits the absorption resonance into two components known as the Autler-Townes components [69]. Various experiments in gases [143] and in solid state systems [144] have studied the Autler-Townes splitting of absorption lines in different contexts. Such a three-level model is not known to give rise to gain unless additional fields are introduced. For example, an incoherent pumping along the probing transition of a V system will give rise to gain [58, 64]. In this chapter, we demonstrate that the VIC in the V systems can produce *gain at frequencies where usually one expects absorption*.

3.1 Basic Equations

Consider the control and probe field set-up shown in Fig. 3.1(a). The transition dipole moments $\vec{d}_{13}$ and $\vec{d}_{23}$ are assumed to be non-orthogonal. It was noted in section 1.3 that non-orthogonal dipole matrix elements are essential for observing the VIC effects. Let θ denote the angle between the two dipole matrix elements. To study the situation as much parallel to the usual case where control and probe fields act on two different arms of the V system, we consider an arrangement of field polarization as shown in Fig. 3.1(b). This enables us to study the VIC effects as well as compare it with the usual situation. Thus the control field ($\vec{E}_c = \vec{E}_{c0}e^{-i\omega_c t} + \text{c.c.}$) with a Rabi frequency $2G_{23} = 2\vec{d}_{23} \cdot \vec{E}_{c0}/\hbar$ drives $|2\rangle \leftrightarrow |3\rangle$

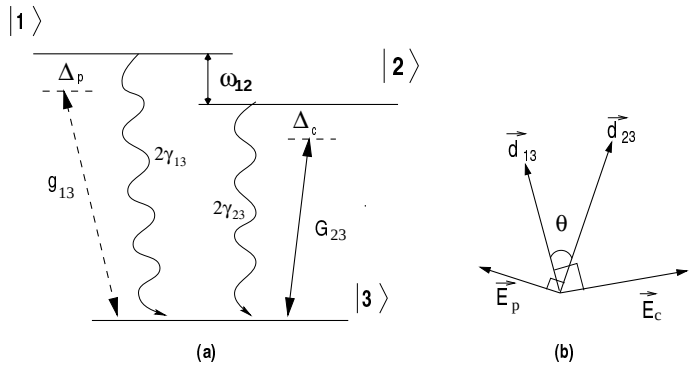

Figure 3.1: (a) Schematic diagram of a three-level V system. The control and probe fields have a frequency detunings Δ_c and Δ_p, respectively. The γ's denote the spontaneous emission rates from the respective levels. (b) The arrangement of field polarization required for single field driving one transition when dipoles are non-orthogonal.

transition ($\vec{d}_{13} \cdot \vec{E}_{c0} = 0$) and similarly the probe field ($\vec{E}_p = \vec{E}_{p0}e^{-i\omega_p t} + \text{c.c.}$) with a Rabi frequency $2g_{13} = 2\vec{d}_{13} \cdot \vec{E}_{p0}/\hbar$ drives $|1\rangle \leftrightarrow |3\rangle$ transition ($\vec{d}_{23} \cdot \vec{E}_{p0} = 0$). We note here that the Rabi frequencies will also depend on θ. But for comparisons we keep the Rabi frequencies same for different values of θ. In practice this can be done by suitably increasing/decreasing the field strength.

The Hamiltonian for this system in the RWA will be

$$\begin{aligned} H &= \hbar\omega_{13}|1\rangle\langle 1| + \hbar\omega_{23}|2\rangle\langle 2| \\ &\quad -\hbar(G_{23}|2\rangle\langle 3|e^{-i\omega_c t} + g_{13}|1\rangle\langle 3|e^{-i\omega_p t} + \text{H.c.}), \end{aligned} \tag{3.1}$$

where $\hbar\omega_{l3}$ ($l = 1, 2$) is the energy of the state $|l\rangle$ when measured with respect to the state $|3\rangle$. Making appropriate canonical transformations, the density matrix equations with inclusion of all the decay terms will be

$$\dot{\rho}_{11} = -2\gamma_{13}\rho_{11} - \eta(\rho_{12} + \rho_{21}) + ig_{13}e^{-i\delta t}\rho_{31} - ig_{13}e^{i\delta t}\rho_{13}, \tag{3.2a}$$

$$\dot{\rho}_{22} = -2\gamma_{23}\rho_{22} - \eta(\rho_{12} + \rho_{21}) + iG_{23}\rho_{32} - iG_{23}\rho_{23}, \tag{3.2b}$$

$$\dot{\rho}_{12} = -(\gamma_{13} + \gamma_{23} + i\omega_{12})\rho_{12} - \eta(\rho_{11} + \rho_{22}) + ig_{13}e^{-i\delta t}\rho_{32} - iG_{23}\rho_{13}, \tag{3.2c}$$

$$\begin{aligned} \dot{\rho}_{13} &= -(\gamma_{13} + i(\Delta_c + \omega_{12}))\rho_{13} - \eta\rho_{23} - iG_{23}\rho_{12} \\ &\quad + ig_{13}e^{-i\delta t}(1 - 2\rho_{11} - \rho_{22}), \end{aligned} \tag{3.2d}$$

$$\dot{\rho}_{23} = -(\gamma_{23} + i\Delta_c)\rho_{23} - \eta\rho_{13} - ig_{13}e^{-i\delta t}\rho_{21} + iG_{23}(1 - \rho_{11} - 2\rho_{22}), \tag{3.2e}$$

where $\delta = \omega_p - \omega_c$. The probe detuning $\Delta_p = \omega_{13} - \omega_p$ and the control field detuning $\Delta_c = \omega_{23} - \omega_c$ are related by $\Delta_p - \Delta_c = \omega_{12} - \delta$. The elements ρ_{13} and ρ_{23} in the

original frame are given by $\rho_{13}e^{-i\omega_c t}$ and $\rho_{23}e^{-i\omega_c t}$. We also use the trace condition $\rho_{11}+\rho_{22}+\rho_{33}=1$. Here $\eta=\sqrt{\gamma_{13}\gamma_{23}}\cos\theta$ is the VIC parameter, which is nonzero when $\theta\neq 90^o$. Note that for the kind of geometry shown in Fig. 3.1(b), θ is always nonzero, though it could be small. In the absence of external fields, as noted in equations (1.54), the VIC effects are important when the separation between the two excited levels is of the order of their natural line width. However, this condition may be relaxed when the system is being driven by external fields as we will see later.

Let us first consider the case when $\theta=90^o$. Making a further canonical transformation on ρ_{13} and ρ_{12}, we can get rid of the explicit time dependence. The imaginary part of ρ_{13} yields the probe absorption. In the limit of a weak probe field ($g_{13}\ll\gamma_{13},\gamma_{23}$), we obtain

$$\rho_{13}=\frac{g_{13}\{(\gamma_{23}^2+\Delta_c^2+G_{23}^2)(\Delta_c-\Delta_p+i(\gamma_{13}+\gamma_{23}))+G_{23}^2(\Delta_c-i\gamma_{23})\}}{(\gamma_{23}^2+\Delta_c^2+2G_{23}^2)[G_{23}^2+(\Delta_p-i\gamma_{13})(\Delta_c-\Delta_p+i(\gamma_{13}+\gamma_{23}))]}. \tag{3.3}$$

The above expression shows that two complex poles exists at $\Delta_p=(\Delta_c+i\gamma_{23}+2i\gamma_{13}\pm\sqrt{(\Delta_c+i\gamma_{23})^2+4G_{23}^2}\ )/2$. In the limit $G_{23}\gg\gamma_{23}$, the probe absorption will have two resonances at $\Delta_p=(\Delta_c\pm\sqrt{\Delta_c^2+4G_{23}^2})/2$. These are the two Autler-Townes components in the absorption spectrum. It can be further shown that $\mathrm{Im}(\rho_{13})>0$.

We now consider the effects of VIC ($\theta\neq 90^o$) [in Appendix B we show the possible systems where dipole matrix elements are non-orthogoanl]. The system of Eqs. (3.2) have been previously studied under different conditions. We would now recall what has been done and in what ways our current work differs from the existing works. (a) We could first consider the case when control field is also replaced by the probe field ($\vec{E}_{c0}\equiv\vec{E}_{p0}$, $\omega_p=\omega_c$). Here the effects of VIC manifest both in emission [117, 120] and absorption spectrum [114, 121, 145]. Zhou and Swain demonstrated the existence of ultra-narrow spectral lines in emission [120]. Cardimona *et al.* showed vanishing of absorption under certain conditions [114] whereas Zhou and Swain demonstrated the possibility of gain with no control field present [121]. (b) Another case which is extensively studied by Knight and coworkers corresponds to degenerate control and probe fields, i.e., $\vec{E}_{c0}\neq\vec{E}_{p0}$, but $\omega_p=\omega_c$ ($\delta=0$). Here the control field can have arbitrary strength while the probe is kept relatively weak. Paspalakis *et al.* showed how VIC can lead to gain without inversion [145]. (c) In the present work we study the general case of non-

degenerate control and probe fields, $\vec{E}_{c0} \neq \vec{E}_{c0}$, $\omega_p \neq \omega_c$. We show how the VIC can invert the traditional Autler-Townes component in the absorption spectrum.

The non-degenerate case has a major complication due to explicit time dependence in the equations of motion (3.2). Since the time dependence in (3.2) is periodic, we can solve these equations by Floquet analysis. The solution can be written as

$$\rho_{lm} = \sum_{\mathrm{n}} \rho_{lm}^{(\mathrm{n})} e^{-i\mathrm{n}\delta t}. \tag{3.4}$$

Thus the absorption and emission spectra get modulated at various harmonics of δ. The dc component in probe absorption spectrum is related to $\rho_{13}^{(+1)}$. The absorption coefficient α per unit length can be shown to be

$$\alpha = \frac{\alpha_0 \gamma_{13}}{g_{13}} \mathrm{Im}(\rho_{13}^{(+1)}), \tag{3.5}$$

where $\alpha_0 = 4\pi N |d_{13}|^2 \omega_p / \hbar \gamma_{13} c$ and N denotes the atomic density. Note that in (3.5) only one term from the entire series (3.4) contributes. For the degenerate case ($\delta = 0$), all the terms in the series (3.4) are important (but numerically easy to evaluate).

3.2 Numerical Results

In order to obtain the probe absorption spectra we solve (3.2) numerically using the series solution (3.4) and the steady state condition $\dot{\rho}_{ij}^{(\mathrm{n})} = 0$. The situation is much simpler for a weak probe when $\rho_{ij}^{(+1)}$ can be computed to first order in g_{13}, otherwise we use Floquet method. In Fig. 3.2 we plot the probe absorption as a function of probe detuning. The dashed curves in Fig. 3.2(a,b) are the usual Autler-Townes components in the absence of VIC effects. The solid curves show the absorption spectra when VIC is included. We observe that *one of the Autler-Townes component flips sign to give rise to significant gain.* This type of behavior is seen for any value of ω_{12} provided the control field strength satisfies the condition $G_{23} = |\omega_{12}|$ for $\Delta_c = 0$. When $\omega_{12} = G_{23}$ and $\Delta_c = 0$, the gain appears at $\Delta_p = -G_{23}$. *The solid curve in Fig. 3.2(b) shows that the effect of VIC is observed even for large ω_{12} compared to γ_{13}, γ_{23}.* This is in contrast to the situation that exist in the absence of external fields where one finds that VIC effects are important when the separation between vacuum coupled levels is of the order of their natural

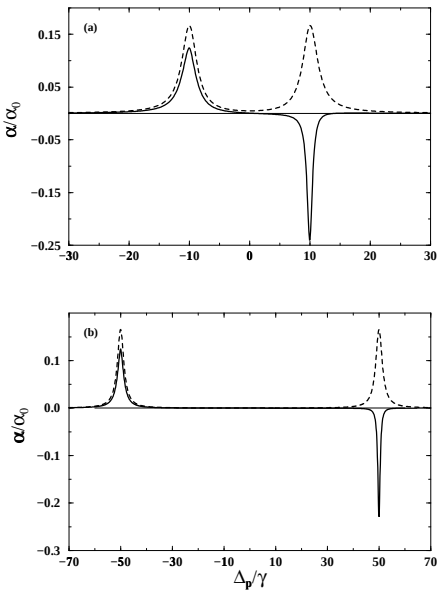

Figure 3.2: The probe absorption spectra both in the presence and in the absence of VIC. In both the frames the dashed curves show the usual Autler-Townes components in the absence of VIC ($\theta = 90^o$) and the solid curves are for $\theta = 15^o$. The common parameters are $g_{13} = 0.01\gamma$, $\gamma_{23} = \gamma_{13} = \gamma$, and $\Delta_c = 0$. Note that α will depend on ω_{12} only when VIC is present and we take $\omega_{12} = -G_{23}$ for the solid curves. In frame (a) we take $G_{23} = 10\gamma$ and in frame (b) we take $G_{23} = 50\gamma$. The solid curve in frame (b) shows that the effect of VIC is retained even for large ω_{12}.

line-width. As can be seen from the Fig. 3.2(b), for strong control fields, such a restriction can be relaxed. Also, one of the Autler-Townes component can be almost suppressed for certain set of parameters as shown in Fig. 3.3. It can be seen that the parameter θ controls the spectra in presence of VIC. The dot-dashed curve in Fig. 3.3 also shows the effect of unequal decays. For $\gamma_{23} > 2\gamma_{13}$ both the Autler-Townes components flip. We analyze the origin of these features in the following sections.

3.3 Quasi-Trapped-States

For a very weak probe field ($g_{13} \ll \gamma_{13}, \gamma_{23}$) we can solve equations (3.2) perturbatively with respect to the strength of the probe field. To the lowest order in g_{13}, the solution may be written as

$$\rho_{lm} = \sigma^0_{lm} + g_{13}\sigma^+_{lm}e^{-i\delta t} + g^*_{13}\sigma^-_{lm}e^{i\delta t}. \tag{3.6}$$

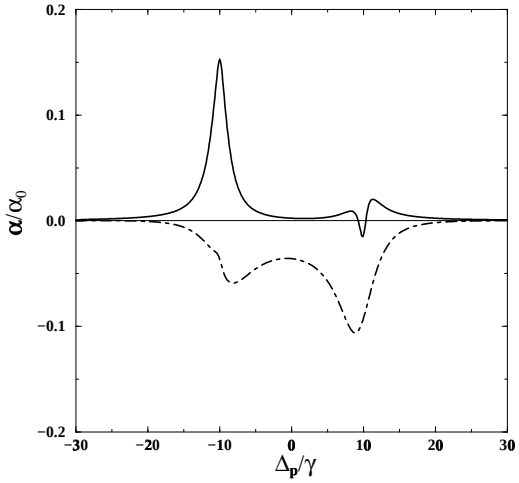

Figure 3.3: Plots show the important role θ and unequal γ's play in the presence of VIC. The common parameters are $G_{23} = 10\gamma$, $g_{13} = 0.01\gamma$, $\Delta_c = 0$, and $\omega_{12} = -G_{23}$. The solid curve presents the case when $\gamma_{23} = \gamma_{13} = \gamma$ and $\theta = 35^o$. The dot-dashed curve arises when $\gamma_{23} = 6\gamma$, $\gamma_{13} = \gamma$ and $\theta = 15^o$.

We first examine the behavior of the system in the presence of control field alone ($g_{13} = 0$). In the absence of VIC effects the system reduces to the well known case of coherently driven two-level atom. But the behavior is quite different in the presence of VIC effects as we show in the following.

It is clear that field G_{23} creates a coherent mixing of states $|2\rangle$ and $|3\rangle$. The new eigenvalues will be

$$\lambda_{\pm} = \frac{\Delta_c \pm \sqrt{\Delta_c^2 + 4G_{23}^2}}{2}, \tag{3.7}$$

and the corresponding dressed energy states can be written as

$$|+\rangle = \cos\psi|2\rangle + \sin\psi|3\rangle, \tag{3.8a}$$

$$|-\rangle = -\sin\psi|2\rangle + \cos\psi|3\rangle, \tag{3.8b}$$

where $\tan\psi = -G_{23}/\lambda_+$. The crucial point to note is that the level $|1\rangle$ is coupled with $|\pm\rangle$ because of the presence of VIC. Thus the population in $|\pm\rangle$ also depends on the VIC. When $|1\rangle$ is degenerate with either $|\pm\rangle$, i.e., when $\omega_{12} = \lambda_{\pm}$, the degenerate levels get strongly coupled via VIC, giving rise to trapping. When $|1\rangle$ and $|-\rangle$ are degenerate, we show that the dynamical behavior of the system can be best

analyzed in the basis given below:

$$|+\rangle, \quad |c\rangle = \frac{\sqrt{2\gamma_{13}}|1\rangle + \sqrt{\gamma_{23}}|-\rangle}{\sqrt{\gamma_{23}+2\gamma_{13}}}, \quad |uc\rangle = \frac{\sqrt{\gamma_{23}}|1\rangle - \sqrt{2\gamma_{13}}|-\rangle}{\sqrt{\gamma_{23}+2\gamma_{13}}}. \tag{3.9}$$

Using the transformations (3.8), (3.9) and Eqs. (3.2) with $g_{13} = 0$, we numerically compute the steady state population in the states (3.9). In Fig. 3.4 we plot the population of these states as a function of Δ_c. Note that in the presence of VIC, σ^0_{ucuc} approaches unity at $\Delta_c = 0$, i.e., when the states $|1\rangle$ and $|-\rangle$ are degenerate, because $\omega_{12} = -G_{23}$. A similar kind of trapping will occur when $|1\rangle$ is degenerate

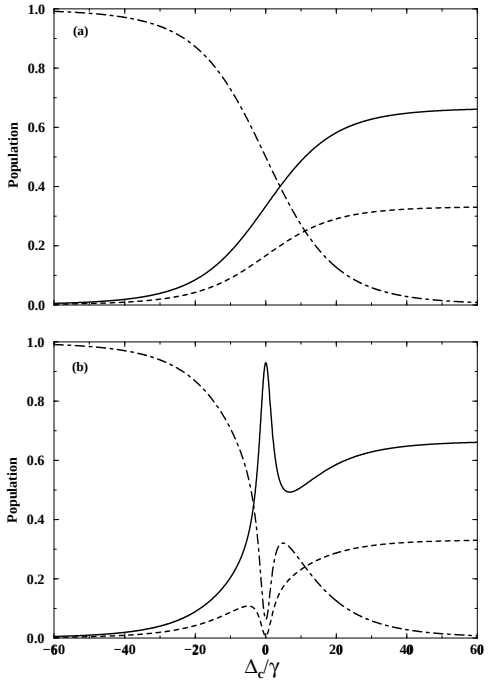

Figure 3.4: The atomic population in the basis (3.9) as a function of control detuning Δ_c/γ in the presence [frame (b), $\theta = 15^o$] and in the absence [frame (a), $\theta = 90^o$] of VIC. The parameters are $G_{23} = 20\gamma$, $\omega_{12} = -G_{23}$, and $\gamma_{13} = \gamma_{23} = \gamma$. The solid curves denote σ^0_{ucuc}, the dashed curves are for σ^0_{cc} and the dot-dashed curves denote σ^0_{++}.

with $|+\rangle$. When $|\omega_{12}| \neq G_{23}$, the trapping occurs for an off-resonant control field. Trapping also requires θ to be small. We show later that σ^0_{ucuc} cannot approach unity, and for this reason we refer to it as 'quasi-trapped-state' (QTS). Figure 3.4 also shows that for $\Delta_c \ll -G_{23}$, all the population remains in $|+\rangle$. This is not an interference effect and happens irrespective of whether VIC is present or absent. When $\Delta_c \ll -G_{23}$, $\lambda_+ \to 0$ and $\sin\psi \to 1$ ($\cos\psi \to 0$) in (3.8). Thus the

level $|+\rangle \approx |3\rangle$ is the ground state and most of the population remains here if the control is highly off-resonant. The building up of population in $|uc\rangle$ is a result of interference among decay channels of $|1\rangle$ and $|-\rangle$ levels. As a consequence, even if ω_{12} is large in bare basis, strong VIC effects can appear when a dressed state is degenerate with the bare state $|1\rangle$.

We next examine how the quasi-trapped-state is formed. For this purpose we transform the equations of motion (3.2) of the density matrix elements in basis (3.9). For $\Delta_c = 0$ and $\omega_{12} = -G_{23}$, a tedious calculation leads to

$$\begin{aligned}
\dot{\sigma}^0_{ucuc} &= -\frac{4\gamma_{13}\gamma_{23}(\gamma_{13}+\gamma_{23})(1-\cos\theta)}{(2\gamma_{13}+\gamma_{23})^2}\sigma^0_{ucuc} + \frac{\gamma_{13}(4\gamma_{13}^2+4\gamma_{13}\gamma_{23}\cos\theta+\gamma_{23}^2)}{(2\gamma_{13}+\gamma_{23})^2}\sigma^0_{cc} \\
&\quad + \frac{\gamma_{13}\gamma_{23}}{2\gamma_{13}+\gamma_{23}}\sigma^0_{++} - \frac{\gamma_{23}\sqrt{\gamma_{13}\gamma_{23}}(2\gamma_{13}-\gamma_{23})(1-\cos\theta)}{\sqrt{2}(2\gamma_{13}+\gamma_{23})^2}(\sigma^0_{ucc}+\sigma^0_{cuc}), \qquad (3.10a) \\
\dot{\sigma}^0_{cc} &= -\frac{(4\gamma_{13}+\gamma_{23})(4\gamma_{13}^2+4\gamma_{13}\gamma_{23}\cos\theta+\gamma_{23}^2)}{2(2\gamma_{13}+\gamma_{23})^2}\sigma^0_{cc} + \frac{2\gamma_{13}\gamma_{23}^2(1-\cos\theta)}{(2\gamma_{13}+\gamma_{23})^2}\sigma^0_{ucuc} \\
&\quad + \frac{\gamma_{23}^2}{2(2\gamma_{13}+\gamma_{23})}\sigma^0_{++} - \frac{\gamma_{13}(2\gamma_{13}-\gamma_{23})\sqrt{2\gamma_{13}\gamma_{23}}(1-\cos\theta)}{(2\gamma_{13}+\gamma_{23})^2}(\sigma^0_{ucc}+\sigma^0_{cuc}) \qquad (3.10b) \\
\dot{\sigma}^0_{++} &= -\frac{\gamma_{23}}{2}\sigma^0_{++} + \frac{(4\gamma_{13}^2+4\gamma_{13}\gamma_{23}\cos\theta+\gamma_{23}^2)}{2(2\gamma_{13}+\gamma_{23})}\sigma^0_{cc} + \frac{2\gamma_{13}\gamma_{23}(1-\cos\theta)}{(2\gamma_{13}+\gamma_{23})}\sigma^0_{ucuc} \\
&\quad + \frac{(2\gamma_{13}-\gamma_{23})\sqrt{\gamma_{13}\gamma_{23}}(1-\cos\theta)}{\sqrt{2}(2\gamma_{13}+\gamma_{23})}(\sigma^0_{ucc}+\sigma^0_{cuc}), \qquad (3.10c) \\
\dot{\sigma}^0_{ucc} &= -\left[\frac{4\gamma_{13}^2\gamma_{23}(1-\cos\theta)}{(2\gamma_{13}+\gamma_{23})^2} + \frac{\gamma_{13}\gamma_{23}\cos\theta+\gamma_{23}^2}{(2\gamma_{13}+\gamma_{23})} + \gamma_{13}\right]\sigma^0_{ucc} - \frac{\gamma_{23}\sqrt{\gamma_{13}\gamma_{23}}}{\sqrt{2}(2\gamma_{13}+\gamma_{23})}\sigma^0_{++} \\
&\quad - \frac{\gamma_{13}\gamma_{23}(1-\cos\theta)(2\gamma_{13}-\gamma_{23})}{(2\gamma_{13}+\gamma_{23})^2}\sigma^0_{cuc} - \frac{\sqrt{\gamma_{13}\gamma_{23}}(1-\cos\theta)}{\sqrt{2}}\sigma^0_{ucuc} \\
&\quad - [8\gamma_{13}^2(1-\cos\theta) + (2\gamma_{13}+\gamma_{23})^2\cos\theta]\frac{\sqrt{\gamma_{13}\gamma_{23}}}{\sqrt{2}(2\gamma_{13}+\gamma_{23})^2}\sigma^0_{cc}, \qquad (3.10d) \\
\dot{\sigma}^0_{+uc} &= -\frac{\gamma_{23}}{2(2\gamma_{13}+\gamma_{23})}[\gamma_{23}+\gamma_{13}(1+6\sqrt{2}-\cos\theta)]\sigma^0_{+uc} \\
&\quad - \frac{\sqrt{\gamma_{13}\gamma_{23}}}{\sqrt{2}(2\gamma_{13}+\gamma_{23})}[2\gamma_{13}+\gamma_{23}\cos\theta-2\gamma_{23}]\sigma^0_{+c}, \qquad (3.10e) \\
\dot{\sigma}^0_{+c} &= -\frac{\sqrt{2\gamma_{13}\gamma_{23}}}{(2\gamma_{13}+\gamma_{23})}[\gamma_{13}(1-\cos\theta)-\gamma_{23}]\sigma^0_{+uc} \\
&\quad - [2\gamma_{13}\gamma_{23}(1+\cos\theta)+4\gamma_{13}^2+3\gamma_{23}^2]\frac{\sigma^0_{+c}}{2(2\gamma_{13}+\gamma_{23})}. \qquad (3.10f)
\end{aligned}$$

The above equations were derived by neglecting terms rotating at $e^{\pm 2iG_{23}t}$ (secular approximation). Note that the above equations are not the usual rate equations because the diagonal elements are coupled with the off-diagonal elements as in (1.54). It is this coupling which leads to quasi-trapping even though σ^0_{ucuc} decays

at a rate

$$\Gamma_{uc} = \frac{4\gamma_{13}\gamma_{23}(\gamma_{13}+\gamma_{23})(1-\cos\theta)}{(2\gamma_{13}+\gamma_{23})^2}. \tag{3.11}$$

Also note that for small non-zero θ the decay from state $|uc\rangle$ is very small, which makes it a highly 'stable' state. We solve Eqs. (3.10) numerically with the initial condition $\sigma^0_{33}(0) = 1$. In Fig. 3.5 we plot the time evolution of the population in states $|+\rangle$, $|c\rangle$, and $|uc\rangle$. Note that both $|+\rangle$ and $|c\rangle$ decay very rapidly, while population gets accumulated in $|uc\rangle$. Here complete trapping will occur [$\sigma^0_{ucuc}(t \to \infty) = 1$] when $\Gamma_{uc} = 0$. This is not possible for the geometry shown in Fig. 3.1(b). However, we have a quasi-trapped-state for small θ.

It should be noted that trapped states were shown to occur in presence of VIC under several conditions [112, 114, 118, 119, 121]. Recently, new trapping states in the presence of VIC have been found for four-level systems [146, 147]. However, the QTS discussed above is due to a control field G_{23} coupling $|2\rangle \leftrightarrow |3\rangle$ transition and thus is *different* from all the previous works.

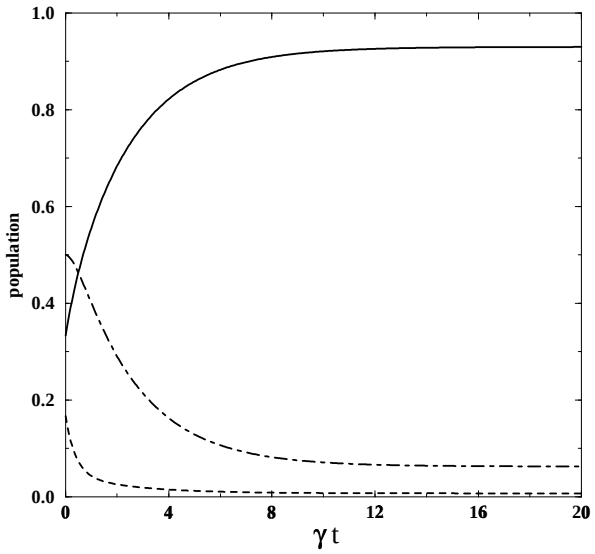

Figure 3.5: Time evolution of the atomic population in the states $|+\rangle$, $|c\rangle$, and $|uc\rangle$ when $\Delta_c = 0$, $\omega_{12} = -G_{23}$ and $\theta = 15^o$. The other parameters are $G_{23} = 20\gamma$, and $\gamma_{13} = \gamma_{23} = \gamma$. The solid curve represents σ^0_{ucuc}, the dashed curve is for σ^0_{cc} and the dot-dashed curve shows evolution of σ^0_{++}.

3.4 Effect of Quasi-Trapping on the Control Field

We now show the effect of the above trapping on the absorption and dispersion profiles of the control field. The trapping leads to an increase in the refractive index and drastically reduces the absorption of the control field. Various models in the past have demonstrated and discussed the importance of such a medium [86, 87, 88, 89]. However, in the present case we show how VIC can be used to control the refractive index of a medium. It is known that a large population difference between the dressed states can result in large dispersion with vanishing absorption [88]. For our system the population of dressed states depends on η and hence in principle we can get a situation where large population difference between dressed states can exist. Consider the case when $\Delta_c = 0$ and $\omega_{12} = -G_{23}$. The coherence σ_{23}^0 can be evaluated using Eqs. (3.2) and (3.6). The optical coherence to all orders in the control field is found to be

$$\begin{aligned}\sigma_{23}^0 &= [G_{23}^2\eta^2\{G_{23}^2(2\gamma_{13}+\gamma_{23})\gamma_{13}+(\eta^2-\gamma_{13}\gamma_{23})(\gamma_{13}+\gamma_{23})^2\} \\ &\quad +iG_{23}(\gamma_{13}\gamma_{23}-\eta^2)\{A\gamma_{23}-\eta^2\gamma_{13}(\gamma_{13}+\gamma_{23})^2\}]/B, \end{aligned} \tag{3.12}$$

where

$$\begin{aligned} A &= G_{23}^2\gamma_{23}^2+4G_{23}^2\gamma_{13}\gamma_{23}+\gamma_{13}^2\gamma_{23}^2+4G_{23}^2\gamma_{13}^2+2\gamma_{13}^3\gamma_{23}+\gamma_{13}^4, \\ B &= (\gamma_{13}\gamma_{23}-\eta^2)\{A(\gamma_{23}^2+2G_{23}^2)+\eta^2G_{23}^2\gamma_{13}(\gamma_{23}+2\gamma_{13})\}+\eta^2G_{23}^4(\gamma_{23}+2\gamma_{13})^2 \\ &\quad +\eta^2(\gamma_{13}+\gamma_{23})^2(3\gamma_{13}\gamma_{23}\eta^2-2\gamma_{13}^2\gamma_{23}^2-\eta^4). \end{aligned} \tag{3.13}$$

It is known that the $\mathrm{Re}(\sigma_{23}^0)$ corresponds to the dispersion and $\mathrm{Im}(\sigma_{23}^0)$ corresponds to absorption. When the alignment parameter θ is small, we have $\eta^2 \approx \gamma_{13}\gamma_{23}$ (for example when $\theta = 15^o$, $\eta^2 = 0.93\gamma_{13}\gamma_{23}$), then we can approximate (3.12) by

$$\sigma_{23}^0 \approx \frac{\gamma_{13}}{\gamma_{23}+2\gamma_{13}} + i\frac{(\gamma_{13}\gamma_{23}-\eta^2)\{A-\gamma_{13}^2(\gamma_{13}+\gamma_{23})^2\}}{G_{23}^3\gamma_{13}(\gamma_{23}+2\gamma_{13})^2}, \tag{3.14}$$

with the constraint that $G_{23} \neq 0$. Thus for $\gamma_{13} \gg \gamma_{23}$, one can have $\mathrm{Re}(\sigma_{23}^0)$ as high as 0.5, while the absorption remains low. In Fig. 3.6 we plot the absorption and dispersion parts of σ_{23}^0 as a function of detuning Δ_c/γ. For comparison, the dashed curves show the result in the absence of VIC. These curves are obtained from the steady state numerical solutions of (3.2) with $g_{13} = 0$. Note that in the presence of the VIC, there is a dip in the absorption and a peak in the dispersion

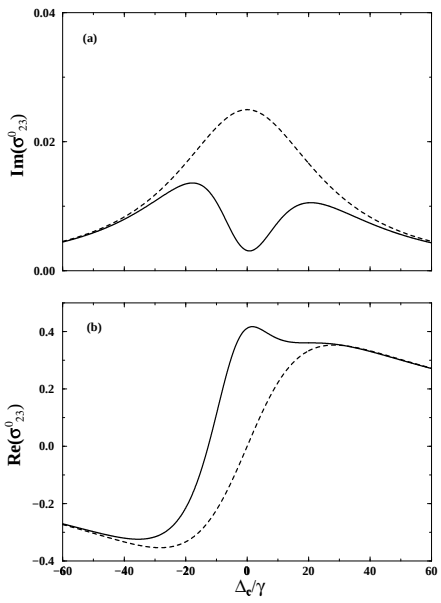

Figure 3.6: Plots show the absorption and dispersion curves for the control field in dimensionless units as a function of control detuning Δ_c/γ. The solid curves show the effect of VIC, $\theta = 15^o$, and the dashed curves are for $\theta = 90^o$. The parameters are $G_{23} = 20\gamma$, and $\gamma_{13} = 10\gamma$, $\gamma_{23} = \gamma$. For the solid curve $\omega_{12} = -G_{23}$.

curve. Due to trapping, most of the population tend to remain in states $|1\rangle$ and $|-\rangle$. For $\omega_{12} = -G_{23}$ and $\Delta_c = 0$ the population in the three dressed states and the coherence σ^0_{+-} were evaluated to be

$$\sigma^0_{11} = \frac{G^2_{23}\eta^2(\gamma_{13}+\gamma_{23})^2(\eta^2-\gamma_{13}\gamma_{23}) - G^4_{23}\eta^2\gamma_{23}(\gamma_{23}+2\gamma_{13})}{B}, \tag{3.15a}$$

$$\begin{aligned}\sigma^0_{--} = {} & \{(\gamma^2_{23}+2G^2_{23})A(\gamma_{13}\gamma_{23}-\eta^2) - \eta^2G^2_{23}(\gamma_{13}\gamma_{23}-\eta^2)(3\gamma^2_{23}+5\gamma_{13}\gamma_{23}+\gamma^2_{13}) \\ & +4G^4_{23}\eta^2\gamma_{13}\gamma_{23} + \eta^2(\gamma_{23}+\gamma_{13})^2(3\eta^2\gamma_{13}\gamma_{23} - 2\gamma^2_{13}\gamma^2_{23} - \eta^4)\}/2B,\end{aligned} \tag{3.15b}$$

$$\begin{aligned}\sigma^0_{++} = {} & (\gamma_{13}\gamma_{23}-\eta^2)\{A(\gamma^2_{23}+2G^2_{23}) + G^2_{23}\eta^2\gamma_{13}(\gamma_{23}+2\gamma_{13}) \\ & +\eta^2(\gamma_{13}+\gamma_{23})^2(G^2_{23} - 2\gamma_1\gamma_{23} + \eta^2)\}/2B,\end{aligned} \tag{3.15c}$$

$$\begin{aligned}\sigma^0_{+-} = {} & [(\eta^2-\gamma_{13}\gamma_{23})(A\gamma^2_{23} - G^2_{23}(\gamma^2_{23}+\gamma_{13}\gamma_{23}-\gamma^2_{13})\eta^2) - \eta^2(\gamma_{13}+\gamma_{23})^2(3\gamma_{13}\gamma_{23}\eta^2 \\ & -2\gamma^2_{13}\gamma^2_{23} - \eta^4) - 2iG_{23}(\eta^2-\gamma_{13}\gamma_{23})(A\gamma_{23} - \eta^2\gamma_{13}(\gamma_{13}+\gamma_{23})^2)]/2B,\end{aligned} \tag{3.15d}$$

which under the condition $\eta^2 \approx \gamma_{13}\gamma_{23}$ reduce to

$$\sigma^0_{11} \approx \frac{\gamma_{23}}{\gamma_{23}+2\gamma_{13}}, \quad \sigma^0_{--} \approx \frac{2\gamma_{13}}{\gamma_{23}+2\gamma_{13}}, \tag{3.16a}$$

$$\begin{aligned}\sigma^0_{++} \approx {} & (\gamma_{13}\gamma_{23}-\eta^2)\{A(\gamma^2_{23}+2G^2_{23}) + G^2_{23}\gamma^2_{13}\gamma_{23}(\gamma_{23}+2\gamma_{13}) \\ & +\gamma_{13}\gamma_{23}(\gamma_{13}+\gamma_{23})^2(G^2_{23} - \gamma_{13}\gamma_{23})\}/(2G^4_{23}\gamma_{13}\gamma_{23}(\gamma_{23}+2\gamma_{13})^2),\end{aligned} \tag{3.16b}$$

$$\mathrm{Im}(\sigma^0_{+-}) \approx \frac{(\gamma_{13}\gamma_{23}-\eta^2)\{A-\gamma_{13}^2(\gamma_{13}+\gamma_{23})^2\}}{G_{23}^3\gamma_{13}(\gamma_{23}+2\gamma_{13})^2}. \tag{3.16c}$$

Because of the factor $(\gamma_{13}\gamma_{23}-\eta^2)$, σ^0_{++} and $\mathrm{Im}(\sigma^0_{+-})$ are very small compared to σ^0_{11} and σ^0_{--}. One can equally write σ^0_{23} as

$$\sigma^0_{23} = (\sigma^0_{--}-\sigma^0_{++})/2 + i\mathrm{Im}(\sigma^0_{+-}), \qquad \text{at} \quad \Delta_c = 0. \tag{3.17}$$

Thus the *large difference in population between states* $|-\rangle$ *and* $|+\rangle$ *gives rise to the large dispersion*. This large difference of population arises because $|1\rangle$ and $|-\rangle$ form the QTS. When $\theta = 90^o$, we find from (3.15b), (3.15c) and (3.15d) that, $\sigma^0_{--} = \sigma^0_{++}$ and $\mathrm{Im}(\sigma^0_{+-}) \neq 0$. Thus the dispersion at $\Delta_c = 0$ is zero with substantial absorption which is consistent with the well known power-broadened absorption and dispersion profiles for a two-level atom.

3.5 Origin of Gain through Quasi-trapped-states

The origin of the Autler-Townes doublet in the absorption spectrum is well understood. The control field dresses the states $|2\rangle$ and $|3\rangle$. The absorption from the dressed states $|\pm\rangle$ leads to the Autler-Townes doublet. The situation changes drastically in presence of VIC which as shown in Sec. 3.3, for a suitable choice of parameters, leads to a quasi-trapped-state $|uc\rangle$. For $\Delta_c = 0$, $\omega_{12} = -G_{23}$, $\gamma_{13} = \gamma_{23}$ and small values of θ the dressed state $|+\rangle$ is almost empty whereas $\sigma^0_{--} > \sigma^0_{11}$ [Eq. (3.16a)]. Thus the probe can be absorbed in the transition $|-\rangle \rightarrow |1\rangle$ whereas the probe will experience gain in the transition $|1\rangle \rightarrow |+\rangle$. We also note that in principle the coherence between two dressed states $|\pm\rangle$ can also contribute to the gain [59]. As discussed in the Sec. 3.3 , the population in the states $|\pm\rangle$ and $|1\rangle$ depend on the angle θ between the two dipole matrix elements. For intermediate values of θ the population in $|1\rangle$ and $|+\rangle$ can be almost same. This can suppress one of the Autler-Townes components as shown by the solid curve in Fig. 3.3. When $\gamma_{23} > 2\gamma_{13}$, it is possible to have $\sigma^0_{11} > \sigma^0_{--}$ for small θ [see result (3.16a)]. Thus both the Autler-Townes components will show gain. This behavior is shown by the dot-dashed curve in Fig. 3.3.

3.6 Summary

In summary, we have studied the *non-degenerate* spectroscopy of the V systems in the presence of VIC effects. In Sec. 3.1 the basic working equations were derived. In Sec. 3.2 the numerical results were presented and comparisons were made with the usual Autler-Townes spectra in a V system. Here the possibility of controlled modification of the Autler-Townes spectra was also shown. In Sec. 3.3 the concept of Quasi-Trapped-States has been introduced, and results were explained in terms of quasi-trapping. We have shown that interference in the dressed basis gives rise to quasi-trapping. In Sec. 3.4 we have discussed a consequence of quasi-trapping on the control field. We have shown the possibility of a spectral region where refractive index is large, but absorption is minimum due to quasi-trapping. Finally, in Sec. 3.5 the gain in Autler-Townes components was explained in terms of quasi-trapped-states.

Chapter 4

Quantum Interferences and Thermodynamic Equilibrium

It is shown in section 1.3 that the quantum coherences can be created in interactions involving a common bath with a set of closely lying states. However, one would like to understand the role of coherences if the bath is at a finite temperature. At the outset one would not expect any coherences if the system is in thermodynamic equilibrium as the density matrix has the form $\exp(-\beta H)$ [$\beta = 1/KT$] which is clearly diagonal in a basis in which H is diagonal. But a microscopic derivation of the master equation for a system interacting with a heat bath does show the appearance of coherence terms in dynamical equations. Clearly, one needs to demonstrate the consistency of the dynamical equation with thermodynamic equilibrium. This then raises a very interesting question: What could be the observational consequence of such coherence terms in the master equation ? The present chapter deals with such aspects. Following the procedure discussed in section 1.3, we derive from first principles the dynamical equation for systems which exhibits coherences and which we show to be consistent with thermodynamic equilibrium.

4.1 Equations of Motion

We consider a collection of three-level atoms, the excited levels $|1\rangle$, $|2\rangle$ and ground level $|3\rangle$ (V system) in a bath of thermal field. Following Sec. 1.3 [see Eq. (1.49)]

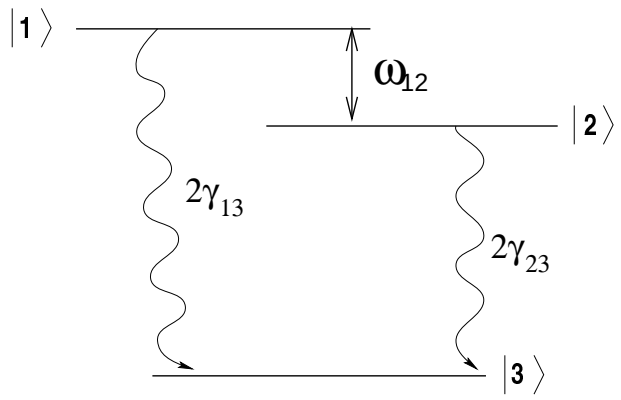

Figure 4.1: Schematic of a V system in a thermal bath. The γ's denote the spontaneous emission rates and the excited levels are assumed to be coupled via vacuum field.

the Hamiltonian for this system in the interaction picture and RWA will be

$$H_I = -\sum_{ks}[\{g_{ks}A_{13}e^{i\omega_{13}t} + f_{ks}A_{23}e^{i\omega_{23}t}\}a_{ks}e^{-i\omega_{ks}t} + \text{H.c.}]. \tag{4.1}$$

However, unlike in section 1.3, here the atoms are in thermal bath and the initial state of the radiation field is given by

$$\rho_R(0) = \frac{\exp\left(-\beta\sum\hbar\omega_{ks}a^\dagger_{ks}a_{ks}\right)}{\text{Tr}\left\{\exp\left(-\beta\sum\omega_{ks}a^\dagger_{ks}a_{ks}\right)\right\}}. \tag{4.2}$$

The master equation derived in the Born and Markov approximation reads as below:

$$\begin{aligned}\frac{\partial\rho}{\partial t} &= -i[\omega_{13}A_{11} + \omega_{23}A_{23}, \rho] - \Gamma_{13}[A_{11}\rho - A_{33}\rho_{11}] - \Gamma_{23}[A_{22}\rho - A_{33}\rho_{22}] \\ -\Gamma_{23}d_r\cos\theta[A_{12}\rho - A_{33}\rho_{21}] &- \frac{\Gamma_{13}\cos\theta}{d_r}[A_{21}\rho - A_{33}\rho_{12}] - \gamma_{13}n_1[A_{33}\rho - A_{11}\rho_{33}] \\ -\gamma_{23}n_2[A_{33}\rho - A_{22}\rho_{33}] &+ (\frac{\gamma_{13}n_1}{d_r} + \gamma_{23}n_2d_r)\cos\theta A_{21}\rho_{33} + \text{H.c.}\end{aligned} \tag{4.3}$$

Here $2\gamma_{j3} = 4|\vec{d}_{j3}|^2\omega^3_{j3}/3\hbar c^3$ $(j = 1, 2)$ is the natural line-width of the level $|j\rangle$ which comes due to the zero-point fluctuation of electromagnetic field, $n_j = (\exp[\beta\hbar\omega_{j3}] - 1)^{-1}$ is the mean number of thermal photons on the transition $|j\rangle \leftrightarrow |3\rangle$ at temperature T and, $\Gamma_j = \gamma_j(n_j + 1)$. The angle between the two dipole matrix elements $\vec{d}_{13}$, $\vec{d}_{23}$ is denoted as θ, and $d_r = |\vec{d}_{13}|/|\vec{d}_{23}|$. As discussed is section 1.3 the above master equation was derived without any secular approximation. The $\cos\theta$ terms in the above equation are the cross (interference) terms which arise due to the two

transitions $|1\rangle \leftrightarrow |3\rangle$ and $|2\rangle \leftrightarrow |3\rangle$ coupling with the same mode of the bath field. Unlike other chapters, for generality, here we do not approximate the interfering decay terms as $\sqrt{\Gamma_{13}\Gamma_{23}}$, as shown in section 1.3. The equations of motion for the various density matrix elements in Schrödinger picture are

$$\dot{\rho}_{11} = -2\Gamma_{13}\rho_{11} + 2\gamma_{13}n_1\rho_{33} - \Gamma_{23}d_r\cos\theta(\rho_{12}+\rho_{21}), \tag{4.4a}$$

$$\dot{\rho}_{22} = -2\Gamma_{23}\rho_{22} + 2\gamma_{23}n_2\rho_{33} - \frac{\Gamma_{13}\cos\theta}{d_r}(\rho_{12}+\rho_{21}), \tag{4.4b}$$

$$\begin{aligned}\dot{\rho}_{12} = &-[\Gamma_{13}+\Gamma_{23}+i\omega_{12}]\rho_{12} - \frac{\Gamma_{13}\cos\theta}{d_r}\rho_{11} - \Gamma_{23}d_r\cos\theta\rho_{22} \\ &+(\gamma_{23}d_r n_2 + \frac{\gamma_{13}n_1}{d_r})\cos\theta\rho_{33},\end{aligned} \tag{4.4c}$$

$$\dot{\rho}_{13} = -[\Gamma_{13}+\gamma_{23}n_2+\gamma_{13}n_1+i\omega_{13}]\rho_{13} - \Gamma_{23}d_r\cos\theta\rho_{23}, \tag{4.4d}$$

$$\dot{\rho}_{23} = -[\Gamma_{23}+\gamma_{13}n_1+\gamma_{23}n_2+i\omega_{23}]\rho_{23} - \frac{\Gamma_{13}\cos\theta}{d_r}\rho_{13}. \tag{4.4e}$$

Traditionally one has the rate equations for population and coherences as simple decay. In such cases in the long time limit, the density matrix is well known to be diagonal and the elements are given by Boltzmann factors. This is in accordance with what one expects in the case of thermodynamic equilibrium. However, in (4.4) the dynamics of the coherence ρ_{12} is coupled with the diagonal elements and vice versa. The crucial question is: *Does this system evolve into a thermodynamic equilibrium even in the presence of such coherences in the density matrix equations ?.*

4.2 Recovering Thermodynamic Equilibrium: Steady State Behavior

We evaluate the steady state for the set of equations (4.4). After a tedious calculation we arrive at the following simplified result.

$$\rho_{11} = \frac{\Gamma_{23}\gamma_{13}n_1}{(\Gamma_{13}\Gamma_{23}+\Gamma_{23}\gamma_{13}n_1+\Gamma_{13}\gamma_{23}n_2)}, \tag{4.5a}$$

$$\rho_{22} = \frac{\Gamma_{13}\gamma_{23}n_2}{(\Gamma_{13}\Gamma_{23}+\Gamma_{23}\gamma_{13}n_1+\Gamma_{13}\gamma_{23}n_2)}. \tag{4.5b}$$

The remaining elements are zero. A clear demonstration of thermodynamic equilibrium can be seen by taking the ratio of populations,

$$\frac{\rho_{11}}{\rho_{22}} = \frac{\exp\left[-\beta\hbar\omega_{13}\right]}{\exp\left[-\beta\hbar\omega_{23}\right]}, \tag{4.6}$$

which is in accordance with Boltzmann distribution. Note that one arrives at the same set of results (4.5) even in the absence of interference terms. This essentially means that, though the system may evolve in a different way, in steady state, the thermodynamic equilibrium is obtained even in the presence of coherence terms in the master equation. To show that the steady state conditions are the same both in the presence and in the absence of interference, we measure the entropy of the system. The entropy is defined as

$$S(t) = -\sum_{i=1}^{3} \Lambda_i \ln \Lambda_i, \tag{4.7}$$

where Λ_i's are the eigenvalues of the density matrix ρ. At $t = 0$ we have $\rho_{33}(0) = 1$, which is a pure state and the entropy will be zero. To numerically evaluate the entropy we make a canonical transformation of $\rho_{j3} \equiv \bar{\rho}_{j3} \exp[-i(\omega_{13} + \omega_{23})t/2]$ $(j = 1, 2)$ in equations (4.4). Note in Fig. 4.2 that both in the presence and in the absence of interference, the system evolves to the same value of entropy. We have also verified that the time derivative of entropy continuously decreases.

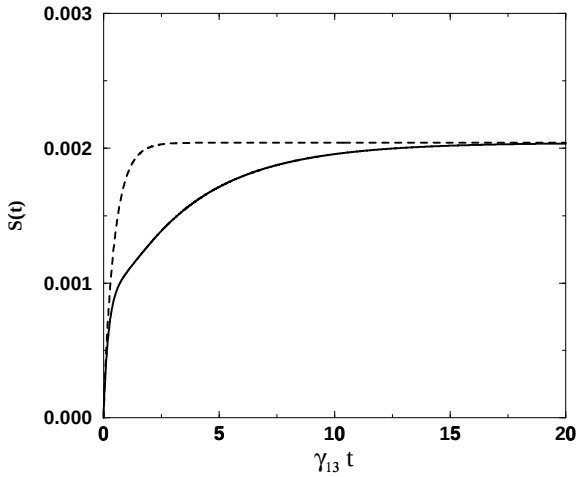

Figure 4.2: Figure shows the dynamical evolution of entropy. The parameters are $\gamma_{13} = \gamma_{23} = \omega_{12}$, $n_1 = n_2 = 10^{-5}$, and $d_r = 1$. The solid line is in the presence of interference ($\theta = 0^o$) and the dashed curve is in the absence ($\theta = 90^o$). In both the cases the long time behaviors are same.

Note that the time taken to reach the equilibrium value is more in the presence of interference. This happens because the interference terms pump the system back to excited levels, and thus the populations decay with an effective life time which is more than the life time in the absence of interference. We note here that the

analysis of Savchenko et al. [125] based on Green's functions seems to imply the existence of coherence under equilibrium conditions. We have shown above that though non-diagonal elements are present in the equations for populations, they do not contribute in steady state. In Appendix C we show that, in general, for the non-degenerate multilevel atoms in a thermal bath, the steady state populations are given by Boltzmann factors.

An exception to the above occurs for the degenerate case, $\omega_{12} = 0$, which is ambiguous when $\theta = 0^o$. A unique straightforward steady state solution of equations (4.4) does not exist. In fact, ρ_{11} and ρ_{22} remain arbitrary. This situation arises because there exists a constant of motion in this case [112]. Consider the states

$$|uc\rangle = \frac{|\vec{d}_{23}||1\rangle - |\vec{d}_{13}||2\rangle}{d}, \qquad |c\rangle = \frac{|\vec{d}_{13}||1\rangle + |\vec{d}_{23}||2\rangle}{d}, \tag{4.8}$$

where $d^2 = |\vec{d}_{13}|^2 + |\vec{d}_{23}|^2$. It is easy to see that $\rho_{ucuc}(t) = p_0$ where p_0 is a constant. In general the steady state solution is given by

$$\rho_{11} = \rho_{22} = \frac{n(1+p_0)+p_0}{2(1+2n)}, \qquad \rho_{12} = \frac{n(1-3p_0)-p_0}{2(1+2n)}, \qquad 0 \leq p_0 \leq 1, \tag{4.9}$$

where $n_1 = n_2 = n$. Clearly, a unique steady state solution exists for a given value of p_0. The above result may seem to violate equilibrium conditions, but it is not surprising as the state $|uc\rangle$ is *decoupled* from the bath. Thus if we initially start with $p_0 = 1$, then the system always remains in $|uc\rangle$. The state $|uc\rangle$ is an example of a trapped state [32] and is very much of current interest in the context of quantum computing using decoherence free subspace [148]. However, there are other situations where the steady state could be different from the one determined by thermodynamic equilibrium. An example is given below.

Asymmetric treatment of spontaneous vs stimulated processes

The decays Γ_{13}, Γ_{23} contain the contribution of both spontaneous (γ_{13}, γ_{23}) and stimulated ($\gamma_{13}n_1$, $\gamma_{23}n_2$) emission processes. Thus the interference exists in both these processes. If we associate a parameter a for interference in stimulated emission and b for interference in spontaneous emission, the master equation in

this case will be

$$\frac{\partial\rho}{\partial t} = -i[\omega_{13}A_{11} + \omega_{23}A_{22}, \rho] - \Gamma_{13}[A_{11}\rho - A_{33}\rho_{11}] - \Gamma_{23}[A_{22}\rho - A_{33}\rho_{22}]$$
$$-\gamma_{23}(an_1 + b)d_r\cos\theta[A_{12}\rho - A_{33}\rho_{21}] - \frac{\gamma_{13}(an_1 + b)\cos\theta}{d_r}[A_{21}\rho - A_{33}\rho_{12}]$$
$$-\gamma_{13}n_1[A_{33}\rho - A_{11}\rho_{33}] - \gamma_{23}n_2[A_{33}\rho - A_{22}\rho_{33}]$$
$$+a(\frac{\gamma_{13}n_1}{d_r} + \gamma_{23}n_2d_r)\cos\theta A_{21}\rho_{33} + \text{H.c.} \tag{4.10}$$

It implies that $a = 0, b = 1$ would mean interference only in spontaneous process and $a = 1, b = 0$ would mean interference only in stimulated process. Such a segregation is not just of theoretical interest, but we will show later that there are other kinds of baths where such conditions can be realized. However for a thermal field, a correct physical situation would imply either $a = b = 1$ or $a = b = 0$. It turns out that the neglect of any one interference term (a or b) results in a steady state, which is at variance from thermal equilibrium. We found the following steady state when $a = 0, b = 1$.

$$\rho_{11} = \{((\Gamma_{13} + \Gamma_{23})^2 + \omega_{12}^2)\Gamma_{23}\gamma_{13}n_1$$
$$+\gamma_{23}\cos^2\theta(\Gamma_{13} + \Gamma_{23})(\gamma_{23}^2d_r^2n_2 - \gamma_{13}^2n_1)\}/D_1, \tag{4.11a}$$
$$\rho_{22} = \{((\Gamma_{13} + \Gamma_{23})^2 + \omega_{12}^2)\Gamma_{13}\gamma_{23}n_2$$
$$+\gamma_{13}\cos^2\theta(\Gamma_{13} + \Gamma_{23})(\frac{\gamma_{13}^2n_1}{d_r^2} - \gamma_{23}^2n_2)\}/D_1, \tag{4.11b}$$
$$\rho_{12} = \frac{-(\Gamma_{13} + \Gamma_{23} - i\omega_{12})(\Gamma_{13}\gamma_{23}^2n_2d_r + \Gamma_{23}\frac{\gamma_{13}^2n_1}{d_r})\cos\theta}{D_1}, \tag{4.11c}$$

where

$$D_1 = \{(\Gamma_{13} + \Gamma_{23})^2 + \omega_{12}^2)(\Gamma_{13}\Gamma_{23} + \Gamma_{23}\gamma_{13}n_1 + \Gamma_{13}\gamma_{23}n_2) - \gamma_{13}\gamma_{23}\cos^2\theta(\Gamma_{13} + \Gamma_{23})^2$$
$$-(\Gamma_{13} + \Gamma_{23})\cos^2\theta(\gamma_{23}d_r^2 - \gamma_{13})(\frac{\gamma_{13}^2n_1}{d_r^2} - \gamma_{23}^2n_2)\}.$$

When $a = 1, b = 0$ we find:

$$\rho_{11} = \{((\Gamma_{13} + \Gamma_{23})^2 + \omega_{12}^2)\Gamma_{23}\gamma_{13}n_1 - \gamma_{13}n_1\gamma_{23}n_2\cos^2\theta(\Gamma_{13} + \Gamma_{23})$$
$$\times(\Gamma_{23} + \gamma_{13}n_1 + \frac{\gamma_{23}^2d_r^2n_2}{\gamma_{13}n_1})\}/D_2, \tag{4.12a}$$
$$\rho_{22} = \{((\Gamma_{13} + \Gamma_{23})^2 + \omega_{12}^2)\Gamma_{13}\gamma_{23}n_2 - \gamma_{13}n_1\gamma_{23}n_2(\Gamma_{13} + \Gamma_{23})\cos^2\theta$$
$$\times(\Gamma_{13} + \gamma_{23}n_2 + \frac{\gamma_{13}^2n_1}{\alpha^2\gamma_{23}n_2})\}/D_2, \tag{4.12b}$$
$$\rho_{12} = \frac{(\Gamma_{13} + \Gamma_{23} - i\omega_{12})(\Gamma_{23}\frac{\gamma_{13}^2n_1}{d_r} + \Gamma_{13}\gamma_{23}^2n_2d_r)\cos\theta}{D_2}, \tag{4.12c}$$

where

$$D_2 = \{((\Gamma_{13}+\Gamma_{23})^2+\omega_{12}^2)(\Gamma_{13}\Gamma_{23}+\Gamma_{13}\gamma_{23}n_2+\Gamma_{23}\gamma_{13}n_1)-(\Gamma_{13}+\Gamma_{23}) \times\gamma_{13}n_1\gamma_{23}n_2(2\Gamma_{13}+2\Gamma_{23}+\gamma_{13}n_1+\gamma_{23}n_2+\frac{\gamma_{13}^2 n_1}{\gamma_{23}n_2 d_r^2}+\frac{\gamma_{23}^2 d_r^2 n_2}{\gamma_{13}n_1})\cos^2\theta\}.$$

In both the cases the *steady state coherence* among excited levels is *non-zero*. In Fig. 4.3 we show the dynamics of $|\rho_{12}|$ for various values of a and b. We take the initial state as $|3\rangle$. Thus for $a = b = 0$, $\rho_{12}(t) = 0$. As seen in the Fig. 4.3, for $a = b = 1$ the *steady state coherence is absent*. In the case of asymmetric treatment, equilibrium conditions are violated.

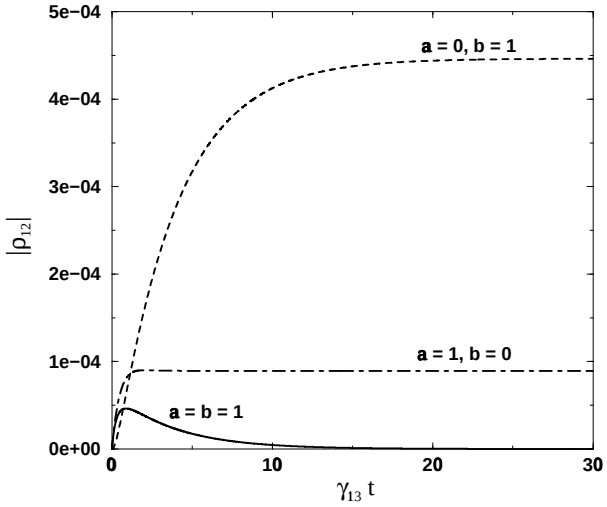

Figure 4.3: Plotted are the absolute values of coherence ρ_{12} as a function of time. The parameters are as in Fig. 4.2.

We now explain why thermodynamic equilibrium does not permit such an asymmetric treatment. We note that the emission (absorption) processes are determined by the antinormally ordered (normally ordered) correlation functions of the electromagnetic field. In thermodynamic equilibrium both these correlations are connected via the *fluctuation-dissipation* theorem and therefore both stimulated and spontaneous processes are to be treated on the same footing. In order to treat them asymmetrically one needs extra freedom and we show in Sec. 4.4 that pumping by broadband lasers provides such a freedom.

4.3 Interference in Emission Spectrum via Thermal Bath

In the previous section we showed that the long time effect of coherence on atomic variables is absent. In this section, we show the effect of coherence on the emitted radiation. We derive the emission spectrum and show the existence of a dark line as a result of atomic coherence via decay terms.

All the nine elements of ρ can be written in a compact matrix equation as below

$$\frac{\partial \Psi}{\partial t} = M\Psi, \tag{4.13}$$

where

$$\Psi^{\dagger} = [\rho_{11},\ \rho_{12},\ \rho_{13},\ \rho_{21},\ \rho_{22},\ \rho_{23},\ \rho_{31},\ \rho_{32},\ \rho_{33}]\,, \tag{4.14}$$

and M is a 9×9 matrix corresponding to the coefficients of ρ in (4.4). The positive frequency part of the radiated electric field operator at a distance $|r|\hat{r}$, in the far field region is given by

$$E^{+}(\vec{r},t) = -\frac{\omega_{13}^2}{c^2 r}[\hat{r}\times\hat{r}\times\vec{d}_{13}]A_{31}(t)e^{-ikr} - \frac{\omega_{23}^2}{c^2 r}[\hat{r}\times\hat{r}\times\vec{d}_{23}]A_{32}(t)e^{-ikr}. \tag{4.15}$$

The emission spectrum is given by

$$\mathcal{S}(\omega) = \lim_{t\to\infty}\int_0^{\infty} \mathrm{Re}\{\exp(-i\omega\tau)\langle E^{-}(t+\tau)\cdot E^{+}(t)\rangle\}d\tau, \tag{4.16}$$

and the two-time field correlation is

$$\begin{aligned}\langle E^{-}(\vec{r},t+\tau)\cdot E^{+}(\vec{r},t)\rangle = \\ \frac{\omega_{13}^4|\vec{d}_{13}|^2\sin^2\phi_1}{c^4r^2}\langle A_{13}(t+\tau)A_{31}(t)\rangle + \frac{\omega_{23}^4|\vec{d}_{23}|^2\sin^2\phi_2}{c^4r^2}\langle A_{23}(t+\tau)A_{32}(t)\rangle \\ +\frac{\omega_{23}^2\omega_{13}^2|\vec{d}_{23}||\vec{d}_{13}|}{c^4r^2}(\cos\theta-\cos\phi_1\cos\phi_2)\{\langle A_{23}(t+\tau)A_{31}(t)\rangle + \langle A_{13}(t+\tau)A_{32}(t)\rangle\}.\end{aligned} \tag{4.17}$$

Here ϕ_1, ϕ_2 are the angles between $\hat{r}$ and $\vec{d}_{13}$, $\vec{d}_{23}$, respectively. From (4.13) we can write

$$\Psi(t+\tau) = L(\tau)\Psi(t), \tag{4.18}$$

where the matrix $L(\tau) = \exp(M\tau)$ and the elements of $\Psi(t)$ are given in (4.14). Using equation (4.18) and regression theorem [7] we find the two time correlation functions in the limit $t\to\infty$ as below:

$$\begin{aligned}\langle A_{13}(t+\tau)A_{31}(t)\rangle &= L_{77}(\tau)\rho_{11}(\infty), \qquad \langle A_{13}(t+\tau)A_{32}(t)\rangle = L_{78}(\tau)\rho_{22}(\infty),\\ \langle A_{23}(t+\tau)A_{32}(t)\rangle &= L_{88}(\tau)\rho_{22}(\infty), \qquad \langle A_{23}(t+\tau)A_{31}(t)\rangle = L_{87}(\tau)\rho_{11}(\infty).\end{aligned}$$

The elements of matrix L required for the above expression are given by $L_{77}(\tau) = \rho_{31}(\tau)$, $L_{87}(\tau) = \rho_{32}(\tau)$, solved with the initial condition $\rho_{31}(0) = 1$, and $L_{88}(\tau) = \rho_{32}(\tau)$, $L_{87}(\tau) = \rho_{31}(\tau)$, with the initial condition $\rho_{32}(0) = 1$. Taking one-sided Fourier transform we get

$$L_{77}(\omega) = \frac{(\Gamma_{23} + \gamma_{13}n_1 + \gamma_{23}n_2 - i(\delta_{\rm em} - \omega_{12}/2))}{D_3}, \tag{4.19a}$$

$$L_{78}(\omega) = \frac{-\Gamma_{23}\alpha\cos\theta}{D_3}, \tag{4.19b}$$

$$L_{88}(\omega) = \frac{(\Gamma_{13} + \gamma_{13}n_1 + \gamma_{23}n_2 - i(\delta_{\rm em} + \omega_{12}/2))}{D_3}, \tag{4.19c}$$

$$L_{87}(\omega) = \frac{-\Gamma_{13}\cos\theta/\alpha}{D_3}, \tag{4.19d}$$

where

$$\begin{aligned} D_3 = {} & (\Gamma_{13} + \gamma_{13}n_1 + \gamma_{23}n_2 - i(\delta_{\rm em} + \omega_{12}/2)) \\ & \times(\Gamma_{23} + \gamma_{13}n_1 + \gamma_{23}n_2 - i(\delta_{\rm em} - \omega_{12}/2)) - \Gamma_{13}\Gamma_{23}\cos^2\theta, \end{aligned}$$

and $\delta_{\rm em} = (\omega_{13} + \omega_{23})/2 - \omega$ is the detuning of the emitted radiation with respect to the center of the two excited levels. The final expression for the spectrum is

$$\begin{aligned} \mathcal{S}(\omega) = {} & {\rm Re}\left[\frac{\omega_{13}^4|\vec{d}_{13}|^2}{c^4r^2}\sin^2\phi_1 L_{77}(\omega)\rho_{11} + \frac{\omega_{23}^4|\vec{d}_{23}|^2}{c^4r^2}\sin^2\phi_2 L_{88}(\omega)\rho_{22}\right. \\ & \left. + \frac{\omega_{13}^2\omega_{23}^2|\vec{d}_{13}||\vec{d}_{23}|}{c^4r^2}(\cos\theta - \cos\phi_1\cos\phi_2)\{L_{78}(\omega)\rho_{22} + L_{87}(\omega)\rho_{11}\}\right]. \end{aligned} \tag{4.20}$$

Here ρ's denote the steady state value. The first two terms above denote the emission from the two excited levels and the last term is due to interference. If we take the ratio $\omega_{13}/\omega_{23} \approx 1$ and assume that the difference $\Gamma_{13} - \Gamma_{23}$ is negligible, the spectrum can be written in a simpler form as a sum of Lorentzian and dispersive contributions as below:

$$\begin{aligned} \mathcal{S}(\omega)/C = {} & A_+\left[\frac{\gamma_0}{(\delta_{\rm em} + \omega_0)^2 + \gamma_0^2)}\right] + A_-\left[\frac{\gamma_0}{(\delta_{\rm em} - \omega_0)^2 + \gamma_0^2)}\right] \\ & + B\left[\frac{\delta_{\rm em} - \omega_0}{(\delta_{\rm em} - \omega_0)^2 + \gamma_0^2} - \frac{\delta_{\rm em} + \omega_0}{(\delta_{\rm em} + \omega_0)^2 + \gamma_0^2}\right], \end{aligned} \tag{4.21}$$

where we take $\phi_1 = \phi_2 = \pi/2$, $A_\pm = \{\gamma_{13}(2\omega_0 \mp \omega_{12})\rho_{11} + \gamma_{23}(2\omega_0 \pm \omega_{12})\rho_{22}]\}/4\omega_0$, $B = \{(\Gamma_{13}\gamma_{23}\rho_{11} + \Gamma_{23}\gamma_{13}\rho_{22})\cos^2\theta\}/2\omega_0$. Here $\omega_0 = \sqrt{(\omega_{12}^2 - 4\Gamma_{13}\Gamma_{23}\cos^2\theta)}/2$, $\gamma_0 = (\Gamma_{13} + \Gamma_{23})/2 + \gamma_{13}n_1 + \gamma_{23}n_2$, and $C = 3\hbar\omega_{13}/2cr^2$. The above result (4.21) is valid

for $\omega_{12} > 2\sqrt{\Gamma_{13}\Gamma_{23}}\cos\theta$. Note that the interference terms appear as dispersive contributions which is a general feature observed among such interference effects [71]. A deviation from this behavior can be seen in certain cases, as observed here, when $\omega_{12} < 2\sqrt{\Gamma_{13}\Gamma_{23}}\cos\theta$. The spectrum in this case will be

$$\begin{aligned}\mathcal{S}(\omega)/C &= B_+\left[\frac{\gamma_0+\gamma'}{\delta_{\rm em}^2+(\gamma_0+\gamma')^2}\right]+B_-\left[\frac{\gamma_0-\gamma'}{\delta_{\rm em}^2+(\gamma_0-\gamma')^2}\right]\\ &\quad+\frac{(\gamma_{23}\rho_{22}-\gamma_{13}\rho_{11})\omega_{12}}{4\gamma'}\left[\frac{\delta_{\rm em}}{\delta_{\rm em}^2+(\gamma_0-\gamma')^2}-\frac{\delta_{\rm em}}{(\delta_{\rm em}^2+(\gamma_0+\gamma')^2}\right], \quad (4.22)\end{aligned}$$

where $B_\pm = \{\gamma'\gamma_{13}\rho_{11}+\gamma'\gamma_{23}\rho_{22} \pm (\Gamma_{13}\gamma_{23}\rho_{11}+\Gamma_{23}\gamma_{13}\rho_{22})\cos^2\theta\}/2\gamma'$ and $\omega_0 = i\gamma'$.

Here even the interference terms appear as Lorentzian. In both the cases the contribution of interference is a sharp dip in the spectrum at averaged frequency of the two excited levels. Thus in the presence of interference the two levels can be resolved even when the two excited levels have separation much less than their line-width. We show the spectrum both in the presence and in the absence of interference in Fig. 4.4. The dark line (at $\delta_{\rm em} = 0$) in the spectrum is the observational effect of interference which arises for the system in thermodynamic equilibrium. For $\gamma_{13} = \gamma_{23} = \gamma$, $n_1 = n_2 = n$ at $\delta_{\rm em} = 0$ the spectrum is proportional

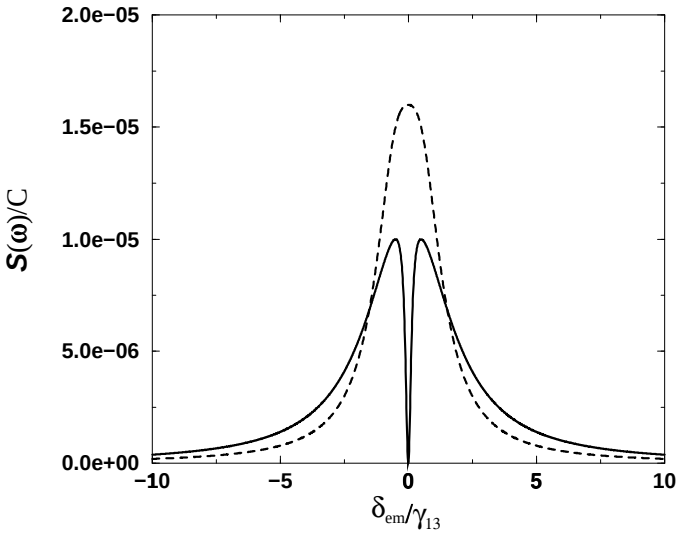

Figure 4.4: The emission spectrum is plotted in dimensionless units. The parameters are $\gamma_{13} = \gamma_{23}$, $\omega_{12} = \gamma_{13}$, $n_1 = n_2 = 10^{-5}$. The solid curve is for $\theta = 0^o$ and the dashed curve for $\theta = 90^o$.

to

$$\mathcal{S}(\omega)/C = \frac{4\gamma^2 n^2}{(1+3n)(\gamma_0^2+\omega_0^2)}, \tag{4.23}$$

when $\theta = 0^o$. Thus the observation of dark line at $\delta_{\rm em} = 0$ depends on n. The smaller the value of n, the better will be the observed interference effect.

4.4 Interference Effects via Broadband Pumping

We have shown earlier that an asymmetric treatment of spontaneous emission and stimulated emission could lead to a variety of different steady states. However, this is not valid for interaction with a thermal bath. We now show that there are other types of baths where such situations could be realized in practice. Consider, for example, the pumping by a broadband pumping laser, where the field is given by

$$\vec{E}(t) = \hat{\epsilon}_1 \varepsilon(t) e^{-i\omega_1 t} + \text{c.c.}, \tag{4.24}$$

and the field amplitude is delta-correlated, $\langle \varepsilon(t)\varepsilon^*(t-\tau)\rangle = 2R\delta(\tau)$. The pumping field is polarized along $\hat{\epsilon}_1$. Below we show the two cases which correspond to $a = 1, b = 0$ and $a = 0, b = 1$ as in Sec. 4.2.

Case I: a = 1, b = 0. As discussed in Sec. 4.2 this would correspond to no interference in spontaneous emission, while interference in stimulated process persists. For this we consider the dipole matrix elements as orthogonal ($\vec{d}_{23} \perp \vec{d}_{13}$). We take a single broadband field, polarized along $\hat{\epsilon}_1$, which makes an angle Φ_1 with $\vec{d}_{13}$ and the central frequency tuned midway between the two excited levels. The master equation for such a bath, in Schrödinger picture can be derived as below.

$$\begin{aligned}\frac{\partial \rho}{\partial t} &= -i[\omega_{13}A_{11} + \omega_{23}A_{22}, \rho] - (\gamma_{13}+p_1)[A_{11}\rho - A_{33}\rho_{11}] \\ &\quad -(\gamma_{23}+p_2)[A_{22}\rho - A_{33}\rho_{22}] - p_1[A_{33}\rho - A_{11}\rho_{33}] - p_2[A_{33}\rho - A_{22}\rho_{33}] \\ &\quad +2\sqrt{p_1 p_2}A_{21}\rho_{33} - \sqrt{p_1 p_2}[A_{12}\rho + A_{21}\rho - A_{33}\rho_{12} - A_{33}\rho_{21}] + \text{H.c.},\end{aligned} \tag{4.25}$$

where $2p_j = 2R|\vec{d}_{j3}\cdot\hat{\epsilon}_1|^2/\hbar^2$, $(j = 1, 2)$ is the radiative broadening due to the pumping field. For simplicity we have taken the dipole matrix elements as real. Note from the equation (4.25) that $\sqrt{p_1 p_2}$ terms are the new coherence terms. This coherence arises due to a polarized broadband field coupling to both the transitions. The

coherence will be important for separation ω_{12} less than the spectral width of the pumping field [87, 117]. Here the interference in spontaneous emission is absent.

Case II: a = 0, b = 1. This would correspond to a situation where interference in stimulated emission is absent, but interference in spontaneous emission is present. Consider a situation where dipole matrix elements are at an angle θ where $\theta \neq 0, \pi/2$. Both the transitions are now pumped by two different broadband fields of the same central frequency ω_1, but of different polarizations $\hat{\epsilon}_1$ and $\hat{\epsilon}_2$ such that $\vec{d}_{23} \cdot \hat{\epsilon}_1 = 0$ and $\vec{d}_{13} \cdot \hat{\epsilon}_2 = 0$ [131, 145]. This would imply that we have two different pumping strengths along the two arms of the V system given by $2p_j = 2R|\vec{d}_{j3} \cdot \hat{\epsilon}_j|^2/\hbar^2$, $(j = 1, 2)$. Further, if the pumping fields $\hat{\epsilon}_1$ and $\hat{\epsilon}_2$ are uncorrelated then the master equation will be

$$\begin{aligned}\frac{\partial \rho}{\partial t} &= -i[\omega_{13}A_{11} + \omega_{23}A_{22}, \rho] - (\gamma_{13} + p_1)[A_{11}\rho - A_{33}\rho_{11}] \\ &\quad -(\gamma_{23} + p_2)[A_{22}\rho - A_{33}\rho_{22}] - p_1[A_{33}\rho - A_{11}\rho_{33}] - p_2[A_{33}\rho - A_{22}\rho_{33}] \\ &\quad -\sqrt{\gamma_{13}\gamma_{23}}\cos\theta[A_{12}\rho + A_{21}\rho - A_{33}\rho_{12} - A_{33}\rho_{21}] + \text{H.c.}, \end{aligned} \tag{4.26}$$

which clearly has else interference in spontaneous emission. For simplifying the interference term, we have taken $\omega_{13}/\omega_{23} \approx 1$.

In both the above cases either spontaneous or stimulated emission has interference. Thus as seen in Sec. 4.2, steady state coherence will be present. If we consider a single, unpolarized, broadband pumping field and nonorthogonal dipole matrix elements, then that will correspond to a situation $a = b = 1$. The observational effect will be a dark line in the emission spectrum as seen in the case of thermal equilibrium. In the case of asymmetric treatment, the observational effects will vary due to the steady state coherence. The dark line arises only for the case of symmetric treatment of spontaneous vs stimulated emission (results not shown).

4.5 Summary

In summary, the consistency of thermal bath induced interference effect with thermodynamic equilibrium has been shown above. In Sec. 4.1 the microscopic equations of motion have been derived for a V system in a thermal bath. We have shown that under appropriate situation interference terms arise in the density matrix equations due to thermal field. In Sec. 4.2 the steady state solutions

of density matrix equations were obtained and the consistency of interference phenomenon with thermodynamic equilibrium has been shown. We have calculated the entropy of the system. In the long time limit entropy is same both in the presence and absence of interference. We have also explained the situations where thermodynamic equilibrium can be violated. We have shown that both spontaneous and stimulated processes should be treated on equal footing for compatibility with thermodynamic principles. In Sec. 4.3 we have shown the effect of interference term in the emission spectrum. We have given analytical expression for the emission spectrum and have shown the presence of a dark line in the emission spectrum due to interference. Finally, in Sec. 4.4 we have considered the case of a broadband pumping instead of a thermal field. We have shown that one can selectively have interference in either spontaneous emission or in stimulated emission. This is an example where coherences exist even under steady state conditions.

Chapter 5

Probing the Vacuum Induced Coherence in the Λ systems

Unlike the V systems, studies of VIC effects in the Λ systems are limited to few cases [126, 127]. In the Λ systems as shown in Sec. 1.3 the coherence is created between the two ground levels. We show below that because of this reason, VIC effect is not observed in the spontaneous emission spectrum of the Λ systems. The aim of the present chapter is to show the origin and consequence of VIC in the Λ systems. We also present a four-level model for probing VIC in a Λ system.

5.1 Origin of VIC in Λ Systems

Consider the Λ system as shown in Fig. 5.1. Following (1.57) the density matrix elements in the Schrödinger picture obey the equations

$$\dot{\rho}_{11} = -2\Gamma_1\rho_{11}, \quad \dot{\rho}_{22} = 2\gamma_{12}\rho_{11}, \tag{5.1a}$$

$$\dot{\rho}_{12} = -(\Gamma_1 + i\omega_{12})\rho_{12}, \quad \dot{\rho}_{13} = -(\Gamma_1 + i\omega_{13})\rho_{13}, \tag{5.1b}$$

$$\dot{\rho}_{23} = -i\omega_{23}\rho_{23} + 2\sqrt{\gamma_{12}\gamma_{13}}\cos\theta_1\rho_{11}, \tag{5.1c}$$

where $\Gamma_1 = \gamma_{12} + \gamma_{13}$, and θ_1 is the angle between the dipole matrix elements $\vec{d}_{12}$ and $\vec{d}_{13}$. Note that the equation for the ground state coherence ρ_{23} is coupled to the population of the excited state. Solving for the coherence ρ_{23} with the initial population in $|1\rangle$, we get

$$\rho_{23}(t) = \frac{2\sqrt{\gamma_{12}\gamma_{13}}\cos\theta_1(e^{-i\omega_{23}t} - e^{-2\Gamma_1 t})}{(2\Gamma_1 - i\omega_{23})}. \tag{5.2}$$

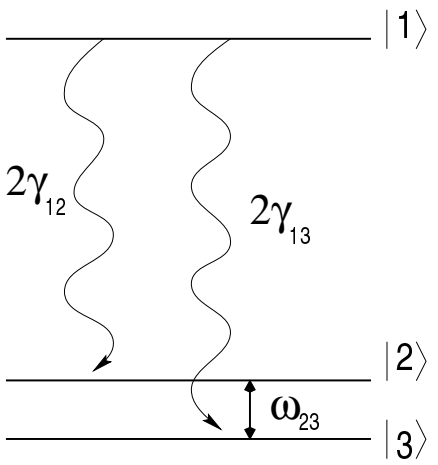

Figure 5.1: Schematic diagram of a three-level Λ system. The γ's denote the spontaneous emission rates and $\hbar\omega_{23}$ is the separation between the two ground levels.

As the equation reads, this coherence is non-zero as a result of interference term. Even in the long time limit ($t \gg 1/\Gamma_1$) this coherence is finite and oscillates with a frequency ω_{23}

$$\rho_{23}(t \to \infty) = \frac{2\sqrt{\gamma_{12}\gamma_{13}}\cos\theta_1 e^{-i\omega_{23}t}}{(2\Gamma_1 - i\omega_{23})}. \tag{5.3}$$

The magnitude of this coherence is especially significant when $\omega_{23} \leq 2\Gamma_1$ and if the dipole matrix elements are parallel. We next address the questions: (a) What leads to the coherence (5.2), and (b) how such a coherence can be measured ?

In the long time limit, the non-zero density matrix in (5.1) will be

$$\rho_{22} = \gamma_{12}/\Gamma_1, \quad \rho_{33} = \gamma_{13}/\Gamma_1, \quad \rho_{23} = \sqrt{\rho_{22}\rho_{33}}B, \tag{5.4}$$

where $B = 2\Gamma_1\cos\theta_1/(2\Gamma_1 - i\omega_{23})$. The oscillation in ρ_{23} has been removed by writing it in the interaction picture. Thus the density matrix ρ can be reduced to an effective matrix $\tilde{\rho}$, where

$$\tilde{\rho} = \begin{bmatrix} \rho_{22} & \rho_{23} \\ \rho_{32} & \rho_{33} \end{bmatrix} \equiv \begin{bmatrix} \rho_{22} & \sqrt{\rho_{22}\rho_{33}}B \\ \sqrt{\rho_{22}\rho_{33}}B^* & \rho_{33} \end{bmatrix}. \tag{5.5}$$

To measure the purity of the state, we calculate $\mathrm{Tr}(\tilde{\rho}^2)$:

$$\mathrm{Tr}(\tilde{\rho}^2) = \frac{\gamma_{12}^2 + \gamma_{13}^2}{\Gamma_1^2} + \frac{8\gamma_{12}\gamma_{13}\cos^2\theta_1}{(4\Gamma_1^2 + \omega_{23}^2)}. \tag{5.6}$$

For $\omega_{23} = 0$ and $\cos\theta_1 = 1$, we get

$$\mathrm{Tr}(\tilde{\rho}^2) = 1, \tag{5.7}$$

which means that the atom would be in a pure state when the VIC is maximum. Generally, one would find the system in a mixed state [$\mathrm{Tr}(\tilde{\rho}^2) < 1$] as $|B| \neq 1$. The entropy of the final state depends on the parameter B.

The case when the atom is left in a pure state is especially interesting as we can introduce the coupled ($|c\rangle$) and uncoupled ($|uc\rangle$) states given by

$$|c\rangle = \frac{|d_{12}||2\rangle + |d_{13}||3\rangle}{|d|}, \qquad |uc\rangle = \frac{|d_{13}||2\rangle - |d_{12}||3\rangle}{|d|}, \tag{5.8}$$

where $|d| = \sqrt{|d_{12}|^2 + |d_{13}|^2}$. The Hamiltonian (1.56) can be written as

$$H = \hbar\omega_{13}|1\rangle\langle 1| + \sum_{ks} \omega_k a_{ks}^\dagger a_{ks} - \sum_{ks} (\mathfrak{g}_{ks}|1\rangle\langle c|a_{ks} + \mathrm{H.c.}), \tag{5.9}$$

where $\mathfrak{g}_{ks} = i(2\pi ck/\hbar L^3)^{1/2}|d|\hat{d}\cdot\hat{\varepsilon}_{ks}e^{i\vec{k}\cdot\vec{r}}$ is the vacuum coupling between state $|1\rangle$ and $|c\rangle$ and $\hat{d}$ is the unit vector parallel to both $\vec{d}_{12}$ and $\vec{d}_{13}$. Note that the state $|uc\rangle$ is not directly coupled to $|1\rangle$. Thus $|uc\rangle$ never gets populated if $\rho_{11}(0) = 1$. The spontaneous emission from state $|1\rangle$ occurs to the coherent superposition state $|c\rangle$ and *not just* to the individual states $|2\rangle$ and $|3\rangle$. Clearly, under these conditions the final state will be $|c\rangle$ which agrees with the result (5.4) for $\omega_{23} = 0$, $\theta_1 = 0$.

For $\omega_{23} \neq 0$, the proper basis corresponds to the two eigenstates $|\psi_\pm\rangle$ of (5.5) and the steady state will be an *incoherent* mixture of $|\psi_+\rangle$ and $|\psi_-\rangle$.

5.2 Emission spectrum in the presence of VIC

We now come to the question as to how can one probe the existence of VIC in a Λ system. Thus one naturally think of the spectrum of spontaneous emission. In a V system the spontaneous emission is significantly affected by the presence of VIC [112, 114, 115]. But for a Λ system, as we show, the emission spectrum is independent of VIC. The emission spectrum corresponds to the normally ordered two-time correlation function of electric field amplitudes [7]. The radiated fields at space-time points $\vec{r}_j, t_j$ ($j = 1, 2$) will have a correlation given by

$$\langle E^{(-)}(\vec{r}_1, t_1)\cdot E^{(+)}(\vec{r}_2, t_2)\rangle = (r_1 r_2)^{-1} \sum_{l,m=2,3} M_{lm}\langle A_{1l}(t_1)A_{m1}(t_2)\rangle, \qquad t_1 > t_2, \tag{5.10}$$

where

$$M_{lm} = \left(\frac{\omega_{1l}\omega_{1m}}{c^2}\right)^2 [\hat{r}_1 \times (\hat{r}_1 \times \vec{d}^{*}_{1l})] \cdot [\hat{r}_2 \times (\hat{r}_2 \times \vec{d}_{1m})],$$

and r_j is much greater than the size of the source. Using quantum regression theorem and equations (5.1), it can be shown that the two-time atomic correlation functions are given by

$$\langle A_{1m}(t_1) A_{m1}(t_2)\rangle = \exp\left[(i\omega_{1m} - \Gamma_1)(t_1 - t_2)\right] \exp\left(-2\Gamma_1 t_2\right), \qquad t_1 > t_2, \tag{5.11}$$

$$\text{and} \qquad \langle A_{1l}(t_1) A_{m1}(t_2)\rangle = 0 \qquad \text{for} \qquad l \neq m.$$

Using (5.11) in (5.10) we get the correlation function of the radiated field

$$\langle E^{(-)}(\vec{r}_1, t_1) \cdot E^{(+)}(\vec{r}_2, t_2)\rangle =$$
$$(r_1 r_2)^{-1} \sum_{m=2,3} M_{mm} \exp\left[(i\omega_{1m} - \Gamma_1)(t_1 - t_2)\right] \exp\left(-2\Gamma_1 t_2\right), \qquad t_1 > t_2. \tag{5.12}$$

This correlation function is the sum of *incoherent* emissions along the two transitions, $|1\rangle \rightarrow |2\rangle$ and $|1\rangle \rightarrow |3\rangle$. Thus we conclude that the spontaneous emission spectrum in a Λ system is *not affected* by VIC. Therefore one has to consider other types of probes to study VIC in such a system.

5.3 Modulated absorption as a probe of VIC

The above result is not surprising because the coherence is created after the spontaneous emission has occurred. An alternative approach to monitor VIC will be to study the absorption of a probe field tuned close to some other transition in the system. We now show that a unique feature in probe absorption appears due to the presence of VIC. The model scheme is as shown in Fig. 5.2. Here the spontaneous emission from state $|1\rangle$ creates VIC between the two near-degenerate ground levels $|2\rangle$ and $|3\rangle$. We now consider another excited *probe* state $|p\rangle$, well separated from $|1\rangle$. A weak coherent field is tuned between state $|p\rangle$ and the two ground states to monitor VIC. The Hamiltonian in the dipole approximation will be

$$\begin{aligned} H &= \hbar\omega_{23} A_{22} + \hbar\omega_{13} A_{11} + \hbar\omega_{p3} A_{pp} \\ &\quad -\{(\vec{d}_{p3} A_{p3} + \vec{d}_{p2} A_{p2}) \cdot \vec{E}_{p0} e^{-i\omega_p t} + \text{H.c}\}, \end{aligned} \tag{5.13}$$

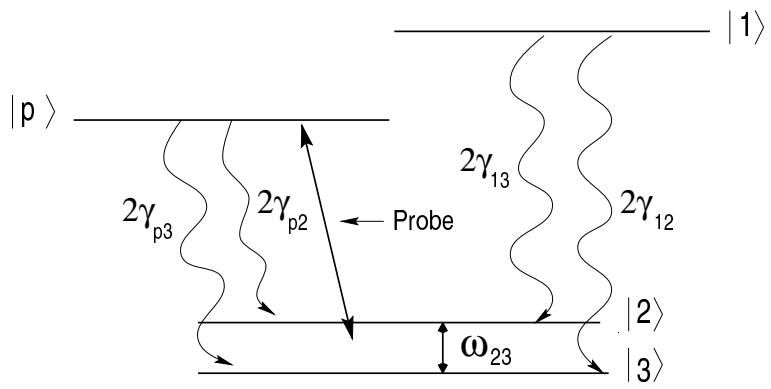

Figure 5.2: Schematic diagram of a four level model proposed for monitoring vacuum induced coherence. The coherence created by spontaneous emission from $|1\rangle$ can be observed in the probe absorption along $|p\rangle \leftrightarrow |2\rangle, |3\rangle$.

where the counter-rotating terms in the probe field have been dropped. The probe field is treated classically here and has a frequency ω_p and a complex amplitude $\vec{E}_{p0}$. The equations for the various density matrix elements can be derived as below.

$$\dot{\rho}_{11} = -2\Gamma_1\rho_{11}, \tag{5.14a}$$

$$\dot{\rho}_{pp} = -2\Gamma_p\rho_{pp} + i[(g_{p2}\rho_{2p} + g_{p3}\rho_{3p})e^{-i\omega_p t} - \text{c.c.}], \tag{5.14b}$$

$$\dot{\rho}_{22} = 2\gamma_{12}\rho_{11} + 2\gamma_{p2}\rho_{pp} - i[g_{p2}e^{-i\omega_p t}\rho_{2p} - \text{c.c.}], \tag{5.14c}$$

$$\dot{\rho}_{2p} = -(\Gamma_p - i\omega_{p2})\rho_{2p} - ig^*_{p3}e^{i\omega_p t}\rho_{23} + ig^*_{p2}e^{i\omega_p t}(\rho_{pp} - \rho_{22}), \tag{5.14d}$$

$$\dot{\rho}_{3p} = -(\Gamma_p - i\omega_{p3})\rho_{3p} - ig^*_{p2}e^{i\omega_p t}\rho_{32} + ig^*_{p3}e^{i\omega_p t}(2\rho_{pp} + \rho_{11} + \rho_{22} - 1), \tag{5.14e}$$

$$\dot{\rho}_{21} = -(\Gamma_1 - i\omega_{12})\rho_{21} + ig^*_{p2}e^{i\omega_p t}\rho_{p1}, \tag{5.14f}$$

$$\dot{\rho}_{31} = -(\Gamma_1 - i\omega_{13})\rho_{31} + ig^*_{p3}e^{i\omega_p t}\rho_{p1}, \tag{5.14g}$$

$$\dot{\rho}_{p1} = -(\Gamma_1 + \Gamma_p - i(\omega_{13} - \omega_{p3}))\rho_{p1} + i(g_{p2}\rho_{21} + g_{p3}\rho_{31})e^{-i\omega_p t}, \tag{5.14h}$$

$$\dot{\rho}_{23} = \eta_1\rho_{11} + \eta_p\rho_{pp} - i\omega_{23}\rho_{23} - ig_{p3}e^{-i\omega_p t}\rho_{2p} + ig^*_{p2}e^{i\omega_p t}\rho_{p3}, \tag{5.14i}$$

where we have used the trace condition $\sum_m \rho_{mm} = 1$ for (5.14e). Here

$$2\gamma_{p2} = \frac{4\omega^3_{p2}|d_{p2}|^2}{3\hbar c^3} \quad \text{and} \quad 2\gamma_{p3} = \frac{4\omega^3_{p3}|d_{p3}|^2}{3\hbar c^3} \tag{5.15}$$

define the spontaneous emission rates from $|p\rangle$ to states $|2\rangle$ and $|3\rangle$, respectively and we write $\Gamma_p = \gamma_{p2} + \gamma_{p3}$. The Rabi frequencies

$$2g_{p2} = 2\vec{E}_{p0}\cdot\vec{d}_{p2}/\hbar, \quad 2g_{p3} = 2\vec{E}_{p0}\cdot\vec{d}_{p3}/\hbar \tag{5.16}$$

are for the probe field acting on transitions $|p\rangle \leftrightarrow |2\rangle$ and $|p\rangle \leftrightarrow |3\rangle$, respectively. Further we can write $g_{p2} = |g_{p2}|e^{-i\phi_2}$ and $g_{p3} = |g_{p3}|e^{-i\phi_3}$, where $\phi = \phi_2 - \phi_3$ gives the relative phase between the complex dipole matrix elements $\vec{d}_{p2}$ and $\vec{d}_{p3}$. The VIC parameters are

$$\eta_1 = 2\sqrt{\gamma_{12}\gamma_{13}}\cos\theta_1, \qquad \eta_p = 2\sqrt{\gamma_{p2}\gamma_{p3}}\cos\theta_p. \tag{5.17}$$

We thus include vacuum induced coherence on all possible transitions.

In order to study probe absorption we solve Eqs. (5.14) perturbatively. We need to know $\rho_{pp}(t)$ to second order in the probe field, assuming that the atom was prepared in the state $|1\rangle$ at $t = 0$. Using (5.14b) we get

$$\rho_{pp}^{(2)}(t) = i\int_0^t d\tau e^{-i\omega_p\tau}[|g_{p2}|e^{-i\phi_2}\rho_{2p}^{(1)}(\tau) + |g_{p3}|e^{-i\phi_3}\rho_{3p}^{(1)}(\tau)]e^{-2\Gamma_p(t-\tau)} + \text{c.c.} \ . \tag{5.18}$$

The first order contribution obtained by integrating (5.14d) is given below:

$$\begin{aligned}\rho_{2p}^{(1)}(t) \ &= \ -i\int_0^t d\tau e^{i\omega_p\tau}\{|g_{p3}|e^{i\phi_3}\rho_{23}^{(0)}(\tau) \\ &\quad -|g_{p2}|e^{i\phi_2}[\rho_{pp}^{(0)}(\tau) - \rho_{22}^{(0)}(\tau)]\}e^{-(\Gamma_p - i\omega_{p2})(t-\tau)}.\end{aligned} \tag{5.19}$$

It can be easily shown that $\rho_{pp}^{(0)}(t) = 0$ and the other zeroth order terms are known from Sec. 5.1. The VIC contribution arises from non-zero $\rho_{23}^{(0)}(t)$ in (5.19). Similarly integrating for $\rho_{3p}^{(1)}(t)$ and combining with Eqs. (5.18) (5.19), and on simplification we find our key result

$$\begin{aligned}\rho_{pp}^{(2)}(t \gg \Gamma_1^{-1}, \Gamma_p^{-1}) \ &\equiv \ \frac{\eta_1|g_{p3}||g_{p2}|e^{-i(\omega_{23}t+\phi)}}{(2\Gamma_p - i\omega_{23})(2\Gamma_1 - i\omega_{23})(\Gamma_p - i(\Delta_p + \omega_{23}/2))} \\ &\quad + \frac{\eta_1|g_{p3}||g_{p2}|e^{i(\omega_{23}t+\phi)}}{(2\Gamma_p + i\omega_{23})(2\Gamma_1 + i\omega_{23})(\Gamma_p - i(\Delta_p - \omega_{23}/2))} \\ &\quad + \frac{|g_{p2}|^2}{4\Gamma_p[\Gamma_p - i(\Delta_p - \omega_{23}/2)]} + \frac{|g_{p3}|^2}{4\Gamma_p[\Gamma_p - i(\Delta_p + \omega_{23}/2)]} + \text{c.c.}\end{aligned} \tag{5.20}$$

When $\eta_1 \to 0$

$$\rho_{pp}^{(2)}(t \gg \Gamma_1^{-1}, \Gamma_p^{-1}) \equiv \frac{|g_{p2}|^2}{4\Gamma_p[\Gamma_2 - i(\Delta_p - \omega_{23}/2)]} + \frac{|g_{p3}|^2}{4\Gamma_p[\Gamma_p - i(\Delta_p + \omega_{23}/2)]} + \text{c.c.}, \tag{5.21}$$

which is the sum of the individual absorptions corresponding to the transitions $|2\rangle \to |p\rangle$, $|3\rangle \to |p\rangle$, as expected. The parameter $\Delta_p = \omega_{p3} - \omega_{23}/2 - \omega_p$ is the probe detuning defined with respect to the center of level $|2\rangle$ and $|3\rangle$. The modulated term in probe absorption (5.20) is the result of VIC. *This modulation is the signature of*

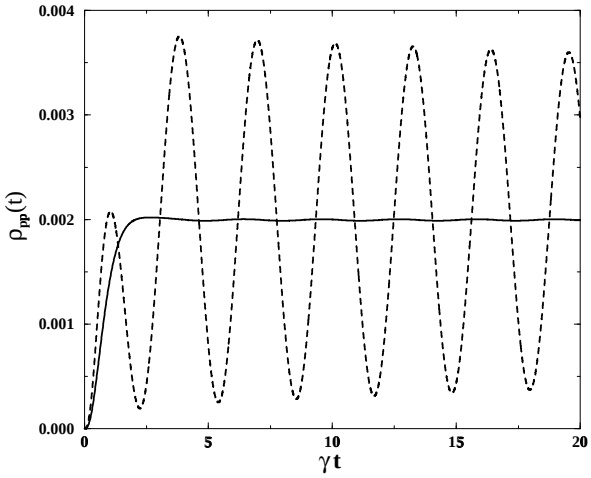

Figure 5.3: The excited state population ρ_{pp} as a function of scaled time γt. Here the probe field is tuned to the center of states $|2\rangle$ and $|3\rangle$, and we take $\gamma_{12} = \gamma_{13} = \gamma_{p2} = \gamma_{p3} = \gamma$. The parameters are $g_{p3} = g_{p2} = 0.1/\gamma$ and $\omega_{23} = 2\gamma$, and phase $\phi = 0$. The dashed oscillating curve is in the presence of VIC and the solid curve in the absence of VIC. This observed modulation is consistent with the analytical result (5.20). Very weak oscillation appears in the solid line because the probe is not exactly tuned to the two transitions.

the VIC produced by the two paths of spontaneous emission $|1\rangle \rightarrow |2\rangle$, $|1\rangle \rightarrow |3\rangle$. Note the interesting phase dependence that arises in the probe absorption due to non-zero η_1. This phase dependence is another outcome of the presence of VIC in a system. Since the probe is treated to second order in its amplitude, the result is independent of the coherence parameter η_p for the transition $|p\rangle \rightarrow |2\rangle$, $|p\rangle \rightarrow |3\rangle$. Needless to say that the Eqs. (5.14) can be integrated numerically to obtain the probe absorption for arbitrary times. For this purpose it is useful to remove the optical frequencies by making the transformations $\tilde{\rho}_{1m} \equiv \rho_{1m} e^{i\omega_{1m}t}$, $\tilde{\rho}_{pm} \equiv \rho_{pm} e^{i\omega_p t}$ $(m = 2, 3)$ and $\tilde{\rho}_{1p} \equiv \rho_{1p} e^{i(\omega_p - \omega_{13})t}$ etc. We solve these using fifth-order Runge-Kutta-Verner method with the initial condition that $\rho_{11}(0) = 1$. We take the probe Rabi frequencies g_{p3}, g_{p2} much smaller than Γ's. The numerical results for excited state population $\rho_{pp}(t)$ as a function of time for both the cases when η_1 is zero and non-zero are plotted in Fig. 5.3. The figure shows the significant difference that arises due to the presence or absence of VIC. The oscillation in the probe absorption is a reflection of oscillation in the coherence ρ_{23} [see (5.2)] and this confirms the analytical result (5.20). The numerical result shows a very slow decay of the envelop of the oscillations. This arises from terms which are of

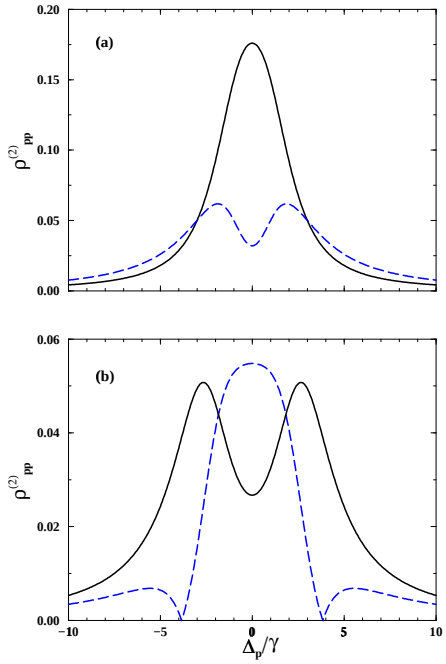

Figure 5.4: The cosine (dashed) and sine (solid) components of the excited state population $\rho^{(2)}_{pp} \times 10^2$ as a function of probe detuning. Plot (a) is for $\omega_{23} = 2\gamma$ and (b) is for $\omega_{23} = 5\gamma$. The parameters are as in Fig. 5.3.

higher order in probe strength.

Finally, we discuss the changes in absorption spectrum that arise due to VIC. The modulated component of the population (5.20) can be written as

$$\begin{aligned}\rho^{(2)}_{pp} \equiv & \frac{2\eta_1|g_{p3}||g_{p2}|}{D}[\{2\Gamma_1\Gamma_p^2 + 2\Gamma_1(\Delta_p^2 - \omega_{23}^2/4) - \Gamma_p\omega_{23}^2\}\cos(\omega_{23}t+\phi) \\ & +\omega_{23}\{2\Gamma_1\Gamma_p + \Gamma_p^2 + \Delta_p^2 - \omega_{23}^2/4\}\sin(\omega_{23}t+\phi)], \end{aligned} \tag{5.22}$$

where

$$D = (4\Gamma_1^2 + \omega_{23}^2)[\Gamma_p^2 + (\Delta_p + \omega_{23}/2)^2][\Gamma_p^2 + (\Delta_p - \omega_{23}/2)^2].$$

Since it is possible to separate the sine and cosine terms by a phase sensitive detection, we plot these in Fig. 5.4 as a function of probe detuning. These two components of the absorption spectrum behave quite differently.

5.4 Summary

In summary, we have studied the origin and problem of detection of VIC in the Λ systems. In Sec. 5.1 we have shown that VIC can result in a non-zero coherence among the ground levels. We have also shown that such a coherence arises because the system tends to remain close to a pure state due to interference, which explains the origin of VIC. In Sec. 5.2 we have evaluated the spontaneous emission spectrum and have shown that VIC does not affect the emission spectrum in the Λ systems. In Sec. 5.3 we have shown that VIC can be monitored via probe absorption. The oscillations of VIC modulates the probe absorption and we show that the sine and cosine components of absorption spectra behave quite differently in the presence of VIC. We have given analytical expressions to substantiate our numerical results.

Chapter 6

Effects of Vacuum Induced Coherence on Coherent Population Trapping

It is now clear as to how the decay of a system of closely lying states induced by interaction with a common bath leads to new types of coherences. In a Λ system, as noted in the previous chapter, this coherence is created among the two ground levels. Javanainen [126] discussed the possibility of VIC effects in the Λ systems. In particular, he examined the case of maximal coherence via VIC in a Λ system driven by a single field of arbitrary intensity. He demonstrated the absence of CPT state in such a situation. More recently, Martinez et al. [127] showed the existence of phase dependent spontaneous emission line shapes when the lower levels in a Λ system, coupled by VIC, are driven by a microwave field. The aim of the present chapter is to study the effect of VIC on CPT and EIT in the Λ systems, using the control and probe field geometry. Unlike the previous study [126], we study the response of the probe field on one arm of a Λ system, driven by a control field on the other arm. We study both the cases when the probe field is weak (as in EIT studies) and when the probe field is strong (as in CPT studies).

6.1 Absorption and Dispersion Line Shapes

To study a situation more parallel to the usual CPT and EIT models, we consider a control field $\vec{E}_c$ coupling to $|1\rangle \leftrightarrow |2\rangle$ transition and the probe field $\vec{E}_p$ coupling to $|1\rangle \leftrightarrow |3\rangle$ transition. Since we allow the separation between the two ground levels $\hbar\omega_{23}$ to be arbitrarily small, the arrangement of the field polarization as shown in Fig. 6.1(b) will be required. This will avoid the complications that arise due

to cross talk among optical transitions as discussed in chapter 2. The control

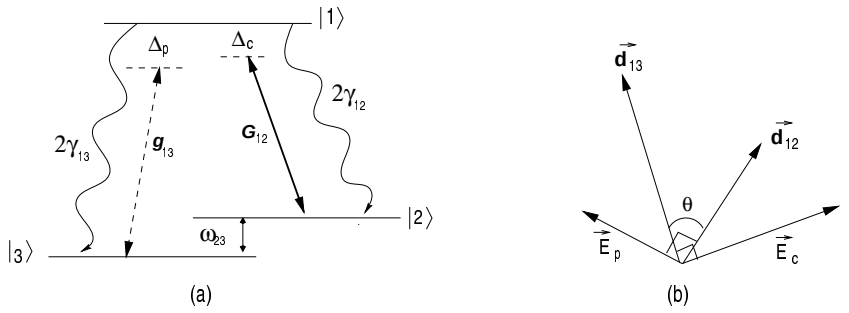

Figure 6.1: (a) Schematic diagram of a three-level Λ system driven by two coherent fields of same frequencies but with Rabi frequencies $2g_{13}$ (probe) and $2G_{12}$ (control), respectively. (b) Arrangement of field polarizations required so that one field drives only one transition.

(probe) field frequency is denoted as ω_c (ω_p) and the detuning as $\Delta_c = \omega_{12} - \omega_c$ ($\Delta_p = \omega_{13} - \omega_p$). The basic equations describing such a model in the RWA will be

$$\dot{\rho_{11}} = -2(\gamma_{13}+\gamma_{12})\rho_{11} + iG_{12}\rho_{21} - iG_{12}^*\rho_{12} + ig_{13}\rho_{31} - ig_{13}^*\rho_{13}, \quad (6.1a)$$

$$\dot{\rho_{22}} = 2\gamma_{12}\rho_{11} + iG_{12}^*\rho_{12} - iG_{12}\rho_{21}, \quad (6.1b)$$

$$\dot{\rho_{12}} = -(\gamma_{13}+\gamma_{12}+i\Delta_c)\rho_{12} + ig_{13}\rho_{32} - iG_{12}(\rho_{11}-\rho_{22}), \quad (6.1c)$$

$$\dot{\rho_{13}} = -(\gamma_{13}+\gamma_{12}+i\Delta_p)\rho_{13} + iG_{12}\rho_{23} - ig_{13}(2\rho_{11}+\rho_{22}-1), \quad (6.1d)$$

$$\dot{\rho_{23}} = -i(\Delta_p-\Delta_c)\rho_{23} + 2\sqrt{\gamma_{13}\gamma_{12}}\cos\theta\rho_{11} + iG_{12}^*\rho_{13} - ig_{13}\rho_{21}. \quad (6.1e)$$

Here we have taken the *control and probe fields of same frequency and thus* $\Delta_p - \Delta_c = \omega_{23}$. In such a model, CPT and EIT can be studied by scanning over the separation between the two ground levels. In (6.1) the Rabi frequencies are denoted as $2G_{12} = 2\vec{d}_{12}\cdot\vec{E}_{c0}/\hbar$ and $2g_{13} = \vec{d}_{13}\cdot\vec{E}_{p0}/\hbar$, where $\vec{E}_{c0(p0)}$ are the electric field amplitudes. It should be noted that for the arrangement in Fig. 6.1(b), both the Rabi frequencies will be θ-dependent. However, we will not explicitly consider this θ-dependence, because Rabi frequencies for different θ can be kept same by adjusting the field intensity.

The general steady state solution for ρ_{13} in all orders of probe and control field is found to be

$$\rho_{13} = \frac{g_{13}G_{12}^2(\Delta_p-\Delta_c)[-g_{13}^2 + 2\cos\theta g_{13}G_{12} - G_{12}^2 + \Delta_p(\Delta_p-\Delta_c) + 2i(\Delta_p-\Delta_c)]}{D}, \quad (6.2)$$

where

$$\begin{aligned} D &= [(g_{13}^2+G_{12}^2)^2(g_{13}^2-2\cos\theta G_{12}g_{13}+G_{12}^2)+(2g_{13}^2+2G_{12}^2-2\cos\theta G_{12}g_{13}) \\ &\times(g_{13}^2-G_{12}^2)\Delta_c(\Delta_p-\Delta_c)+(4G_{12}^2+4g_{13}^2+4G_{12}^2g_{13}^2+2\cos\theta g_{13}G_{12}^3-2G_{12}^4 \\ &+(g_{13}^2+G_{12}^2)\Delta_c^2)(\Delta_p-\Delta_c)^2+2G_{12}^2\Delta_c(\Delta_p-\Delta_c)^3+G_{12}^2(\Delta_p-\Delta_c)^4], \end{aligned}$$

where we have set $\gamma_{13}=\gamma_{12}=\gamma$, and all the parameters are reduced to dimen-

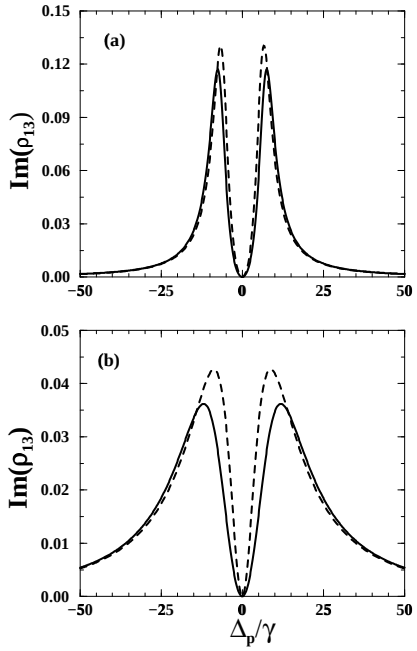

Figure 6.2: Energy absorption from probe $\mathrm{Im}(\rho_{13})$ for $G_{12}=7\gamma$, $\Delta_c=0$ and $\gamma_{13}=\gamma_{12}=\gamma$. For the dashed curve $\theta=45^o$ and the solid curve is the usual case $\theta=90^o$. For frame (a) $g_{13}=2.12\gamma$ and frame (b) $g_{13}=7\gamma$.

sionless units by scaling with γ. For a weak probe ($g_{13}\ll G_{12}$)

$$\rho_{13}\approx\frac{-g_{13}(\Delta_p-\Delta_c)}{[G_{12}^2+(\Delta_p-\Delta_c)(2i-\Delta_p)]}, \tag{6.3}$$

which is independent of the VIC parameter. We also note from (6.2) that $\mathrm{Im}(\rho_{13})=0$ when $\Delta_p=\Delta_c$ for all values of θ allowed by Fig. 6.1. For the arrangement in Fig. 6.1(b), the term $G_{12}^2-2\cos\theta G_{12}g_{13}+g_{13}^2$ is non-zero (for $\theta=0$, both the fields are perpendicular to the dipoles). Thus CPT and EIT phenomena are preserved for the arrangement shown in Fig. 6.1(b), even in the presence of VIC. From (6.2) we also see that the line profiles will start showing significant deviations if the probe field

becomes large so as to saturate the transition. These features are demonstrated in Figs. 6.2 and 6.3. In Figs. 6.2 and 6.3 we also show, for comparison, the results when the VIC effect is absent. Note that $\mathrm{Im}(\rho_{13}) = 0$ at $\Delta_p = \Delta_c$ in all the cases, however, the width of the transparency window is reduced when probe field is strong. For large values of $\Delta_p - \Delta_c$, the difference between the two profiles disappear. As noted earlier, this is because the effect is important only for small values of energy separation between $|2\rangle$ and $|3\rangle$. Similar results are obtained for unequal γ's.

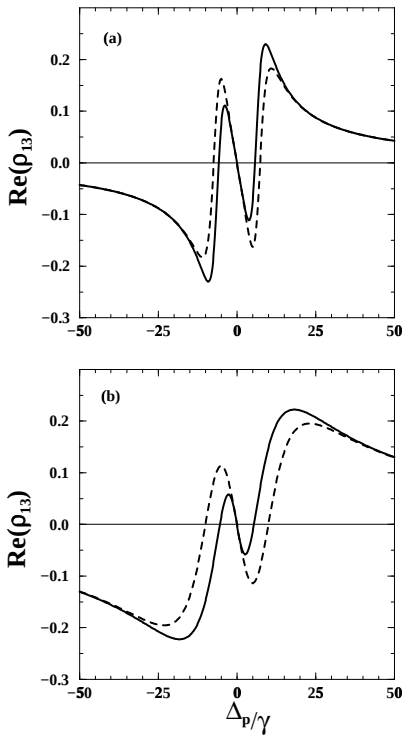

Figure 6.3: Plots for $\mathrm{Re}(\rho_{13})$ as a function of probe detuning. The parameters are the same as in Fig. 6.2.

6.2 Effect of VIC on the Dynamics

We also study the dynamic evolution of this system to the CPT state by solving equations (6.1) numerically with initially all the atoms in state $|3\rangle$. The time evolution of the ground state coherence is shown in Fig. 6.4. We perform an eigenvalue analysis of the 8×8 matrix in equations (6.1) to ascertain the time scales involved

with both strong and weak probes. Typically, for $G_{12} = g_{13} = 7\gamma$, $\Delta_c = \Delta_p = 0$ and equal decay rates, we diagonalise the matrix with $\theta = 45^o$ ($\theta = 90^o$) and obtain the eigenvalues: -2.85+19.95i, -2.85-19.95i, -1.0-9.95i, -1.0-9.95i, -1.0+9.95i, -1.0+9.95i, -1.99, -0.288 (-2.5+19.9i, -2.5-19.9i, -1.0-9.95i, -1.0+9.95i, -1.0-9.95i, -1.0+9.95i, -2.0, -0.99). It is observed that the lowest eigenvalue, which is inversely related to time scale, reduces from -0.99 to -0.28 in the presence of VIC. Thus the time scale to evolve to the CPT state increases as shown in Fig. 6.4. For smaller probe strength ($g_{13} = 0.07\gamma$) the lowest eigenvalue changes form -0.985 to -0.97, hardly affecting the time scale.

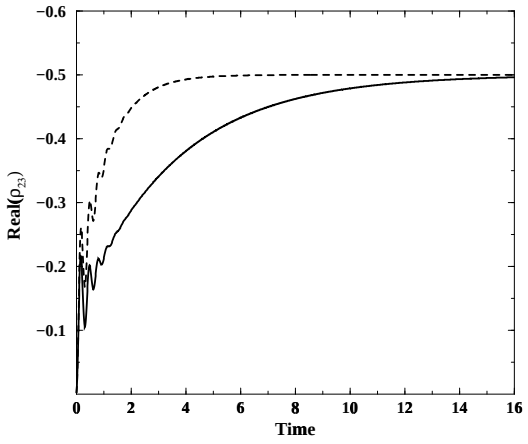

Figure 6.4: Dynamic evolution of the system to the CPT state. The solid (dashed) curve is in the presence (absence) of VIC. The parameters are $G_{12} = g_{13} = 7\gamma$, $\Delta_p = \Delta_c = 0$, $\gamma_{13} = \gamma_{12} = \gamma$, and $\theta = 45^o$. Time is measured in units of γ^{-1}.

6.3 Coupled and Uncoupled States

We now show how the above numerical results can be understood by analyzing the original density matrix equations (6.1) in a field dependent basis given by

$$|1\rangle, \qquad |c\rangle = \frac{G_{12}|2\rangle + g_{13}|3\rangle}{\Omega}, \qquad |uc\rangle = \frac{g_{13}|2\rangle - G_{12}|3\rangle}{\Omega}, \tag{6.4}$$

where $\Omega = \sqrt{G_{12}^2 + g_{13}^2}$ and $|c\rangle$ and $|uc\rangle$ refer to the *coupled* and *uncoupled* states as discussed previously. We assume the CPT condition $\Delta_p = \Delta_c$ throughout this section. Note that the basis (6.4) is different form the dressed state basis which also involves mixing of $|1\rangle$ and $|c\rangle$ states. For understanding the numerical results,

the basis (6.4) turns out to be useful. We can now transform the density matrix equations (6.1) using

$$\rho_{cc} = (G_{12}^2\rho_{22} + g_{13}^2\rho_{33} + G_{12}g_{13}\rho_{23} + G_{12}g_{13}\rho_{32})/\Omega^2, \tag{6.5a}$$

$$\rho_{ucuc} = (g_{13}^2\rho_{22} + G_{12}^2\rho_{33} - G_{12}g_{13}\rho_{23} - G_{12}g_{13}\rho_{32})/\Omega^2, \tag{6.5b}$$

$$\rho_{1c} = (G_{12}\rho_{12} + g_{13}\rho_{13})/\Omega, \tag{6.5c}$$

$$\rho_{1uc} = (g_{13}\rho_{12} - G_{12}\rho_{13})/\Omega. \tag{6.5d}$$

In the new basis we get the equations

$$\dot{\rho}_{11} = -2\Gamma\rho_{11} + i\Omega\rho_{c1} - i\Omega\rho_{1c}, \tag{6.6a}$$

$$\dot{\rho}_{1c} = -\Gamma\rho_{1c} + i\Omega(\rho_{cc} - \rho_{11}), \tag{6.6b}$$

$$\dot{\rho}_{cc} = (\Gamma + \Gamma')\rho_{11} + i\Omega\rho_{1c} - i\Omega\rho_{c1}, \tag{6.6c}$$

$$\dot{\rho}_{ucuc} = (\Gamma - \Gamma')\rho_{11}, \tag{6.6d}$$

$$\dot{\rho}_{1uc} = -\Gamma\rho_{1uc} + i\Omega\rho_{cuc}, \tag{6.6e}$$

$$\dot{\rho}_{cuc} = i\Omega\rho_{1uc} - \Gamma'\frac{(G_{12}^2 - g_{13}^2)}{2G_{12}g_{13}}\rho_{11}, \tag{6.6f}$$

where $\Gamma' = 2\Gamma G_{12}g_{13}\cos\theta/\Omega^2$. Equation (6.6) can be interpreted in terms of the diagram shown in Fig. 6.5. We note that the CPT state $|uc\rangle$ is populated at the rate $\Gamma_{\rm CPT}$, where

$$\Gamma_{\rm CPT} = \Gamma\left(1 - \frac{2G_{12}g_{13}\cos\theta}{\Omega^2}\right). \tag{6.7}$$

It is important to see that for the geometry considered in the Fig. 6.1(b), this rate

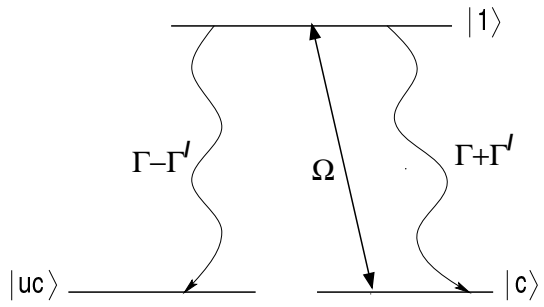

Figure 6.5: Equivalent level scheme of Fig. 6.1(a) in the new basis $|1\rangle$, $|c\rangle$ and $|uc\rangle$. The population oscillates between the state $|1\rangle$ and $|c\rangle$ with an effective Rabi frequency Ω and decays to the CPT state $|uc\rangle$ at the rate $\Gamma - \Gamma'$.

of change of population of the CPT state can never be zero, i.e., $\Gamma_{\rm CPT} \neq 0$. Note

further that the population gets cycled between the levels $|1\rangle$ and $|c\rangle$ because of the effective pumping field Ω. It is clear form this physical picture that optical pumping would lead to the state $|uc\rangle$, i.e., the CPT would occur.

This analysis also explains why Javanainen [126] finds a very different result for the case of a single field. His case corresponds to setting $g_{13} = G_{12}$, $\theta = 0$ leading to $\Gamma_{\rm CPT} = 0$. Thus the CPT state does not get populated and no optical pumping to this state occurs. In this case one has a conservation law

$$\dot{\rho}_{ucuc} = 0. \tag{6.8}$$

Thus the final population in $|uc\rangle$ state is the same as that given by the initial condition. The case considered by Javanainen is equivalent to that of a two level system with state $|1\rangle$ and $|c\rangle$.

Finally, the above equations also enable us to understand the numerical results of the Fig. 6.4. In the absence of VIC, $\Gamma' = 0$ and the CPT state $|uc\rangle$ is populated at the rate Γ, i.e, the CPT state is populated slowly in the presence of VIC. This is precisely what our numerical results of Fig. 6.4 show. The field dependence of Γ' should be borne in mind.

$$\Gamma' = \frac{2\Gamma \cos\theta (g_{13}/G_{12})}{1 + (g_{13}/G_{12})^2}. \tag{6.9}$$

Thus important changes in time scales would occur only when g_{13} and G_{12} are comparable.

6.4 Phase Dependent Absorption Line Shapes.

The usual EIT experiments with well separated ground levels in the Λ systems do not depend on the relative phase between the two applied fields. But, in case of a closely spaced levels, as our numerical simulation reveals, VIC makes the system quite sensitive to the relative phase between the two applied fields. Explicitly, we consider phases ϕ_c and ϕ_p of the control and probe fields, respectively. Then one can rewrite the Rabi-frequencies as $G_{12} \equiv G_{12}e^{-i\phi_c}$ and $g_{13} \equiv g_{13}e^{-i\phi_p}$. Redefining the atomic variables in (6.1) as $\tilde{\rho}_{12} \equiv \rho_{12}e^{i\phi_c}$, $\tilde{\rho}_{13} \equiv \rho_{13}e^{i\phi_p}$, and $\tilde{\rho}_{23} \equiv \rho_{23}e^{i\Phi}$, where $\Phi = \phi_p - \phi_c$, we get equations for the redefined density matrix elements $\tilde{\rho}_{ij}$ which are found to be identical to (6.1) with the VIC term replaced by

$$\sqrt{\gamma_{12}\gamma_{13}}\cos\theta \equiv \sqrt{\gamma_{12}\gamma_{13}}\cos\theta e^{i\Phi}. \tag{6.10}$$

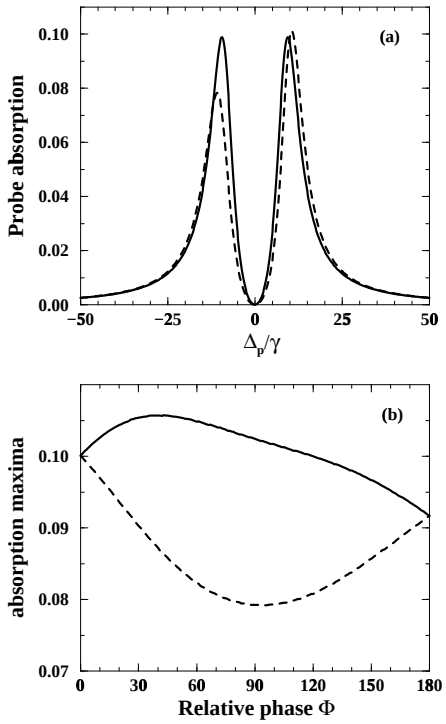

Figure 6.6: Figures show dependence of line profiles on the relative phase Φ between the two applied fields. Frame (a) shows an appreciable difference in the line profiles corresponding to $\Phi = 90^o$ (dashed curve) and $\Phi = 0^o$ (solid curve). Frame (b) is normalized probe absorption maxima $\frac{(\mathrm{peakAbs.})_\Phi}{(\mathrm{peakAbs.})_{\Phi=0}}$ as a function of Φ in the presence of VIC. Solid (dashed) curve is for maxima in the region $\Delta_p > 0$ ($\Delta_p < 0$). Other parameters are $G_{12} = 7\gamma$, $g_{13} = 2.12\gamma$, $\theta = 45^o$ and $\Delta_c = 0$ for both (a) and (b).

The absorption of the probe is now obtained from the imaginary part of $\rho_{13}^{\tilde{}}$. Clearly as long as line shapes depend on the parameter θ, it would also depend on the relative phase between the two fields. We display this dependence of the line shapes on the relative phase of the control and probe fields in Fig. 6.6. It should be noted that the parameters like γ_{13}, γ_{12} are independent of the phases of the dipole matrix elements, whereas the VIC being cross term, depends on the phases of the two dipole matrix elements.

6.5 Summary

In summary, we have studied the effect of VIC on CPT and EIT in the Λ systems. In Sec. 6.1 we have derived the basic equations and analytical expression for

ρ_{13} which corresponds to the absorption and dispersion of the probe field. We have numerically shown the presence of CPT/EIT and the *quantitative* changes in the line profiles due to the VIC. In Sec. 6.2 we have presented the dynamics of CPT in the presence of VIC. We have shown the changes in time scales in the formation of CPT state due to VIC. In Sec. 6.3 we have performed a coupled and uncoupled state analysis to explain our numerical results. We have given analytical expression for the new decay rates, which explains the changes in time scales and formation of CPT state in the presence of VIC. We have also explained the results of Javanainen [126]. In Sec. 6.4 we have studied the phase dependent behavior of VIC. We have shown the possibility of different EIT signatures that can be obtained in the presence of VIC by just changing the phase of the external control field.

Concluding Remarks

In conclusion, this thesis reports new atomic coherence effects in systems with near-degenerate levels. New quantum optical effects are predicted in various chapters and in chapters 4 and 5 fundamental questions are also addressed. Both numerical and analytical results are provided to substantiate our claims. Important conclusions from various chapters and future outlook regarding these problems are given below.

In chapter 2, we have shown the possibility of new gain features via cross talk among optical transitions in the Λ systems. We have elucidated a detailed numerical study of probe absorption and dispersion characteristics under various parameter regimes. We have also presented the effect of relative control and probe field polarization on the response of the medium. We have explained various features of the absorption spectra via a dressed state basis, and have shown certain spectral regions where transparency and high refractive index is observed. We have given examples of atomic systems where our predictions can be demonstrated. We have also shown the possibility of superluminal propagation via cross talk and the example of ^{39}K vapor was considered to measure the negative group index. Nonetheless, many related problems need further investigation. These include, for example, replacement of control field by a modulated field, effect of cross talk on nonlinear phenomena like four wave mixing, and extension of cross talk effect in the V-type and Ξ-type systems.

In chapter 3, we have presented the effect of VIC on the standard Autler-Townes doublet in the V systems. We have shown new gain features that arise in the absorption spectra due to quasi-trapped-states. It has been shown that the quasi-trapping generates a spectral region with low absorption and high dispersion. We also arrive at an important conclusion that in the presence of strong control field, VIC effects can be observed even when the separation between the two excited levels is much larger than their natural line width. This opens up

new possibilities for experimental study of VIC in alkali vapors, where observation of VIC is hindered by the large separation between states of same F or J (see Appendix B for a detailed discussion).

In chapter 4 we have addressed the fundamental question of compatibility of thermal bath induced coherence with thermodynamic equilibrium. We have shown that for time scales greater than the inverse decay rate of the systems, thermodynamic equilibrium will be attained irrespective of such coherences in the dynamical equations. We have given analytical and numerical results and have shown that the thermal bath induced coherence can be probed via emission spectrum. The coherence gives rise to a dark-line in the emission spectrum. We have also discussed the possibility of thermal bath replaced by a broadband laser field. The extra freedom with broadband pumping gives rise to non-zero steady state coherence, unlike thermal field. The rich parameter regime due to tailored baths can allow modification of spectral features in a controlled way.

In chapter 5 we have addressed the question of detection of VIC in the Λ systems. We have shown that the emission spectrum remains unaffected due to VIC. However, a probe absorption gets modulated via VIC, and can be used to monitor VIC in Λ systems. In chapter 6 the effect of VIC on population trapping was elucidated. We arrive at the important conclusion that both CPT and EIT phenomena remain intact even in the presence of VIC. We have presented a physical picture to explain all our numerical results and our analysis also explains previous studies in this context. Note that the coherence created between two ground levels via external field in the Λ systems is known to give rise to highly efficient four-wave-mixing process [106] and it would be interesting to analyze the role of VIC in four wave mixing processes.

Appendix: A

Temperature Dependence of EIT-Spectra in the Λ Systems

Under normal circumstances collisional and thermal fields are the major cause for broadening the EIT window for a weak control field. For example, in a Λ system, if the relaxation rates among the two lower level is larger than the Rabi frequency of the applied fields, the transparency window will be unobservable. Such relaxation rates are one of the major hurdles in observing trapping effects in solid state systems [84] and molecules. Moreover, weak control field is essential for observing subluminal group velocity [92, 93, 94], and hence a large nonlinearity with few photons [110, 111]. In this appendix, the effect of such incoherent processes in the Λ systems is elucidated. An analytically expression for the probe response of such a system in the presence of both homogeneous and inhomogeneous broadening is derived below. Such a result can be useful in trapping related experiments in Λ systems where temperature effects are inevitable. The schematic of a Λ system is shown in Fig. A.1. The energy separation between states $|l\rangle$ and $|m\rangle$ is denoted as $\hbar\omega_{lm}$. The control (probe) field have Rabi frequencies $2G_{12}$ ($2g_{13}$) and frequency detuning $\Delta_c = \omega_{12} - \omega_c$ ($\Delta_p = \omega_{13} - \omega_p$), respectively. The density matrix elements in the RWA will be

$$\dot{\rho}_{11} = -2(\gamma_{13}+\gamma_{12})\rho_{11} + iG_{12}\rho_{21} - iG_{12}^{*}\rho_{12} + ig_{13}\rho_{31} - ig_{13}^{*}\rho_{13}, \quad \text{(A.2a)}$$

$$\dot{\rho}_{22} = 2\gamma_{12}\rho_{11} - iG_{12}\rho_{21} + iG_{12}^{*}\rho_{12} - 2\nu_1\rho_{22} + 2\nu_2\rho_{33}, \quad \text{(A.2b)}$$

$$\dot{\rho}_{12} = -(\gamma_{13}+\gamma_{12}+\nu_1+i\Delta_c)\rho_{12} + ig_{13}\rho_{32} - iG_{12}(\rho_{11}-\rho_{22}), \quad \text{(A.2c)}$$

$$\dot{\rho}_{13} = -(\gamma_{13}+\gamma_{12}+\nu_2+i\Delta_p)\rho_{13} + iG_{12}\rho_{23} - ig_{13}(2\rho_{11}+\rho_{22}-1), \quad \text{(A.2d)}$$

$$\dot{\rho}_{23} = -(\nu_1+\nu_2+i(\Delta_p-\Delta_c))\rho_{23} + iG_{12}^{*}\rho_{13} - ig_{13}\rho_{21}. \quad \text{(A.2e)}$$

Here ν's denote the incoherent population transfer rate among the two ground levels due to finite temperature. In general, ν can be expressed as

$$\nu = \nu_{rad} + \nu_{non}, \quad \text{(A.3)}$$

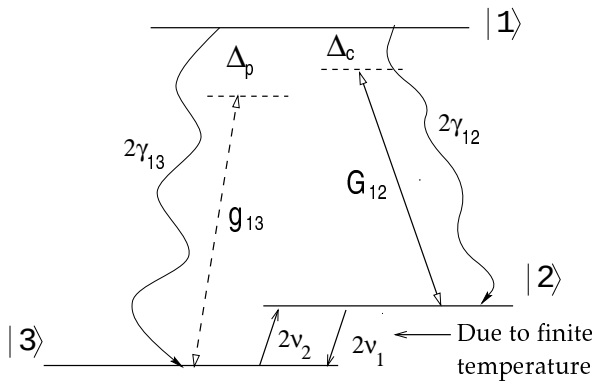

Figure A.1: Schematic of a Λ system with control and probe fields. The γ's denote the spontaneous emission rates.

with both radiative (thermal photons) and non-radiative (inelastic collisions) contributions. In atomic vapors, the two lower levels are dipole forbidden and thus only the non-radiative effects are important. In solid state and molecular systems, both radiative and non-radiative effects can be significant. Agarwal and Jha [34] have show the effect of such relaxation rates on the spontaneous Ramam spectrum. In particular, they have show that when Rabi frequencies of the coherent fields are weak compared to the such relaxation rates, the splitting of spectral lines due to coherent fields disappear. In principle, one can also have a thermally induced transition rate between the optically separated levels like $|1\rangle$ and $|3\rangle$. But such rates would be negligible small for laboratory cases. In the absence of any external fields, at thermal equilibrium one can write

$$\frac{\nu_2}{\nu_1} = \frac{\rho_{22}}{\rho_{33}} = \exp\left[-\frac{\hbar\omega_{23}}{KT}\right], \tag{A.4}$$

where the last term comes due to thermal distribution of population in the two ground levels. In Cs the hyperfine separation between the two ground levels (F $= 1, 2$) is approximately 9 GHz. For $T = 500^{\circ}$K, $\nu_1 \approx \nu_2$ and it is true even for T as low as 50°K.

Steady State Solution

The probe absorption linear in g_{13} will be given by the imaginary part of the optical coherence $\rho_{13}^{(1)}$. The final result of such a calculation is given below.

$$\frac{\gamma_{13}\rho_{13}^{(1)}}{g_{13}} = \frac{i\gamma_{13}|G_{12}|^2(\rho_{11}^{(0)} - \rho_{22}^{(0)})}{A_1(\gamma_{13} + \gamma_{12} + \nu_1 - i\Delta_c)} - \frac{i\gamma_{13}[\nu_1 + \nu_2 + i(\Delta_p - \Delta_c)](2\rho_{11}^{(0)} + \rho_{22}^{(0)} - 1)}{A_1}. \tag{A.5}$$

where

$$A_1 = (\gamma_{13} + \gamma_{12} + \nu_2 + i\Delta_p)(\nu_1 + \nu_2 + i(\Delta_p - \Delta_c)) + |G_{12}|^2 \tag{A.6}$$

The zeroth order response was found to be

$$\rho_{11}^{(0)} = \frac{\nu_2|G_{12}|^2(\gamma_{13} + \gamma_{12} + \nu_1)}{(\gamma_{13} + \gamma_{12})(\nu_1 + \nu_2)[(\gamma_{13} + \gamma_{12} + \nu_1)^2 + \Delta_c^2] + |G_{12}|^2(\gamma_{13} + \gamma_{12} + \nu_1)(\gamma_{13} + \nu_1 + 2\nu_2)}$$

$$\rho_{22}^{(0)} = \frac{\nu_2(\gamma_{13} + \gamma_{12})[(\gamma_{13} + \gamma_{12} + \nu_1)^2 + \Delta_c^2] + \nu_2|G_{12}|^2(\gamma_{13} + \gamma_{12} + \nu_1)}{(\gamma_{13} + \gamma_{12})(\nu_1 + \nu_2)[(\gamma_{13} + \gamma_{12} + \nu_1)^2 + \Delta_c^2] + |G_{12}|^2(\gamma_{13} + \gamma_{12} + \nu_1)(\gamma_{13} + \nu_1 + 2\nu_2)}.$$

From (A.6) the resonances in probe absorption can be found. In the limit $\gamma_{12}, \gamma_{13} \gg G_{12}$ and $\gamma_{12}, \gamma_{13} > \nu_1, \nu_2$ the roots of Δ_p in (A.6) are given by

$$\Gamma_{\rm EIT} = (\nu_1 + \nu_2) + \frac{|G_{12}|^2}{(\gamma_{13} + \gamma_{12} - \nu_1)}, \tag{A.7a}$$

$$\Gamma_{\rm total} = (\gamma_{12} + \gamma_{13} + \nu_2) - \frac{|G_{12}|^2}{(\gamma_{12} + \gamma_{13} - \nu_1)}. \tag{A.7b}$$

Here $\Gamma_{\rm EIT}$ is the width of the transparency window and $\Gamma_{\rm total}$ is the width of the total absorption spectrum. It is clear from (A.7a) that the transparency window will broaden due to decay among the ground levels. Such a broadening is a major hurdle is observing subluminal group velocities, and techniques are being developed to create ultra-narrow transparency window [93, 94]. In Fig. A.2 we plot the probe absorption for different values of ν_1, ν_2. The increasing values of ν can be realized as increasing temperature. It is clear from the plots that for increasing ν the transparency at $\Delta_p = \Delta_c$ decreases and the transparency window broadens.

Analysis with the Inclusion of Doppler Broadening

When both the pump and probe beams are co-propagating ($\vec{k}_p \parallel \vec{k}_c \parallel$ z-axis), we can rewrite the above equations in the presence of Doppler broadening by replacing Δ_p by Δ_{pv} and Δ_c by Δ_{cv} where

$$\Delta_{pv} = \Delta_p - v_z\omega_p/c \qquad \text{and} \qquad \Delta_{cv} = \Delta_c - v_z\omega_c/c.$$

Here v_z is the velocity of the atom along z axis. By taking $\omega_c \approx \omega_p$ and $\Delta_c = 0$, we get $\Delta_{cv} = \Delta_{pv} - \Delta_p$. Doppler averaging of coherence $\rho_{13}^{(1)}$ is given be

$$\rho_{13}^{(1)}(\Delta_p) = \frac{2\sqrt{\ln 2/\pi}}{\omega_D} \int_{-\infty}^{\infty} \rho_{13}^{(1)}(\Delta_{1c}) \exp\left[-4\ln 2(\Delta_{pv} - \Delta_p)^2/\omega_D^2\right] \, d\Delta_{pv}, \tag{A.8}$$

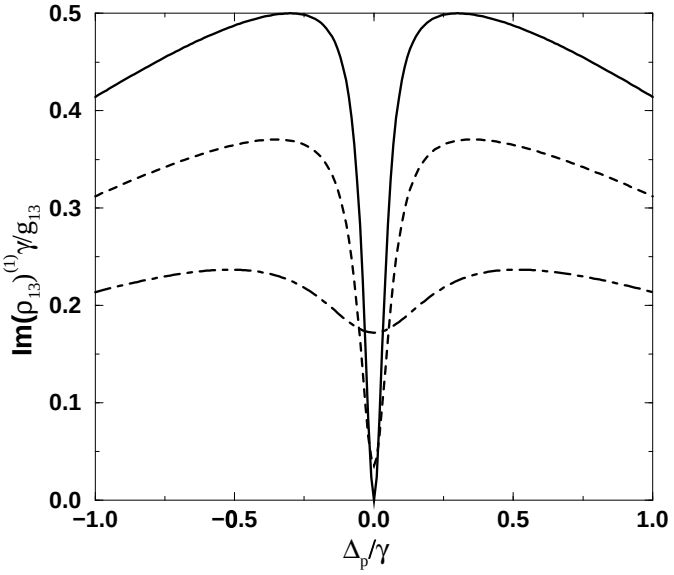

Figure A.2: Normalized probe absorption as a function of probe detuning in dimensionless units from the analytical result (A.5). The parameters $\gamma_{13} = \gamma_{12} = \gamma$, $G_{13} = 0.3\gamma$ and $\Delta_c = 0$. The solid curve is for $\nu_1 = \nu_2 = 0$, the dashed curve is for $\nu_1 = \nu_2 = 0.01\gamma$ and the dot-dashed curve is for $\nu_1 = \nu_2 = 0.1\gamma$.

where $\omega_D = (8 \ln 2 \omega_p^2 KT/c^2 M)^{1/2}$ is the Doppler FWHM.

In the limit $\gamma \gg \nu$ (where, for simplicity we take $\gamma = \gamma_{13} = \gamma_{12}$ and $\nu = \nu_1 = \nu_2$), one can write

$$\rho_{13}^{(1)}(\Delta_{pv}) = \frac{i(2\nu + i\Delta_p)}{2A_2} + \frac{i|G_{12}|^2\gamma(2\nu + i\Delta_p)}{2A_2A_3} - \frac{i\nu|G_{12}|^2[2\gamma + i(\Delta_{pv} - \Delta_p)]}{A_2A_3} \tag{A.9}$$

where

$$\begin{aligned} A_2 &= (2\gamma + i\Delta_{pv})(2\nu + i\Delta_p) + |G_{12}|^2, \\ A_3 &= 2\nu[4\gamma^2 + (\Delta_{pv} - \Delta_p)^2] + \gamma|G_{12}|^2. \end{aligned}$$

When $\omega_D \gg \gamma$ (eg. D_1 and D_2 lines of Rb) the above integration (A.8) can be analytically evaluated in the Doppler limit $[\exp\{-4\ln 2(\Delta_{1c} - \Delta_p)^2/\omega_D^2\} \approx 1]$. We find that

$$\rho_{13}^{(1)}(\Delta_p) = \frac{i\sqrt{\pi \ln 2}}{\omega_D}\left[1 + \frac{\sqrt{\nu}|G_{12}|^2}{A_5} - \frac{i|G_{12}|^2\gamma(\Delta_p + 2i\nu)}{2A_4A_5}\right], \tag{A.10}$$

where

$$\begin{aligned} A_4 &= \left(\frac{\gamma|G_{12}|^2}{2} + 4\gamma^2\nu\right)^{1/2}, \\ A_5 &= \{(\Delta_p - 2i\nu)\sqrt{\nu} - iA_4\}(\Delta_p - 2i\nu) - \sqrt{\nu}|G_{12}|^2. \end{aligned}$$

The complex poles for solution (A.10) exist at

$$\Delta_p = i(\gamma + A_4/2\sqrt{\nu} + \nu) \pm \sqrt{|G|^2 - (\gamma + A_4/2\sqrt{\nu} - \nu)^2} \tag{A.11}$$

For $(\gamma + A_4/2\sqrt{\nu} - \nu)^2 \gg |G_{12}|^2$ the roots are

$$\Gamma_{\rm EIT} = 2i\nu + \frac{i|G_{12}|^2}{2(\gamma - \nu + A_4/2\sqrt{\nu})}, \tag{A.12a}$$

$$\Gamma_{\rm total} = i(2\gamma + A_4/\sqrt{\nu}) - \frac{i|G_{12}|^2}{2(\gamma - \nu + A_4/2\sqrt{\nu})}. \tag{A.12b}$$

In Fig. A.3 below we show the comparisons between the analytical result (A.10)

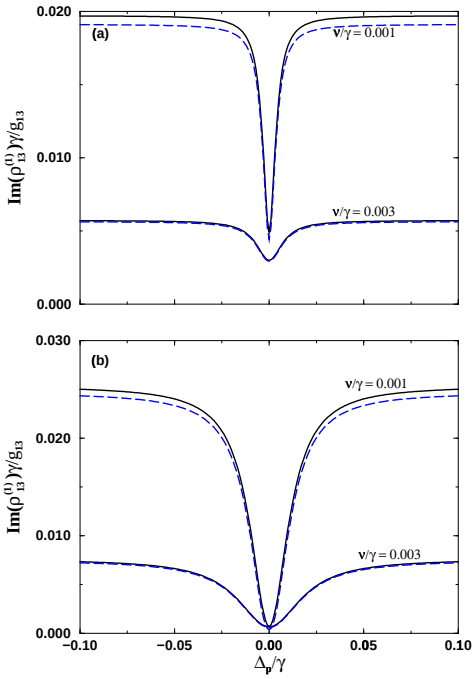

Figure A.3: Plots show the probe absorption in dimensionless units as a function of probe detuning. The frame (a) is for $G_{12} = 0.1\gamma$ and frame (b) for $G_{12} = 0.3\gamma$. The Doppler width ω_D is increased in direct proportion with ν; for $\nu = 0.001\gamma$, $\omega_D = 100\gamma$ and for $\nu = 0.003\gamma$, $\omega_D = 300\gamma$. In both the frames the solid curve corresponds to the analytical result (A.10). The dashed curve corresponds to the numerical integration (A.8) with velocity dependent $\rho_{13}^{(1)}$ obtained from (A.5).

and the numerical integration of (A.8). The parameters are as given in the figures. Comparing the numerical and analytical result in Fig. A.3, it is clear that the Doppler limit invoked in deriving (A.10) holds good for $\nu \neq 0$.

Appendix: B

In this appendix we note the *possible systems where the VIC effects can be studied*. As shown previously, the VIC will be observed when the energy levels have non-orthogonal dipole matrix elements. In alkali vapor there exist many transitions involving hyperfine magnetic sublevels where dipole matrix elements are non-orthogonal: For example, the excited hyperfine sublevels $|\mathrm{F}=3,\mathrm{m_F}=+3\rangle$, $|\mathrm{F}=4,\mathrm{m_F}=+3\rangle$ in the $6\mathrm{P}_{1/2}$ level and the ground level $|6\mathrm{S}_{1/2},\mathrm{F}=4,\mathrm{m_F}=+4\rangle$ in ^{133}Cs. Here the two allowed dipole matrix elements will be along $(\hat{x}+i\hat{y})/\sqrt{2}$ if $\hat{z}$ is the quantization axis. However, all such transitions encountered in alkali vapors are open systems. When all the $\mathrm{m_F}$ (or $\mathrm{m_J}$) sublevels of a given F (or J) level are taken into account, it has been shown that [114, 116] both the excited levels should have the same F and $\mathrm{m_F}$ levels for VIC to be effective in V-type systems. Generally, levels with the same F have separation much larger than their natural line-width. However, Rydberg states and molecular levels have a more complicated structure, and near-degenerate levels with the same F (or J) are possible. Xia et al. [119] used Rydberg levels of Na-dimer, and here the spin-orbit coupling gave rise to VIC effect. Also, recently experiments involving atoms in specific magnetic sublevels [92, 94, 130] were performed very efficiently. Thus the stringent requirement of same F and $\mathrm{m_F}$ levels can be surpassed with the use of atoms in specific magnetic sublevels and optical pumping.

Another possibility of observing non-orthogonal matrix elements is by mixing of energy levels. Harris and Imamoglu [52] have shown that a laser field coupling a metastable state with an excited state gives rise to dressed levels with interfering decay channels. It can be shown the such a mixing gives rise to non-orthogonal dipole matrix elements and have been studied in different contexts [149]. A classic example of non-orthogonal matrix elements is via dc-Stark mixing of energy levels in hydrogen. A dc electric field of $4\mathrm{kV/cm}$ or greater can give rise to mixing of $|2s\rangle$

and $|2p\rangle$ levels [103] given by

$$|1\rangle = \sin\phi|2s\rangle + \cos\phi|2p\rangle, \tag{B.1a}$$

$$|2\rangle = -\sin\phi|2p\rangle + \cos\phi|2s\rangle. \tag{B.1b}$$

It is straight forward to see that $\vec{d}_{13}$ and $\vec{d}_{23}$ will be parallel where $|3\rangle \equiv |1s\rangle$ is the ground state of Hydrogen atom. Various authors [118, 150] have proposed the use of Stark mixed levels to observe VIC kind of effects. In general, the mixing between two levels will not give rise to parallel dipole matrix elements. When spontaneous emission is taken into account, the angle between dressed dipole matrix elements will be

$$\cos\theta = \frac{\sin\phi\cos\phi(\gamma_{b3} - \gamma_{a3})}{\left\{\gamma_{a3}\gamma_{b3} + \sin^2\phi\cos^2\phi(\gamma_{b3} - \gamma_{a3})\right\}^{1/2}} \tag{B.2}$$

where $|2s\rangle$ and $|2p\rangle$ are replaced by $|a\rangle$ and $|b\rangle$, respectively in (B.1). If the decay $\gamma_{a3} \ll \gamma_{b3}$ as in the case of $|2s\rangle$ and $|2p\rangle$ levels of hydrogen, $\cos\theta \approx 1$. It should be noted that γ_{a3} may also denote non-radiative decay like collisions. Thus the angle θ can in practice be tailored using appropriate buffer gas or doping such atoms in crystals where local effects can modify the decay rates. The mixing (B.1) in general can arise due to different possibilities like transverse static magnetic field [151], via stray fields in solid state systems, or spin-orbit coupling as in the case of [119].

There exists a vast range of phenomena where interference effect is similar to the VIC but the conditions are different. The VIC occurs due to two probability amplitudes leading to the same final electromagnetic field state. Similar interference can also occur in autoionizing and tunneling processes. As noted in the early work of Harris [50], all these interference effects give rise to asymmetry in absorption and emission processes. Experiments have been done involving interference effects in both autoionizing levels [152] and tunneling processes [153]. The results discussed in this thesis need to be further analyzed for interfering autoionizing levels and tunneling processes. They will be considered for future investigation. Further, there also exists a wide variety of problems where interfering terms arise due to modified environment. Tailored environment allows one to relax the requirement of non-orthogonal dipole matrix elements as in the case of broadband pumping [87], optical cavities [154] and photonic crystals [155]. Recently, Agarwal [156] has given a general treatment, which shows that *anisotropic* vacuum field will give rise to interfering terms analogous to the VIC.

Appendix: C

Multilevel atom in a thermal bath

In this appendix we prove a general result on the equilibrium state of a multilevel atom interacting with a thermal bath. The Hamiltonian for a multi-level atom in a thermal bath can be written as below

$$H = \sum_{\mu} E_{\mu} A_{\mu\mu} + \sum_{ks} \hbar\omega_{ks} a_{ks}^{\dagger} a_{ks} + \sum_{\mu\neq\nu} V_{\mu\nu} A_{\mu\nu}, \tag{C.1}$$

where

$$V_{\mu\nu}(t) = -i \sum_{ks} \left(\frac{2\pi ck}{L^3\hbar}\right)^{1/2} \vec{d}_{\mu\nu} \cdot (\hat{\epsilon}_{ks} a_{ks} e^{-i\omega_{ks}t} - \hat{\epsilon}_{ks}^{*} a_{ks}^{\dagger} e^{i\omega_{ks}t}) \tag{C.2}$$

The generalized reduced master equation for this Hamiltonian in the Born-Markoff approximation is given by [157]

$$\begin{aligned} \frac{\partial\rho}{\partial t} &= -i\left[\sum_{\mu} E_{\mu} A_{\mu\mu}, \rho\right] \\ &+ \sum_{\mu\nu\kappa\lambda} (A_{\kappa\nu}\rho_{\lambda\mu} - A_{\mu\lambda}\rho\delta_{\nu\kappa})\Gamma^{+}_{\mu\nu\kappa\lambda} + (A_{\mu\lambda}\rho_{\nu\kappa} - \rho A_{\kappa\nu}\delta_{\lambda\mu})\Gamma^{-}_{\kappa\lambda\mu\nu}, \end{aligned} \tag{C.3}$$

where

$$\begin{aligned} \Gamma^{+}_{\mu\nu\kappa\lambda} &= \int_0^{\infty} \langle V_{\mu\nu}(t) V_{\kappa\lambda}(0)\rangle \exp(-i\omega_{\kappa\lambda}t) dt, \\ \Gamma^{-}_{\kappa\lambda\mu\nu} &= \int_0^{\infty} \langle V_{\kappa\lambda}(0) V_{\mu\nu}(t)\rangle \exp(-i\omega_{\kappa\lambda}t) dt, \end{aligned} \tag{C.4}$$

$\langle V_{\mu\nu}(t)V_{\kappa\lambda}(0)\rangle = \mathrm{Tr}_R\{\rho_R(0)V_{\mu\nu}(t)V_{\kappa\lambda}(0)\}$ is the reservoir correlation function, $\hbar\omega_{\mu\nu} = (E_{\mu} - E_{\nu})$, and $\delta_{\mu\nu}$ is the Kronecker delta function. Here the energy spacings are assumed to be non-degenerate. In dealing with degenerate levels one needs to be careful about states decoupled with the reservoir as discussed at the end of Sec.

III. The reservoir initially has a thermal distribution of photons given by (4.2). It should be noted here that the above master equation (C.3) is a generalized form which includes the non-secular terms as well as the terms usually dropped under rotating wave approximation. From (C.4) and (4.2) we find that

$$\Gamma^{+}_{\mu\nu\kappa\lambda} = \begin{cases} \frac{2(\vec{d}_{\mu\nu}\cdot\vec{d}_{\kappa\lambda})\omega^{3}_{\kappa\lambda}}{3\hbar c^{3}} N(\omega_{\kappa\lambda}); & \omega_{\kappa\lambda} > 0, \\ \frac{2(\vec{d}_{\mu\nu}\cdot\vec{d}_{\kappa\lambda})\omega^{3}_{\lambda\kappa}}{3\hbar c^{3}} (1 + N(\omega_{\lambda\kappa})); & \omega_{\kappa\lambda} < 0, \end{cases} \tag{C.5}$$

$$\Gamma^{-}_{\mu\nu\kappa\lambda} = \begin{cases} \frac{2(\vec{d}_{\mu\nu}\cdot\vec{d}_{\kappa\lambda})\omega^{3}_{\kappa\lambda}}{3\hbar c^{3}} (1 + N(\omega_{\kappa\lambda})); & \omega_{\kappa\lambda} > 0, \\ \frac{2(\vec{d}_{\mu\nu}\cdot\vec{d}_{\kappa\lambda})\omega^{3}_{\lambda\kappa}}{3\hbar c^{3}} N(\omega_{\lambda\kappa}); & \omega_{\kappa\lambda} < 0, \end{cases} \tag{C.6}$$

Let us assume that a solution of the form $\rho = \exp\left(-\beta \sum_{\mu} E_{\mu} A_{\mu\mu}\right)$ exists for equation (C.3). Substituting this solution in (C.3) we find that

$$\sum_{\mu\nu\kappa} A_{\mu\nu} \exp\left(-\beta E_{\kappa}\right) \left[\Gamma^{+}_{\kappa\nu\mu\kappa} + \Gamma^{-}_{\kappa\nu\mu\kappa} - \Gamma^{+}_{\mu\kappa\kappa\nu} \exp\left(-\beta\hbar\omega_{\nu\kappa}\right) - \Gamma^{-}_{\mu\kappa\kappa\nu} \exp\left(-\beta\hbar\omega_{\mu\kappa}\right)\right] = 0. \tag{C.7}$$

From (C.5) and (C.6) it can be shown that

$$\Gamma^{+}_{\kappa\nu\mu\kappa} = \Gamma^{-}_{\mu\kappa\kappa\nu} \exp\left(-\beta\hbar\omega_{\mu\kappa}\right) \tag{C.8}$$

$$\Gamma^{-}_{\kappa\nu\mu\kappa} = \Gamma^{+}_{\mu\kappa\kappa\nu} \exp\left(-\beta\hbar\omega_{\nu\kappa}\right). \tag{C.9}$$

Using (C.8) and (C.9) we find that (C.7) is satisfied. Thus it shows that the steady state solution is in fact Boltzmann distribution for populations. And as far as there are no atomic states decoupled from the reservoir, the steady state solution is unique.

References

[1] C. H. Townes, *How the Lasers Happened: Adventures of a Scientist*, (Oxford, New York, 1999).

[2] For English translation of original work see, D. Ter Harr, *The old quantum theory* (Pergamon, Oxford, 1967).

[3] G. N. Lewis, Nature **118**, 874 (1926).

[4] A. Einstein, Phys. Z **18**, 121 (1917).

[5] R. Loudon, *The quantum theory of light*, (Oxford, 1983).

[6] J. D. Jackson, *Classical electrodynamics*, (Wiley, New York, 1962).

[7] G. S. Agarwal, *Quantum Statistical Theories of Spontaneous Emission and Their Relation to Other Approaches*, (Springer-Verlag, Berlin, 1974).

[8] A. I. Brushtein, Sov. Phys. JETP **21**, 567 (1965); M. Newstein, Phys. Rev. **167**, 89 (1968); B. R. Mollow, Phys. Rev. **188**, 1969 (1969).

[9] F. Schuda, C. R. Stroud Jr., and M. Hercher, J. Phys. B: Atom. Molec. Phys. **198**, L7 (1974); F. Y. Wu, R. E. Grove, and S. Ezekiel, Phys. Rev. Lett. **35**, 1426 (1975).

[10] I. I. Rabi, Phys. Rev. **51** 652 (1937).

[11] B. R. Mollow, Phys. Rev. A **5**, 2217 (1972).

[12] S. Haroche and F. Hartmann, Phys. Rev. A **6**, 1280 (1972); S. L. McCall, Phys. Rev. A **9**, 1515 (1974).

[13] F. Y. Wu, S. Ezekiel, M. Ducloy, and B. R. Mollow, Phys. Rev. Lett. **38**, 1077 (1977); M. T. Gruneisen, K. R. MacDonald, and R. W. Boyd, J. Opt. Soc. Am.

B **5**, 123 (1988); W. V. Davis, A. L. Gaeta, R. W. Boyd, and G. S. Agarwal, Phys. Rev. A **53**, 3625 (1996).

[14] G. Khitrova, J. F. Valley, and H. M. Gibbs, Phys. Rev. Lett. **60**, 1126 (1988); A. Lezama, Y. Zhu, M. Kanskar, and T. W. Mossberg, Phys. Rev. A **41**, 1576 (1990).

[15] C. Cohen-Tannoudji and S. Reynaud, J. Phys. B **10**, 345 (1977); For a detailed discussion see, C. Cohen-Tannoudji, J. Dupont-Roc, and G. Grynberg, *Atom-Photon Interactions: Basic Processes and Applications* (Wiley, New York, 1992), Chap. VI.

[16] G. S. Agarwal, Phys. Rev. A **19**, 923 (1979); G. Grynberg and C. Cohen-Tannoudji, Opt. Commun. **96**, 150 (1993).

[17] D. Grandclement, G. Grynberg, and M. Pinard, Phys. Rev. Lett. **59**, 44 (1987); G. Grynberg and P. R. Berman, Phys. Rev. A **39**, 4016 (1989).

[18] For a comprehensive literature on two level phenomena, see, L. Allen and J. H. Eberly, *Optical resonance & two-level atoms*, (Wiley, New York, 1975).

[19] D. F. Walls and P. Zoller, Phys. Rev. Lett. **47**, 709 (1981).

[20] Z. H. Lu, S. Bali, and J. E. Thomas, Phys. Rev. Lett. **81**, 3635 (1998).

[21] H. J. Carmichael et al. Phys. Rev. Lett. **58**, 2539 (1987); H. Ritsch and P. Zoller, Opt. Commun. **64**, 523 (1987); S. Swain, Phys. Rev. Lett. **73**, 1493 (1998).

[22] G. Yu. Kryuchkyan, Opt. Commun. **54**, 19 (1985); G. S. Agarwal, Y. Zhu, D. J. Gauthier, and T. W. Mossberg, J. Opt. Soc. Am. B **8**, 1163 (1991); Z. Ficek and K. S. Freedhoff, Phys. Rev. A **48**, 3092 (1993).

[23] Q. Wu, D. J. Gauthier, and T. M. Mossberg, Phys. Rev. A **49**, R1519 (1994); **50**, 1474 (1994); C. C. Yu, J. R. Bochinski, T. M. Kordich, and T. W. Mossberg, Phys. Rev. A **56**, R4381 (1997).

[24] E. T. Jaynes and F. W. Cummings, Proc. IEEE **1**, 89 (1963).

[25] F. W. Cummings, Phys. Rev. A **140**, 1051 (1965); J. H. Eberly, N. B. Narozhny and J. J. Sanchez-Mondragon, Phys. Rev. Lett. **44**, 1323 (1980);

N. B. Narozhny, J. J. Sanchez-Mondragon and J. H. Eberly, Phys. Rev. A **3**, 236 (1981).

[26] J. J. Sanchez-Mondragon, N. B. Narozhuy, and J. H. Eberly, Phys. Rev. Lett. **51**, 550 (1983).

[27] G. S. Agarwal, Phys. Rev. Lett. **53**, 1732 (1984); J. Opt. Soc. Am. B **2**, 480 (1985).

[28] M. G. Raizen, R. J. Thompson, R. J. Bercha, H. J. Kimble and H. J. Carmichael, Phys. Rev. Lett. **63**, 240 (1989); R. J. Thompson, G. Rempe, and H. J. Kimble, Phys. Rev. Lett. **68**, 1132 (1992).

[29] G. Alzetta, A. Gozzini, L. Moi and G. Orriols, Nuovo Cimento Soc. **36 B**, 5 (1976).

[30] R. M. Whitley and C. R. Stroud Jr., Phys. Rev. A **14**, 1498 (1976); E. Arimondo and G. Orriols, Lett. Nuovo Cimento **17**, 333 (1976).

[31] H. R. Grey, R. M. Whitley and C. R. Stroud Jr., Opt. Lett. **3**, 218 (1978).

[32] For a review article see E. Arimondo in *Progress in Optics*, Vol XXXV ed. by E. Wolf (North Holland, Amsterdam, 1996) p257 and references therein.

[33] C. Cohen-Tannoudji and S. Reynaud, J. Phys. B: At. Mol. Phys. **10** 2311 (1977).

[34] G. S. Agarwal and S. S. Jha, J. Phys. B: At. Mol. Phys. **12**, 2655 (1979).

[35] G. S. Agarwal, Phys. Rev. Lett. **37**, 1383 (1976); S. Swain, Adv. At. Mol. Phys. **16**, 159 (1980).

[36] B. J. Dalton and P. L. Knight, J. Phys. B, **15**, 3997 (1982).

[37] F. T. Hioe and C. E. Carroll, Phys. Rev. A **37**, 3000 (1988); V. S. Smirnov, A. M. Tumaikin and V. I. Yudin, Sov. Phys. JETP, **69** 913 (1989).

[38] G. S. Agarwal, Phys. Rev. Lett. **71**, 1351 (1993); M. Fleischhauer, Phys. Rev. Lett. **72**, 989 (1994).

[39] P. M. Radmore and P. L. Knight, J. Phys. B: At. Mol. Phys. **15**, 561 (1982).

[40] I. V. Jyotsna and G. S. Agarwal, Phys. Rev. A **52**, 3147 (1995); *ibid.* **53**, 1690 (1996).

[41] F. Renzoni and E. Arimondo, Phys. Rev. A **58**, 4717 (1998); F. Renzoni, A. Lindner and E. Arimondo, Phys. Rev. A **60**, 450 (1999).

[42] J. E. Thomas, P. R. Hemmer, S. Ezekiel, C. C. Leiby Jr., R. H. Picard, and C. R. Wills, Phys. Rev. Lett. **48**, 867 (1982); P. L. Knight, Nature **297**, 16 (1982).

[43] D. R. Walls and P. Zoller, Opt. Commun. **34**, 260 (1980); G. P. Agarwal, Phys. Rev. A **24**, 1399 (1981); J. Mlynek, F. Mitschke, R. Deserno and W. Lange, Appl. Phys. B **28**, 135 (1982).

[44] A. Aspect, E. Arimondo, R. Kaiser, N. Vansteenkiste and C. Cohen-Tannoudji, Phys. Rev. Lett. **61**, 826 (1988).

[45] U. Gaubatz, P. Rudecki, S. Schiemann, and K. Bergmann, J. Chem. Phys. **92**, 5363 (1990); N. Dam, L. Oudejans, and J. Reuss, Chem. Phys. **140** 217 (1990).

[46] A. Godone, F. Levi, and J. Vanier, Phys. Rev. A **59**, R12 (1999).

[47] A. Javan, Phys. Rev. **107**, 1579 (1956); T. W. Hänsch and P. E. Toschek, Z. Phys. **236**, 213 (1970); T. Popov, A. Popov, and S. Ravtian, JETP Lett. **30**, 466 (1970).

[48] V. Arkhipkin and Yu. Heller, Phys. Lett. **48A**, 12 (1983).

[49] O. A. Kocharovskaya and Ya. I. Khanin, Sov. Phys. JETP Lett. **48** 630 (1988).

[50] S. E. Harris, Phys. Rev. Lett. **62**, 1033 (1989).

[51] U. Fano, Phys. Rev. **124** 1866 (1961); U. Fano and J. W. Cooper, Phys. Rev. **137**, 1364 (1965).

[52] A. Imamoglu and S. E. Harris, Opt. Lett. **14**, 1344 (1989).

[53] M. O. Scully, S.-Y. Zhu, and A. Gavridiles, Phys. Rev. Lett. **62**, 2813 (1989).

[54] G. S. Agarwal, Phys. Rev. Lett. **67**, 980 (1991).

[55] G. S. Agarwal, S. Ravi, and J. Cooper, Phys. Rev. A **41**, 4721 (1990); 4727 (1990); B. Prasad and G. S. Agarwal, Opt. Commun. **86**, 409 (1991).

[56] A. Imamoğlu, J. E. Field, and S. E. Harris, Phys. Rev. Lett. **66**, 1154 (1991).

[57] L. M. Narducci, H. M. Doss, P. Ru, M. O. Scully, S.-Y. Zhu, and C. H. Keitel, Opt. Commun. **81**, 379 (1991).

[58] Y. Zhu, Phys. Rev. A **45**, R6149 (1992); Y. F. Zhu, and M. Xiao, *ibid.* **49**, 2203 (1994).

[59] G. S. Agarwal, Phys. Rev. A **44**, R28 (1991).

[60] J. Gao, H. Z. Zhang, H. F. Cui, Z. X. Guo, Y. Jiang, W. Q Wang, X. G. Jin and S. J. Li, Opt. Commun. **110**, 590 (1994).

[61] S. E. Fry, X. Li, D. Nikonov, G. G. Padmabandu, M. O. Scully, V. A. Smith, K. F. Tittel, C. Wang, R. S. Wilkinson and S.-Y. Zhu, Phys. Rev. Lett. **70**, 3235 (1993).

[62] A. Nottelman, C. Peters, and W. Lange, Phys. Rev. Lett. **70**, 1783 (1993).

[63] W. E. van der Veer, J. R. van Dienst, A. Dönselmann and H. B. van Linden van den Huevell, Phys. Rev. Lett. **70**, 3243 (1993).

[64] A. S. Zibrov, M. D. Lukin, D. E. Nikonov, L. Hollberg, M. O. Scully, V. L. Velichansky, and H. G. Robinson, Phys. Rev. Lett. **75**, 1499 (1995).

[65] G. G. Padmabandu, G. R. Welch, I. N. Shubin, E. S. Fry, D. E. Nikonov, M. D. Lukin, and M. O. Scully, Phys. Rev. Lett. **76**, 2053 (1996).

[66] For review articles see, O. Kocharovskaya, Phys. Rep. **219**, 175 (1992); P. Mandel, Contemporary Phys. **34**, 235 (1993); M. O. Scully, Quantum Opt. **6**, 203 (1994). For a general article see, M. O. Scully and M. Fleischhauer, Science **263**, 337 (1994).

[67] S. E. Harris, Phys. Today **50(7)**, 36 (1997).

[68] K. J. Boller, A. Imamoglu, and S. E. Harris, Phys. Rev. Lett. **66**, 2593 (1991); J. E. Field, K. H. Hahn, S. E. Harris, *ibid.* **67**, 3062 (1991).

[69] S. H. Autler and C. H. Townes, Phys. Rev. **100**, 703 (1955).

[70] Y. Li and M. Xiao, Phys. Rev. A **51** 4959 (1995).

[71] G. S. Agarwal, Phys. Rev. A **55**, 2467 (1997).

[72] J. G. Banacloche, Y. Li, S. Jin, and M. Xiao, Phys. Rev. A **51**, 576 (1995); M. Xiao, Y. Li, S. Jin, and J. G. Banacloche, Phys. Rev. A **74**, 666 (1995); Y. Li and M. Xiao, Phys. Rev. A **51**, R2703 (1995).

[73] R. R. Moseley, S. Shepherd, D. J. Fulton, B. D. Sinclair and M. H. Dunn, Phys. Rev. Lett. **74**, 670 (1995); Opt. Commun. **119**, 61 (1995).

[74] D. J. Fulton, S. Shepherd, R. R. Moseley, B. D. Sinclair and M .H. Dunn, Phys. Rev. A **52** 2302 (1995); J. R. Boon, E. Zekou, D. McGloin, and M. H. Dunn, Phys. Rev. A **59**, 4675 (1998).

[75] M. Mitsunaga, T. Mukai, K. Watanabe, and T. Mukai, J. Opt. Soc. Am B **13**, 2696 (1998); S. A. Hopkins, E. Usadi, H. X. Chen, and A. V. Durrant, Opt. Commun. **138** 185 (1997); A. V. Durrant, H. X. Chen , S. A. Hopkins, and J. A. Vaccaro, *ibid.* **151**, 136 (1998).

[76] For a topical review, see, J. Marangos, J. Mod. Opt. **45**, 471 (1998).

[77] S. E. Harris, Phys. Rev. Lett. **77**, 5357 (1996).

[78] G. S. Agarwal and R. Boyd, Phys. Rev. A **60**, R2681 (1999).

[79] A. Kasapi, Phys. Rev. Lett. **77**, 1035 (1996).

[80] S. E. Harris, Phys. Rev. Lett. **70**, 552 (1993); R. Grobe et al., Phys. Rev. Lett. **73**, 3183 (1994); S. E. Harris and Z.-F. Luo, Phys. Rev. A **52**, R928 (1995).

[81] M. Mitsunaga and N. Imoto, Phys. Rev. A **59**, 4773 (1999); for a theoretical work, see, H. Y. Ling, Y.-Q. Li, and M. Xiao, Phys. Rev. A **57**, 1338 (1998).

[82] G. S. Agarwal and W. Harshawardhan, Phys. Rev. Lett. **77**, 1039 (1996).

[83] S. E. Harris and Y. Yamamoto, Phys. Rev. Lett. **81**, 3611 (1998).

[84] Y. Zhao, C. Wu, B. S. Ham, M. K. Kim, and E. Awad, Phys. Rev. Lett. **79**, 641 (1997).

[85] B. S. Ham, M. S. Shahriar, and P. R. Hammer, Opt. Lett. **22**, 1138 (1997); K. Ichimura, K. Yamamoto, and N. Gemma, Phys. Rev. A **58**, 4116 (1998).

[86] M. O. Scully, Phys. Rev. Lett. **67**, 1855 (1991); M. O. Scully and S. -Y. Zhu, Opt. Commun. **87**, 134 (1992).

[87] M. Fleischhauer, C. H. Keitel, M. O.Scully, and C. Su. Opt. Commun. **87**, 109 (1992).

[88] O. Kocharovskaya, P. Mandel, and M. O. Scully, Phys. Rev. Lett. **74**, 2451 (1991); M. Löffler, D. E. Nikonov, O. Kocharovskaya, and M. O. Scully, Phys. Rev. A **56**, 5014 (1997).

[89] A. S. Zibrov, M. D. Lukin, L. Hollberg, D. E. Nikonov, M. O. Scully, H. G. Robinson, L. V. Velichansky, Phys. Rev. Lett. **76**, 3935 (1996).

[90] M. O. Scully and M. Fleischhauer, Phys. Rev. Lett. **69**, 1360 (1992); M. Fleischhauer and M. O. Scully, Phys. Rev. A **49**, 1973 (1994)

[91] S. E. Harris, J. E. Field and A. Kasapi, Phys. Rev A **49**, R29 (1992).

[92] L. V. Hau, S. E. Harris, Z. Dutton, and C. H. Behroozi, Nature (London) **397**, 549 (1999).

[93] M. M. Kash, V. A. Sautenkov, A. S. Zibrov, L. Hollberg, G. R. Welch, M. D. Lukin, Y. Rostovtev, E. S. Fry, and M. O. Scully, Phys. Rev. Lett. **82**, 5229 (1999).

[94] D. Budker, D. F. Kimball, S. M. Rochester, and V. V. Yashchuk, Phys. Rev. Lett. **83**, 1767 (1999).

[95] M. Fleischhauer and M. D. Lukin, Phys. Rev. Lett. **84**, 5094 (2000); M. D. Lukin, S. F. Yelin and M. Fleischhauer, *ibid.* **84**, 4232 (2000).

[96] G. S. Agarwal and R. R. Puri, Phys. Rev. A **41**, 3782 (1990).

[97] S. Wielandy and A. L. Gaeta, Phys. Rev. Lett. **81**, 3359 (1998).

[98] A. D. Cronin, R. B. Warrington, S. K. Lamoreaux, and E. N. Fortson, Phys. Rev. Lett. **80**, 3719 (1998).

[99] A. K. Patnaik and G. S. Agarwal, Opt. Commun. **179**, 97 (2000).

[100] S. P. Tewari and G. S. Agarwal, Phys. Rev. Lett. **56**, 1811 (1986).

[101] S. E. Harris, J. E. Field, and A. Imamoglu, Phys. Rev. Lett. **64**, 1107 (1990).

[102] S. P. Tewari and G. S. Agarwal, Phys. Rev. Lett. **66**, 1797 (1991).

[103] K. Hakuta, L. Marmet, and B. P. Stoicheff, Phys. Rev. Lett. **66**, 596 (1991); Phys. Rev. A **45**, 5152 (1992).

[104] G. Z. Zhang, K. Hakuta, and B. P. Stoicheff, Phys. Rev. Lett. **71**, 3099 (1993); G. Z. Zhang, M. Katsuragawa, K. Hakuta, R. I. Thompson, and B. P. Stoicheff, Phys. Rev. A **52**, 1584 (1995).

[105] M. Jain, G. Y. Gin, and S. E. Harris, Opt. Lett. **18**, 998 (1993).

[106] M. Jain, H. Xia, G. Y. Yin, A. J. Merriam, and S. E. Harris, Phys. Rev. Lett. **77**, 4326 (1996). For a non-perturbative theory of such process' see, W. Harshawardhan and G. S. Agarwal, Phys. Rev. A **58**,598 (1998).

[107] H. Schmidt and A. Imamoglu, Opt. Lett. **21**, 1936 (1996).

[108] P. R. Hemmer, D. P. Katz, J. Donoghue, M. Cronin-Golomb, M. S. Shahriar, and P. Kumar, Opt. Lett. **20**, 982 (1995); M. D. Lukin, P. R. Hemmer, M. Löffler, and M. O. Scully, Phys. Rev. Lett. **81**, 2675 (1998).

[109] M. D. Lukin, M. Fleischhauer, A. S. Zibrov, H. G. Robinson, V. L. Velichansky, L. Hollberg, and M. O. Scully, Phys. Rev. Lett. **79**, 2959 (1997).

[110] S. E. Harris and L. V. Hau, Phys. Rev. Lett. **82**, 4611 (1999).

[111] A. S. Zibrov, M. D. Lukin, and M. O. Scully, Phys. Rev. Lett. **83**, 4049 (1999).

[112] See pg. 93-96 in Ref. [7].

[113] D. A. Cardimona and C. R. Stroud, Jr., Phys. Rev. A **27**, 2456 (1983).

[114] D. A. Cardimona, M. G. Raymer, and C. R. Stroud, Jr., J. Phys. B **15**, 55 (1982).

[115] G. S. Agarwal, S. L. Haan and J. Cooper, Phys. Rev. A **29**, 2565 (1984); D. Agassi, Phys. Rev. A **30**, 2449 (1984); S.-Y. Zhu, R. C. F. Chan, and C. P. Lee, Phys. Rev. A **52**, 710 (1995).

[116] A. Imamŏglu, Phys. Rev. A **40**, 2835 (1989).

[117] G. C. Hegerfeldt and M. B. Plenio, Phys. Rev. A **46**, 373 (1992); *ibid.* **47**, 2186 (1993).

[118] S.-Y. Zhu and M. O. Scully, Phys. Rev. Lett. **76**, 388 (1996); H. Huang, S.-Y. Zhu and M. S. Zubairy, Phys. Rev. A. **55**, 744 (1997); H. Lee, P. Polynkin, M. O. Scully, and S.-Y. Zhu, Phys. Rev. A **55**, 4454 (1997).

[119] H.-R. Xia, C. Y. Ye, and S.-Y. Zhu, Phys. Rev. Lett. **77** 1032 (1996); for an intutive picture of spontaneous emission cancellation, see, G. S. Agarwal, Phys. Rev. A **55**, 2457 (1997).

[120] P. Zhou and S. Swain, Phys. Rev. Lett. **77**, 3995 (1996); Phys. Rev. A **56**, 3011 (1997).

[121] P. Zhou and S. Swain, Phys. Rev. Lett. **78**, 832 (1997).

[122] C. H. Keitel, Phys. Rev. Lett. **83**, 1307 (1999); F. Li and S. -Y. Zhu, Phys. Rev. A **59**, 2330 (1999).

[123] E. Paspalakis and P. L. Knight, Phys. Rev. Lett. **81**, 293 (1998); E. Paspalakis, C. H. Keitel, and P. L. Knight, Phys. Rev. A **58**, 4868 (1998).

[124] E. Paspalakis, N. J. Kylstra, and P. L. Knight, Phys. Rev. Lett. **82**, 2079 (1999); *ibid.*, Phys. Rev. A **61**, 045802 (2000).

[125] V. I. Savchenko, N. J. Fisch, A. A. Panteleev, and A. N. Starostin, Phys. Rev. A **59**, 708 (1999).

[126] J. Javanainen, Europhys. Lett. **17**, 407 (1992).

[127] M. A. G. Martinez, P. R. Herczfeld, C. Samuels, L. M. Narducci, and C. H. Keitel, Phys. Rev. A **55**, 4483 (1997).

[128] C. Cohen-Tannoudji and S. Reynaud, J. Phys. B: At. Mol. Phys. **10**, 365 (1977).

[129] S. Menon and G. S. Agarwal, Phys. Rev. A **59**, 740 (1998).

[130] L. J. Wang, A. Kuzmich, and A. Dogariu, Nature **406**, 277 (2000).

[131] S. Menon and G. S. Agarwal, Phys. Rev. A **61**, 013807 (2000); *Frontiers of Laser Physics and Quantum Optics*, eds. Z. Xu, S. Xie, S.-Y. Zhu, and M. O. Scully, (Springer, 2000), p. 541.

[132] G. S. Agarwal and S. Menon, to appear in Phys. Rev. A.

[133] S. Menon and G. S. Agarwal, Laser Phys. **9**, 813 (1999).

[134] S. Menon and G. S. Agarwal, Phys. Rev. A **57**, 4014 (1998).

[135] W. J. Brown, J. R. Gardner, and D. J. Gauthier, Phys. Rev. A **56**, 3255 (1997).

[136] J. L. Bowie, J. C. Garrison and R. Y. Chiao, Phys. Rev. A **61**, 053811 (2000).

[137] L. Brillouin, *Wave Propagation and Group Velocity* (Academic, New York, 1960); C. G. B. Garrett and D. E. McCumber, Phys. Rev. A **1**, 305 (1969).

[138] S. Chu and S. Wong, Phys. Rev. Lett. **48**, 738 (1982).

[139] E. L. Bolda and R. Y. Chiao, Phys. Rev. A **48**, 3890 (1993).

[140] M. W. Mitchell and R. Y. Chiao, Am. J. Phys. **66**, 14 (1998).

[141] A. M. Steinberg and R. Y. Chiao, Phys. Rev. A **49**, 2017 (1994); E. Bolda, J. C. Garrison, and R. Y. Chiao, Phys. Rev. A **49**, 2938 (1994).

[142] G. Diener, Phys. Lett. A **223**, 327 (1996).

[143] P. B. Hogan, S. J. Smith, A. T. Georges, and P. Lambropoulos, Phys. Rev. Lett. **41** 229 (1978); H. R. Gray and C. R. Stroud Jr., Opt. Commun. **25**, 359 (1978).

[144] R. Shimano and M. Kuwata-Gonokami, Phys. Rev. Lett. **72** 530 (1994).

[145] E. Paspalakis, S.-Q. Gong, and P. L. Knight, Opt. Commun. **152**, 293 (1998); S.-Q. Gong, E. Paspalakis, and P. L. Knight, J. Mod. Optics **45**, 2433 (1998).

[146] F. Li and S.-Y. Zhu, Opt. Commun. **162**, 155 (1999).

[147] F. Plastina and F. Piperno, Opt. Commun. **161** 236 (1999).

[148] D. A. Lidar, I. L. Chuang, and K. B. Whaley, Phys. Rev. Lett. **81**, 2594 (1998); A. Beige, D. Braun, B. Tregenna and P. L. Knight, Phys. Rev. Lett. **85**, 1762 (2000); U. Akram, Z. Ficek, and S. Swain, Phys. Rev. A **62**, 013413 (2000).

[149] A. K. Patnaik and G. S. Agarwal, J. Mod. Opt. **45**, 2131 (1998); Z. Ficek and T. Rudolph, Phys. Rev. A **60**, R4245 (1999).

[150] P. R. Berman, Phys. Rev. A **58**, 4886 (1998); for an early work see, P. R. Fontana and R. P. Srivastava, Phys. Rev. A **7**, 1866 (1973).

[151] For a discussion on static field induced mixing of magnetic sub-levels see, E. B. Alexandrov, M. P. Chaika, and G. I. Khvostenko, *Interference of Atomic States* (Springer-Verlag, Berlin, 1993), pg. 229.

[152] K. H. Hahn, D. A. King, and S. E. Harris, Phys. Rev. Lett. **65**, 2777 (1990).

[153] J. Faist, C. Sirtori, S. Zhu, L. Pfeiffer, and K. West, Opt. Lett. **21**, 985 (1996); J. Faist, F. Capasso, C. Sirtori, K. West, and L. Pfeiffer, Nature(London), **390**, 589 (1997); H. Schmidt, K. Campman, A. Gossard, and A. Imamoğlu, Appl. Phys. Lett. **70**, 3455 (1997).

[154] A. K. Patnaik and G. S. Agarwal, Phys. Rev. A **59**, 3015 (1999); P. Zhou and S. Swain, Opt. Commun. **179**, 267 (2000); P. Zhou, quant-ph/0003088; P. Zhou, S. Swain, L. You, and T. Kennedy, quant-ph/0004001.

[155] E. Paspalakis, N. J. Klystra, and P. L. Knight, Phys. Rev. A **60**, R33 (1999).

[156] G. S. Agarwal, Phys. Rev. Lett. **84**, 5500 (2000).

[157] G. S. Agarwal, *Progess in Optics*, Vol. XI, ed. by E. Wolf (North-Holland, Amsterdam, 1973), p. 40; W. H. Louisell, *Quantum statistical properties of radiation* (Wiley, New York, 1973), p. 349; C. Cohen-Tannoudji, *Frontiers in laser spectroscopy*, Vol. 1, eds. R. Balian, S. Haroche, and S. Liberman (North-Holland, Amsterdam, 1977), p. 33.

List of Publications

A. Journals

1. *Effects of Spontaneously Generated Coherence on Pump-Probe Spectroscopy of a Λ System*,
   Sunish Menon and G. S. Agarwal, Phys. Rev. A **57**, 4014-4018 (1998).

2. *Gain from Cross Talk Among Optical Transitions*,
   Sunish Menon and G. S. Agarwal, Phys. Rev. A **59**, 740-749 (1999).

3. *Probing the Vacuum Induced Coherence in a Λ System*,
   Sunish Menon and G. S. Agarwal, Laser Phys. **9**, 813-819 (1999).

4. *Gain Components in Autler-Townes Doublet from Quantum Interference in Decay Channels*,
   Sunish Menon and G. S. Agarwal, Phys. Rev. A **61**, 013807(1-8) (2000).

5. *Quantum Interference and the Question of Thermodynamic Equilibrium*,
   G. S. Agarwal and Sunish Menon, Phys. Rev. A **62**, (2001) [in press].

B. Proceedings of Conference/Symposia

1. *Gain Components in Autler-Townes Doublet from Quantum Interference in Decay Channels*,
   Sunish Menon and G. S. Agarwal, "Frontiers of Laser Physics and Quantum Optics" (*Springer*), Pg. 541, eds. Z. Xu, S. Xie, S.-Y. Zhu and M. O. Scully, held at Shanghai, China, Aug. 1999.

2. *Effects of Spontaneously Generated Coherence on Pump-Probe Response of a Λ System*,

Sunish Menon, "Proceedings of the National Laser Symposium ",Pg. 215, held at Physical Research Laboratory, Ahmedabad, 10-12 Dec., 1997.

3. *Is Coherent Population Trapping Phenomena Preserved in the Presence of Inherent Interference Effects ?*,
   Sunish Menon, "Abstracts of Seminar on Physics with Cooled and Trapped Atoms and Ions", Pg. 20, held at Bhabha Atomic Research Centre, Mumbai, 5-6 March, 1998.

4. *Gain From Cross Talk Among Optical Transitions*,
   Sunish Menon, "Proceedings of National Laser Symposium", Pg. 88, held at Indian Institute of Technology, Kanpur, 14-16 Dec., 1998.

5. *Quasi-Trapped-States in V Systems due to Interference in Decay Channels*,
   Sunish Menon, "Proceedings of the National Laser Symposium ", Pg. 279, held at Univ. of Hyderabad, Hyderabad, 15-17 Dec., 1999.